Non-line of Sight Underwater Optical Wireless Communications

Al-Amin Umar Barambu

A thesis submitted in partial fulfilment of the requirements for the degree of

Doctor of Philosophy

School of Engineering

June, 2021

Dedicated to my Lovely Mother Haj. Zainab Umar Barambu, and my favourite sister Halima (Mama Lesh) for their love and support

TABLE OF CONTENTS

LIST OF FIGURES

LIST OF TABLES

LIST OF ABBREVIATIONS

AMOUR	-	Autonomous modular optical underwater robot.
AOP	-	Apparent optical properties.
APD	-	Avalanche photodiode.
AUV	-	Autonomous underwater vehicles.
AWGN	-	Additive white Gaussian noise.
BCH	-	Bose – Chaudhuri – Hockenheim.
BER	-	Bit error rate.
BL	-	Beer Lambert.
BPSK	-	Binary phase shift keying.
CDF	-	Cumulative density function.
CDOM	-	Coloured dissolved organic matter.
CIR	-	Channel impulse response.
CM	-	Coherent modulation.
CP	-	Cyclic prefix.
CPM	-	Continuous phase modulation.
CRC	-	Cyclic redundancy check.
DD	-	Direct detection.
DGF	-	Double Gamma function.
DPIM	-	Digital pulse interval modulation.
DPSK	-	Differential phase shift keying.
ELF	-	Extremely low frequency.
EGC	-	Equal gain combiner.

FEC	-	Forward error correction.
FFP	-	Fournier forrand phase.
FFT	-	Fast fourier transform.
FOV	-	Field of view.
FSO	-	Free space optics.
GA	-	Gaussian approximation.
HG	-	Henyey Greenstein.
IFFT	-	Inverse fast fourier transform.
IM	-	Intensity modulation.
IOP	-	Inherent optical properties.
IOUT	-	Internet of underwater things.
ISI	-	Inter-symbol interference.
ISM	-	Industrial scientific and medicine.
LEDs	-	Light emitting diodes.
LDPC	-	Low density parity check.
LOS	-	Line of sight.
MATLAB	-	Matrix laboratory.
MC	-	Monte carlo.
MGF	-	Moment generating function.
MIMO	-	Multiple input multiple output.
MISO	-	Multiple input single output.
NLOS	-	Non-line of sight.
NRZ	-	Non-return to zero.

OFDM	-	Orthogornal frequency division multiplexing.
OOK	-	On-Off keying.
OWC	-	Optical wireless communication.
PDF	-	Probability density function.
PMT	-	Photomultiplier tube.
PPM	-	Pulse position modulation.
PSK	-	Phase shift keying.
PWM	-	Pulse width modulation.
QAM	-	Quadrature amplitude modulation.
QPSK	-	Quadrature phase shift keying.
QSSA	-	Quassi-scattering approximation.
RF	-	Radio frequency.
ROV	-	Remotely operated vehicles.
RS	-	Reed Solomon.
RTE	-	Radiative transfer equation.
RV	-	Random variable.
RX	-	Receiver.
SIMO	-	Single input multiple output.
SISO	-	Single input single output.
SNR	-	Single to noise ratio.
SPA	-	Saddle point approximation.
SPF	-	Scattering phase function.
SSA	-	Single – scattering approximation.

TTHG	-	Two term Henyey-Greenstein.
TX	-	Transmitter.
UOWC	-	Underwater optical wireless communication.
UWC	-	Underwater wireless communication.
UWSN	-	Underwater wireless sensor network.
VSF	-	Volume scattering phase function.
WDGF	-	Weighted double Gamma function.
ZFE	-	Zero forcing equalizer.

ACKNOWLEDGEMENTS

Alhamdulillah Praise and Gratitude to Allah for everything, for giving me the guidance, strength and perseverance in this PhD journey.

I would like to express my gratitude to Petroleum Technology Development Fund of the Federal Ministry of Petroleum Resources, Nigeria for sponsorship of the research undertaken. I am grateful for the facilities provided to me by the School of Engineering at the University of Warwick.

Most Importantly, I would like to express my deepest gratitude to my supervisor, Dr. Mark S. Leeson for his valuable time, guidance, support and kindness throughout the PhD journey. I am also indebted to you for your constructive feedback, advice and support throughout the writing up period. Mark, I thank you for helping to keep my research on the right track.

Specially for my beloved parents Haj. Zainab Umar Barambu and Alh. Umar Barambu, and my family, thank you for the endless prayers for my success, health, happiness and for being in spirit every step of the way despite being physically an ocean away. Your love, faith and confidence in me, kept me going all these years.

A special thanks to Deeja Tukur who has being supporting me, motivating me and making me happy from the start to the end of this journey. I will not forget that and will forever be grateful.

Last but not the least, to all my friends in Warwick, UK and Nigeria, thank you for the amazing and memorable experience. Your support and friendship means more than I can ever express.

DECLARATION

This thesis is submitted in partial fulfilment for the degree of Doctor of Philosophy under the regulations set out by the Graduate School at the University of Warwick. All work reported in the thesis has been carried out by Al-Amin Umar Barambu, except where stated otherwise, between the dates of October 2017 and June 2021. No part of this thesis has been previously submitted to the University of Warwick or any other academic institution for admission to a higher degree.

Al-Amin Umar Barambu

June 2021

ABSTRACT

Underwater optical wireless communication (UOWC) has recently become a major research subject as it offers high data rates in the order of Megabits per second (Mbps) to Gigabits per second (Gbps) and lower latency due to the high speed of light in water than the incumbent acoustic technology. Presently, there is an increase in the number of unmanned devices such as remotely operated vehicles (ROVs) and the autonomous underwater vehicles (AUVs) deployed underwater which require high capacity and high bandwidth to transfer information underwater. Such AUVs and ROVs are capable of performing tasks at a depth inaccessible to divers due to the danger and risk associated deep down in the underwater world. This thesis concentrates on and explores the performance of Non-line of sight (NLOS) UOWC because it is a more realistic approach towards designing practical systems. This is because in practical scenarios, line of sight (LOS) communication links are not always possible due to obstructions from sea creatures, bubbles, large suspended particles and features of the seabed, especially in coastal and turbid water environments. LOS links are also unsuitable when the transmitter and receiver are non-stationary nodes.

Following an introduction to and literature review of UOWC, the thesis considers the characteristics of a NLOS UOWC link with multiple scattering based on Monte Carlo (MC) simulation. For the first time, the channel response of an NLOS-UOWC system with different channel modulation schemes is then addressed. The resultant channel impulse (CIR) response varies with the type of water considered and the receiver field of view (FOV). Thus, the CIR for clear ocean, coastal water and turbid water for FOV values of 30° and 60° are investigated. Then, the CIR obtained using different modulation formats is determined in coastal water since this is a likely application medium. This is followed by evaluation of the bit error rate (BER) and throughput of the system, including variation in the receiver bandwidth. The system provides BER values of 10^{-4} or better and throughput of 2.1 Mbps. Furthermore, the impulse response of a NLOS UOWC link is determined using analytical models for the phase scattering from underwater propagation. These are used to obtain temporal dispersion results for NLOS UOWC links in coastal and harbour water environments. Curve fitting using the analytical models shows correlation coefficients of between 0.98 and 0.99, demonstrating the utility of the models employed.

Finally, for the first time, the thesis presents the performance of a multiple-input multiple-output (MIMO) NLOS UOWC system employing continuous phase modulation (CPM), which is shown to offer sensitivity benefits of several dBs over on–off keying (OOK) without coherent reception. The CIR is obtained by using MC simulation. Turbulence is included by conditioning the CIR on log-normal statistics. To mitigate the resultant fading, spatial diversity with receiver side equal gain combining is employed. Shot noise is included by photon counting, followed by BER calculations using Saddle point and Gaussian approximations. The results show that spatial diversity offers performance improvements, for example an 8 dB sensitivity gain at 10^{-9} BER using 1 Gbps 3×1 multiple-input single-output (MISO) transmission over a 20 m link with 0.16 log-amplitude variance. The last part of the thesis also determines using an upper bound that Intersymbol Interference (ISI) has a significant impact at high bit rates, producing error floors for multiple-output arrangements.

PUBLICATIONS ASSOCIATED WITH THIS RESEARCH WORK

The following papers have been published/ submitted as a result of the work contained within this thesis.

A. B. Umar and M. S. Leeson, "Underwater Optical Wireless Communications: Non-Line-of-Sight Links", *International Optics and Photonics Conference, London, UK,* December 9-10, 2019.

A. B. Umar, M. S. Leeson and I. Abdullahi, "Modelling Impulse Response for NLOS Underwater Optical Wireless Communications," *2019 IEEE 15th International Conference on Electronics, Computer and Computation (ICECCO), Abuja, Nigeria,* 2019.

A. B. Umar and M. S. Leeson, "Performance of Non-Line-of-Sight Underwater Optical Wireless Communications," *2019 IEEE 2nd British and Irish Conference on Optics and Photonics (BICOP), London, United Kingdom,* 2019.

A. B. Umar and M. S. Leeson, "Performance of Non-Line of Sight Underwater Optical Wireless Communication Links", *International Journal of Photonics and Optical Technology,* vol. 6, no. 1, pp: 5-10, 2020.

A. B. Umar and M. S. Leeson, "Advances in Underwater Optical Wireless Communications", *International Journal of Photonics and Optical Technology,* vol. 7, no. 1, pp. 1-14, 2021.

Al-Amin. B. Umar and Mark. S. Leeson, "Performance of Non-line of sight Underwater optical wireless communication links with spatial diversity", *Accepted in American journal of Electrical and Computer Engineering, 2021.*

CHAPTER 1

Introduction

1.1 Background

In terrestrial environmental communications, the ever evolving free space optics (FSO), also referred to as optical wireless communications (OWC), has become an increasingly significant technology as a complementary approach to radio frequency (RF) communication technology as a result of its low power, high data rates and large unlicensed bandwidth advantages [1]. Inspired by the appealing performance and characteristics of FSO in the terrestrial environment, OWC technology is now seen as a potential technology for many applications in the underwater environment. Humans have never stopped exploring the ocean over the past thousands of years, since more than 70% of the earth's surface is covered with water. Moreover, about 97 % of earth's water is in the form of ocean according to the United States National Atmospheric and Oceanic Administration [2]. There has been a growing interest in the research of ocean exploration systems in recent years due to the ever-increasing global climate change and resource depletion. The ocean represents one of the ultimate frontiers for exploration, science, and technology. Underwater wireless communication (UWC) technology attracts much attention as it enables the realization of ocean exploration systems.

Acoustic waves have enjoyed great success for communications underwater due to their ability to operate over large distances, but their performance is limited by low bandwidth, high latency, high transmission losses and time-varying multipath propagation. Acoustic underwater communication currently supports data rates of up to hundreds of kbps for few meters (short distances) and tens of kbps for few kilometers (long distances) [3]. Presently, there is an increase in the number of unmanned devices such as remotely operated vehicles (ROVs) and Autonomous underwater vehicles (AUVs) deployed underwater which require high capacity and high

bandwidth to transfer information underwater. Recent advances in visible light technology combined with the low attenuation blue-green wavelength window of seawater has made Underwater optical wireless communications (UOWC) a viable and attractive alternative or a complementary solution, offering higher bandwidths and data rates (of the order of Gbps), lower latency (due to the extremely large propagation speed of light), and better security for underwater communications [4]. A range of applications such as inshore environmental monitoring, offshore oil explorations, oil and gas monitoring and security, tactical surveillance, pollution monitoring, and oceanography research could benefit tremendously from UOWC but the such systems also suffer from significant channel absorption and scattering, and may be blocked by a myriad of underwater obstructions.

Duntley in 1963 proposed that seawater shows a low absorption (The process in which the photon disappear with its energy being converted to another form such as chemical or heat) window to light in the blue/green (from 450 nm to 550 nm) wavelength region in the visible spectrum (Fig 1) [5] based on nearly 2 decades theoretical and experimental study of light propagation in the ocean. His conclusion was then confirmed experimentally by Gabriel *et al.* in [6]. This creates a surge of interest and provides a foundation for the development of UOWC. Interest in UOWC was then limited to military applications over the decades as can be seen in [7] [8] [9]. Only a few products were commercialised recently. These include the Ambalux UOWC system [10] which can provide a maximum data rate of 10 Mbps over a 40 m range, the BlueComm UOWC system commercialised by Sonardyne [11] in the early 2010s which can achieve data transmission of 20 Mbps operating over a distance of 200 m and a tele-submarine built using 70 or more Light emitting diodes (LEDs) per plate holding a 120 degree field of view (FOV) developed by Penguin Automated Systems Inc. providing data rates of up to 100 Mbps [12]. Researchers have proposed Underwater Wireless Sensor Network (UWSN) concept to satisfy the rising demands for ocean exploration with reliable high data rates transmission which has

greatly promote the development of UOWC and hence UOWC market has begun to show a future guarantee. From the literature review conducted in chapter two of this thesis, it can be said that UOWC is still a maturing field (i.e. still at the research stage).

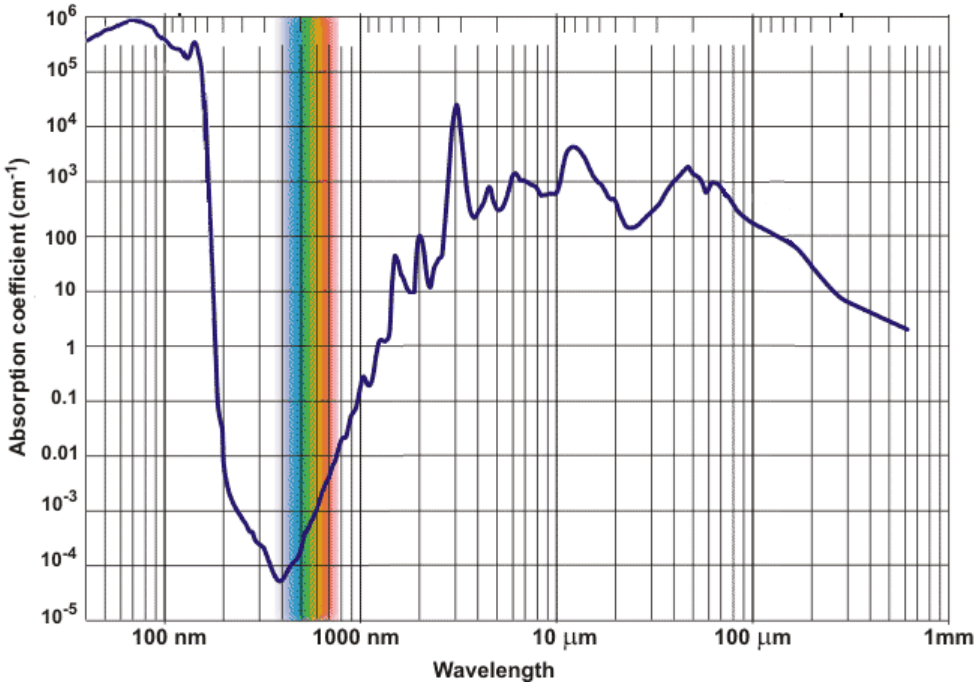

Fig. 1.1: Electromagnetic absorption in water [5].

1.2 Applications Areas of UOWC

Communication under the water is believed to be fundamental for ocean observations and exploration since the underwater environment is an essential source to almost all living organisms. UWSNs are one of the main examples of UOWC applications. The UWSN at its basics comprises many distributed nodes such as relay buoys, seabed sensors, AUVs and ROVs capable of accomplishing processing, sensing and overall communication function (such as transmitting and receiving data) that maintain the monitoring to the underwater world. The mobile nodes can also be used to perform deployment, recovery, and relocation functions [13]. The AUVs and ROVs can also be used in other fields based on sub-sea operations such as surveillance, real time data transfer, inspection and equipment maintenance under the water. The concept of UWSNs is illustrated in Figure

1.2. [14]. The onshore data centre above the sea surface processes the data and communicates with ships and satellite through FSO or RF links.

Below is a brief list of some areas of potential UOWC application.

- Ocean sampling: Ocean observing and prediction system, ocean biology (monitoring the ocean biological changes like global warming on marine biology and impact of human generated pollutants to the climate). The network of AUVs and optical underwater sensors can perform different functions such as measuring the physical properties of ocean, sampling of three-dimensional coastal of oceans and ecosystem productivity. Some of the famous projects developed for ocean sampling are Bermuda Bio-Optics project [15], Coastal ocean dynamics [16] and autonomous ocean sampling network [17].
- Environmental Monitoring: Environmental monitoring application of UOWC are particularly related to Monitoring of underwater exploration, monitoring of underwater habitat (fish farm monitoring, marine life monitoring, coral reef monitoring), and monitoring of water quality. Water is covering most of the earth's surface and there are abundant resources in the underwater environment such as oil and gas which needs to be explored. The dry parts of the earth are connected by pipelines and underwater cables. Hence, UOWC can be used to monitor these pipelines and underwater cables as well as explore the precious resources under the water. In [18], an underwater monitoring system which combines AUVs and ROVs was proposed to discover the mineral resources under the water.
- Navigation: UWSNs are the promising technology to assist the navigation in the underwater world. The authors in [19] have proposed an assistive navigation system for underwater sensor networks using AUVs. Received signal strength (RSS) and novel time of arrival (ToA) based distributed localization schemes are developed in [20] for underwater optical wireless networks.
- Surveillance: Underwater surveillance is important especially for intruder detection. Underwater sensor networks can be used for Onshore surveillance (battleships detection and logistics arrival) and offshore

surveillance (offshore oil and gas exploration, undersea pipelines and oil wells surveillance). A novel blueprint for underwater surveillance which consist of surface sensors has been proposed in [21]. The authors in [22] have proposed electromagnetic waves based different architectures for surveillance under the water.

- Mine Reconnaissance: Sensors to detect underwater mines, teleoperation and determining accurate positions. It is rational that sensors can detect underwater mines since sensors are able to sense different physical parameters. An underwater mine detection systems which considers image processing techniques to localize the mines have been proposed in [23].
- Military: Route surveys, mission coordination, transferring data, controlling assets, securing submarines, and ports. The US military has recently launched a project named 'Ocean of things' worth 37 million US dollars which involves the development of intelligent underwater surveillance network with two major purposes: developing data processing techniques to get useful information and building efficient low-cost underwater sensors [24].
- Disaster prevention (Earthquake, volcano, tsunami, floods, oil spills): Investigating seaquakes, monitoring underwater earthquakes and volcanoes is very important otherwise it can result to immense destruction. In [25], an efficient architecture of underwater sensor network utilizing seismic pressure to detect and transmit the information to the surface station was presented.

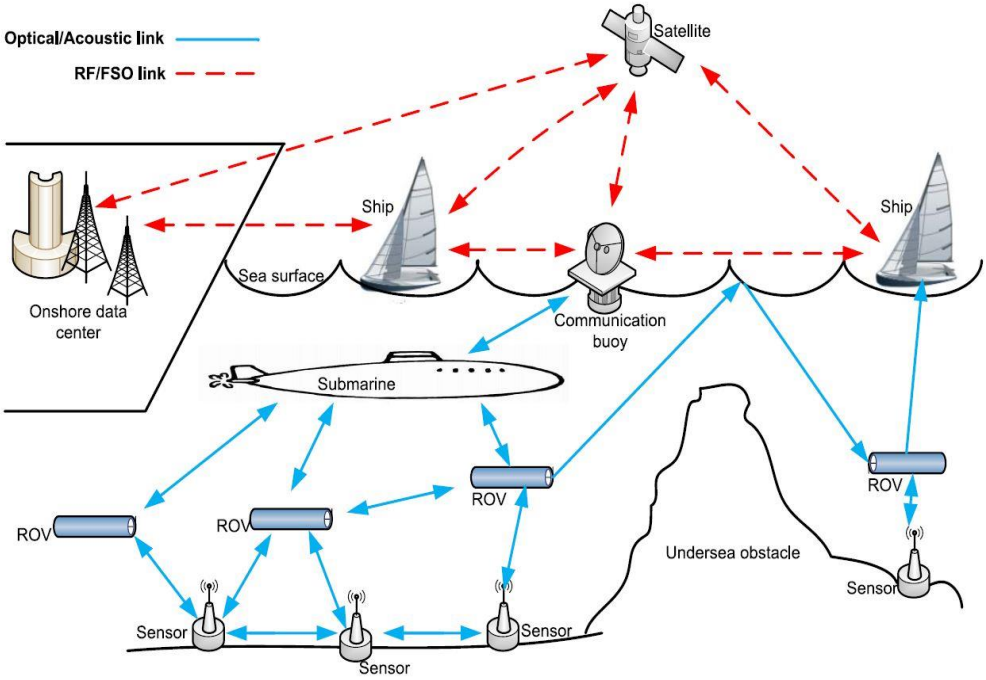

Fig. 1.2: Concept of UWSNs [13]

1.3 Motivations and Aims

Inspired by the significant advantages that UOWC can provide, researchers in both the industry and academia have contributed in exploring the underwater world. But as strange as it may seem, the underwater domain has not been given the required attention needed compared to other planets. A total of twelve astronauts have walked on the moon as of today whereas only three men have reached the challenger deep in the pacific ocean with a depth of approximately 10900 meters (Don Walsh and Jacques Piccard manned the *Trieste* in 1960, James Cameron with the *Deepsea Challenger* in 2012). UOWC is of great interest as mentioned in the applications section, the aforementioned devices (AUVs and ROVs) are capable of performing tasks at a depth inaccessible to divers due to the danger and risk associated deep down in the underwater world. These devices can go there and accomplish advanced projects. Recently, a humanoid robot built from Stanford university with a haptic feedback system [26] known as Ocean One was used to recover a vase from a ship that sunk in 1664 by a team of deep sea archaeologists. Also, collection and

analysis of data and information from the Earth's Ocean using wireless carriers and in real time with tsunami warning systems, pollution monitoring and many other commercial, scientific and defence applications.

The UOWC technology can be tailored to customer needs in order to successfully perform and deliver the specific required tasks, for example inspecting oil pipelines for the oil and gas industry, exploration and thermal imaging applications in areas that are difficult and too risky to be reached by a diver. Specific unmanned vehicles could also offer the feasibility to carry out specific required tasks for repairing and maintaining the integrity of underwater pipeline networks, among others.

UOWC is still a maturing field and various aspect of work and research within it have focused on understanding the channel to understand and develop UOWC systems. The majority of UOWC work to date has concentrated on the case when there is a clear path between the transmitter and the detector, the line-of-sight (LOS) configuration [27] because it is the simplest and assume an unobstructed connection between the transmitter and receiver. In practical scenarios, LOS communication links are not always possible due to obstructions from sea creatures, bubbles, large suspended particles and features of the seabed, especially in coastal and turbid water environments. LOS links are also unsuitable when the transmitter and receiver are non-stationary nodes [28]. Thus, non-LOS (NLOS) UOWC techniques are needed to fully explore the underwater channel but very little work has been reported so far regarding it. Details of the link configurations will be given in chapter two. So, this thesis concentrates mainly on the NLOS UOWC channel and its performance and as such the overall aim of this research is to investigate methods to design and simulate a UOWC system using approaches such as orthogonal frequency-division multiplexing (OFDM). Using a suitable channel model, bit error rate (BER) performance will be considered and numerical simulations carried out in the Matrix Laboratory (MATLAB) software.

This research has the following objectives in order to achieve its aim:

- To review the state of the art of UOWC.
- To simulate NLOS UOWC and investigate its performances with respect to different modulation schemes.
- To model the impulse response for NLOS UOWC using different analytical models considering various scattering phase functions as well.
- To undertake a theoretical investigation and simulation of the performance of spatially diverse NLOS UOWC system taking into account all the degrading effects of the channel (absorption, scattering and turbulence).

1.4 Thesis Outline

In addition to the introductory and concluding chapters as chapter one and seven, this thesis is structured into five main chapters as outlined below.

Chapter two presents an overview of the state of the art including the history of underwater wireless communications, discussion on the physical carriers used for underwater wireless communications, different link configurations used in UOWC and UOWC system design with some highlights of the contributions and related works by other researchers.

Chapter three discusses the physics of light in the underwater environment, the optical properties of the ocean including absorption and scattering as the two main causes of light attenuation in water. In addition to that, channel modelling schemes are also presented which includes the widely used Beer Lambert's law and its limitation, the main equation that describes the behaviour of light underwater: the Radiative transfer equation (RTE) is highlighted and methods of solving it with the respective complexities and the advantages and disadvantages of the methods. Finally, the underwater channel disruption is briefly discussed. The majority of the work in chapter two and three are published in [29].

Chapter four focuses on the numerical channel modelling technique: MC simulation used in this thesis, its principles and theories are discussed highlighting its advantages and disadvantages compared with the analytical

and experimental method. The details of the mathematical equations used in modelling the UOWC channel are described. In addition to that, simulation of the performance of NLOS UOWC links with multiple scattering using MC method using different modulation scheme and including variation in the receiver FOV is carried out with the presentation of the results and discussions. Partial publication of this chapter can be found in [30] with its extended version in [31].

In chapter five, the temporal dispersion of NLOS UOWC links as a result of the effects of multiple scattering in coastal and harbour water environments have been investigated. Different scattering phase function models, namely the (Henyey Greenstein) HG function, Two-term HG function and the Fournier-Forand phase (FFP) function are considered. The channel impulse response is then modelled using Double-Gamma function (DGF) and weighted DGF for NLOS UOWC links in coastal and harbour water and the chapter concludes with the presentation of results and discussions. This chapter is associated with [32] published paper.

Chapter six focuses on the performance studies of MIMO NLOS UOWC employing continuous phase modulation (CPM). All the degrading effects of the channel (absorption, scattering and turbulence) are included. The fading statistics of the channel are presented, the MIMO system architecture is also given, spatial diversity is used to mitigate the turbulence induced fading. This chapter proceeds to BER analysis and modelling and finally concludes with presentation of results and discussions. [33] is associated with this chapter.

Lastly, conclusions and highlights of future perspective of this thesis are summarized in chapter seven.

CHAPTER 2

Overview of the State of the Art

Underwater wireless communication (UWC) encompasses the transmission of data in an unguided water medium using wireless carriers, namely acoustic, radio frequency (RF) and optical waves. UWC is of great interest to the military, industry and the scientific community as a whole, due to its numerous applications that include exploration for environmental monitoring and natural resource discovery. In comparison to RF and the incumbent acoustic technology, Underwater optical wireless communications (UOWC) can provide a much higher data rate, higher bandwidths and reduced latency. A background on UOWC will be presented in this chapter which includes a brief history of UWC, physical carriers used for UWC systems highlighting their advantages and disadvantages, and UOWC link configurations. A review on UOWC system components, modulation, channel coding schemes is also carried out, concluding with experimental work and prototypes.

2.1 History of Underwater Wireless Communications

Almost 97% of the water covering the earth is in the form of Oceans according to the most current study by the national atmospheric and oceanic administration of the united states [34]. The early oceanography study dates back thousands of years, involving the acquisition of knowledge of ocean currents, waves and tides. However, the British government were the first to announce an expedition to undertake proper scientific investigation of the oceans in the late 18th century. Results of this particular expedition titled *"Report Of The Scientific Results of the Exploring Voyage of H.M.S. Challenger during the years 1873-76"* [35] were published in 1882. Following that, numerous books have been published on modern oceanography including *"The Oceans* [36]*", "The Sea* [37]*", "The depths of the oceans* [38]*", "Encyclopedia of Oceanography* [39]*", "Handbuch der Ozeanographie* [40]*", and "Geography of the oceans* [41]*".* The ocean

represents one of the ultimate frontiers for exploration, science, and technology. There has been a growing interest in ocean exploration system research in recent years due to the increasing global climate change and resource depletion [42]. UWC technology, the transmission of data in a random water environment by wireless carriers, attracts much attention as it enables the realization of ocean exploration systems. The physical carriers used are radio frequency (RF), acoustic and optical waves which will be discussed briefly in section 2.2.

Since the RF and acoustic methods have limited bandwidth, the use of optical wireless as the carrier has become a viable and attractive alternative for high capacity underwater data communication. In fact, for thousands of years light has been used as a wireless communications method in different forms. For example, around 1000 BC, the ancient Chinese used beacon towers to pass military information. The ancient Roman and Greek armies around 800 BC used reflects sunlight for signalling purpose using polished shields. Alexander Graham Bell used sunlight as a transmission medium to develop a wireless telephone system in 1880 regarded as the world's first optoelectronic communication system [43]. The invention of lasers in the 1960s as an optical source changed the future of optical wireless communication systems.

The relative recency is the most surprising about the history of UWC. The first demonstration of acoustic underwater systems was around world war I with influence from the use of submarines and underwater mines. The first scientific paper on acoustics underwater was published in 1919 describing sound waves refraction theoretically by salinity and temperature gradients in the ocean [44]. Since then, the fundamental understanding of propagation of acoustic technology has increased and the urgency to use the technology in world war II began comprehensive research in acoustic underwater communication.

The development of optical propagation models of the ocean began in the 60s and 70s. Various research groups around the world such as Duntley in 1971 [45], Preisendorfer in 1976 [46] and Jerlov in 1976 [47] developed the

instruments to measure the propagation of light underwater and interpreted it's consequences with respect to imaging underwater and ocean oxygen production. After the invention of laser devices, some members of the defence research community envisioned underwater laser-based communication system [9]. However, there were no practical demonstrations of underwater optical wireless communications at that time because of the limitations in existing blue/green laser technology.

Throughout the 20th century, acoustics remained the leading technology, its development was largely driven by the cold war after world war II. This resulted in advances in the practical and theoretical understanding of the acoustics underwater technology promoted by computer-based methods. The applications of underwater acoustic technology began to diversify expanding into sensor networks and environmental monitoring against the advances in warfare driving technology. In the 90s, the bandwidth requirements for these applications evolved in correspondence with a prospering in terrestrial wireless communication trends. As a result, both the terrestrial and the underwater applications were looking for wireless technology capable of offering higher capacity by the millennium.

Optical wireless communications came as a popular solution to high bandwidth wireless communications. Developments in optical transmitters especially that of high-powered LEDs and lasers technology in the early 2000s within the visible spectrum [48] meant that the optical underwater systems conceived in the late 70s became practically feasible. This leads to the revival of underwater wireless optical communication research pioneered by studies such as in [49] and [50] where the new generation of ROVs and AUVs formed the foundation of applications. The union of wireless optical communications with autonomous submersible vehicle technology meant that with minimal human intervention, substantial amounts of data and information could be sent and collected typically for the purpose of applications such as environmental studies, defence and mapping. Autonomous underwater submersible vehicles technology has significantly advanced over the past 15 years whilst the developments in

wireless underwater optical communication systems have been gradual with link length and capacity increasing slowly. Recently, there has been progress towards commercialization, as discussed by Zeng *et al.* [14]. Of particular note are the Ambalux system, which can provide a 10 Mbps data rate over a range of 40 m, the Sonardyne BlueComm system that offers 20 Mbps over a distance of 200 m and tele-submarine developed by Penguin Automated System Inc. providing data rates of up to 100 Mbps.

2.2 Physical carriers for UWC

This section intends to give a brief overview of all the primary physical carriers that are used for underwater wireless communication system. These are RF, Acoustic and Optical waves.

2.2.1 RF waves

RF waves are defined as waves with a frequency of less than 300 GHz. The use of such waves in UWC can be seen an expansion of terrestrial RF communication. It offers two major advantages when compared to optical and acoustic waves. First, the passage of RF through air/water interfaces is relatively seamless, which can be used to accomplish cross-boundary communication integrating terrestrial and underwater RF communication systems. Secondly, the RF approach is more tolerant to turbidity and water turbulence [51]. However, the short RF link range is a drastic limitation that hinders the development of the underwater RF system. RF waves in seawater can only propagate a few meters at an extremely low frequency (ELF) i.e.30 – 300 Hz due to the conductive nature of the transmission medium (since seawater contains substantial quantities of salt) [52]. RF frequencies in MHz range can propagate a distance of up to 100 m in seawater by using dipole radiation with high transmission powers in the order of 100 W, as reported in [52] but it requires this high transmission power and sophisticated antenna designs.

In 1968, the pioneer ELF project was developed for communication between deeply submerged naval submarines [53] where terrestrial radio

links with an alerting system was used to call the naval submarines to the surface for high bandwidth communication. In [54], an experiment for a Wi-Fi network using 700 MHz, 2.4 GHz, and 5 GHz was demonstrated in fresh water for its applicability in underwater communication. It was shown that at 700 MHz, the system is capable of providing long distance communication but with low data rates (5 m with bit rates of up to 550 kbps) while high data rates can be achieved at 2.4 and 5 GHz but at short ranges (a few centimetres) as the path loss in water increases as the propagation distance increases. An experimental measurement was performed by Lloret in [55] using 2.4 GHz in the unlicensed Industrial, scientific and medicine (ISM) band using the binary phase shift keying (BPSK) and quadrature phase shift keying (QPSK) modulation schemes in an underwater environment where they covered a distance of 16 cm. The authors in [56] compare RF and acoustic communication technology where maximum propagation distances were given for several frequency ranges (22 m at 1 kHz, 16 m at 10 kHz and 6m at 100 kHz). MIMO schemes can be used to improve the data rate of RF underwater communications as reported in [57] where four transmit antennas using the QPSK modulation scheme were shown to be capable of transmitting 48 kbps over a 2 km distance at 23 kHz bandwidth. In [58], towed antenna system was shown to allow real-time communication with autonomous unmanned undersea vehicle (UUV). An experimental model for underwater communications in fresh water using EM waves in the 2.4 GHz ISM frequency band was presented in [55]. The propagation characteristics of high frequency RF in seawater was discussed in [59] where the simulated result has been experimentally validated by comparing the computed available range against the measured data based on water tank test. Re-evaluating the role of EM signals in underwater environments was presented in [51].

2.2.2 Acoustic waves

The most established technology uses acoustic waves, presently responsible for most underwater wireless communications due to their relatively low

absorption and consequent ability to cover long distances. Acoustic technology is also used in navigation, positioning and imaging apart from being used in communication systems but the acoustic approach also has certain limitations. The transmission data rate is relatively low (kbps) since the typical frequencies associated with it are between tens of Hz and hundreds of kHz, which is generally insufficient for video transmission [52]. Acoustic links also suffer from severe communication delays due to the slow propagation of sound waves in water; moreover, acoustic transceivers are generally costly, bulky and consume much energy, making them uneconomical in the large scale implementation of underwater wireless sensor networks [60]. Acoustic communication technology can also distress marine life such as whales and dolphins that uses sound waves for navigation [61].

Many researchers have developed methods for channel estimation and have designed different algorithms to achieve more effective underwater communications using acoustic waves over the years as in [39] [62]. The orthogonal frequency division multiplexing (OFDM) approach has also been used to achieve high data rates in underwater acoustic communications [63] [64].

2.2.3 Optical waves

Underwater wireless communications using optical waves offers higher achievable data rates in the order of Gbps, immunity to latency due to the high speed of light in water, higher communication security thanks to the omnidirectional nature of light, more energy efficient and has the lowest implementation cost than the RF and Acoustic methods [65]. The high-speed benefit of the optical waves will guarantee the realization of numerous real-time applications for example underwater video transmission. However optical signals in underwater environment are subjected to extreme challenges due to water absorption and scattering caused by suspended particles.

In many publications, various experimental and theoretical studies have been carried out to characterize the behavior of light under the water providing evidence of high capacity transmission over moderate distances [66] [67] [68]. The first experimental work was demonstrated in 1992 using a 514 nm laser (argon-ion) for 50 Mbps over a 9 m distance [4]. In [69] a 10 Mbps data rate at 20 m optical communication underwater was achieved using LED based theoretical analysis. The work was later extended to over 25 m in [50]. In [70] laboratory work was carried out to achieve a 1 Gbps communication using a laser source over a 2 m range. The authors in [13] presented unidirectional optical wireless links for an underwater sensor network capable of sending 320 kbps data up to a distance of 2 m. Later, in 2006 an underwater optical communication link was tested for seafloor observatories using LED based system [71].

Table 2.1 summarizes the advantages and disadvantages of the physical carriers used for UWC. However, implementing UOWC is not a trivial issue because optical signals in the underwater environment are subjected to extreme challenges due to water absorption and scattering caused by suspended particles, link misalignment of the transceivers in addition to the need for reliable underwater devices which will all be discussed in chapter three.

Table 2.1: Comparison of UWC technologies.

Carrier	**Advantages**	**Disadvantages**
RF	➢ Tolerance of turbidity. ➢ Lenient pointing requirements. ➢ Easily crosses air ↔ water. ➢ Moderate transmission rate (Mbps).	➢ Short link range at ELF. ➢ Energy consuming devices. ➢ Costly and Bulky (large transmission antenna).

Acoustic	➢ Long range (typically several km). ➢ Most mature UWC technology. ➢ Low absorption.	➢ High Latency. ➢ Low transmission rate (kbps). ➢ Requires high power. ➢ Possible harm to marine life. ➢ Transceivers are costly, bulky and high power.
Optical	➢ High transmission data rates (Gbps). ➢ Immune to latency. ➢ Better security. ➢ Low cost. ➢ Small volume transceivers. ➢ Energy Efficient. ➢ Low transmission power.	➢ Suffers from attenuation. ➢ Can be scattered. ➢ Line-of-sight can be blocked. ➢ Moderate link range (10 m to 100 m typically).

2.3 UOWC Link Configurations

Fig. 2.1 shows the four basic types of underwater optical link configuration: point-to-point line of sight (LOS), diffused LOS, retroreflector and non-line of sight (NLOS) links, which will now be described.

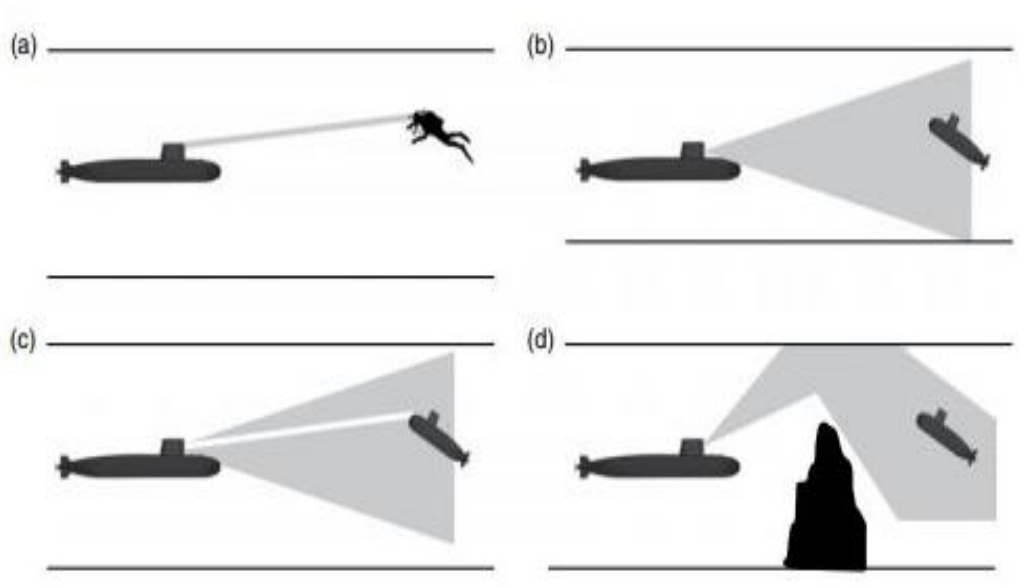

Fig. 2.1: Four UOWC link configurations: (a) point to point LOS; (b) diffused LOS; (c) retro-reflector; (d) NLOS. [28].

2.3.1 Point-to-point LOS

This is the simplest and most widely used link configuration in UOWC connection [72], in which there is an unobstructed path between the transmitter and the receiver. Its disadvantage is that it requires precise pointing between the transmitter and receiver, limiting UOWC performance in turbulent water and posing a problem for non-stationary nodes such as ROVs and AUVs [28]. The received power of the signal in a LOS link configuration is given as [72]:

$$P_{R\_LOS} = P_T \eta_R \eta_T L_P \left(\lambda, \frac{d}{\cos\theta}\right) \frac{A_R \cos\theta}{2\pi d^2 (1-\cos\theta_d)} \qquad (2.1)$$

where $P_T, \eta_T, \eta_R, L_p, d, \theta, A_R, \theta_d$ are the average optical power of the transmitter, optical efficiency of the transmitter, optical efficiency of the receiver, the propagation loss factor, the perpendicular distance between the transmitter and receiver plane, the angle between the perpendicular to the receiver plane, the receiver aperture area, and laser beam divergence angle respectively.

A 10 Mbps LOS link of up to 40 m on different water types, discussed in [4] has been demonstrated using a range of modulation techniques, namely QPSK, BPSK, 8-PSK and 32-quadrature amplitude modulation (32-QAM) in a laboratory environment. A 70 MHz carrier was employed with a 3W solid state laser and 5 Mbps achieved even in turbid water. Back scatter suppression in a LOS link was presented by Cox *et al.* in [73] using polarization shift keying along with channel coding.

2.3.2 Diffused LOS

This configuration employs different light sources with large divergence angles such as high-powered LEDs to accomplish broadcasting from one node to multiple nodes. However, its disadvantage compared to point-to-point LOS is that it suffers from aquatic attenuation because of the large intersection area with water. Lower data rates and relatively short communication distances are the two main drawbacks of this configuration [14].

2.3.3 Retroreflector Links

In this arrangement, a passive reflection device is employed at one end. This makes it suitable for duplex UOWC systems with the UW sensor nodes having limited weight and power budgets. Since the optical signal goes through the channel twice, additional attenuation will be experienced by the received signal [14]. The received power in this configuration is given as:

$$P_{R\_RETRO} = P_T \eta_R \eta_T \eta_{RETRO} L_P \left(\lambda, \frac{d}{\cos\theta}\right) \frac{A_{RETRO} \cos\theta}{2\pi d^2 (1 - \cos\theta_d)} \times \left[\frac{A_R \cos\theta}{\pi (d \tan\theta_{RETRO})^2}\right] \quad (2.2)$$

where $\eta_{RETRO,} A_{RETRO}, \theta_{RETRO}$ are the optical efficiency of the retroreflector, retroreflector aperture area, divergence angle of the retroreflector and other parameters are defined above in (2.1).

The retroreflector link configuration is prone to the unwanted backscattered light that will increase the receiver noise level [74]. The authors in [75] use a polarization discrimination technique to solve the

interference problem in this link geometry. Performance analysis of different configuration link types was performed in [14] and the modulating retroreflector was observed to be the most affected by the water turbidity.

2.3.4 NLOS Links

Here, the transmitter projects the light beam to the sea surface with an incident angle greater than the critical angle so that total internal reflection is experienced by the beam [76]. NLOS links can be achieved by using arrays of high divergence transmitter sources such as LEDs or by intentionally diverging the transmit beam. Such links do not require strict tracking and pointing especially in turbid water environments in contrast to LOS links, which require very strict pointing and tracking system also with a significant risk of beam blockage due to underwater suspended particles, bubbles and marine life. NLOS is a more realistic approach to designing practical systems and greater understanding of UW channels. The majority of the work in this thesis focuses on NLOS links. In [77]and [30] the effect of multi-scattering in NLOS is studied. Baiden built a spherical transmitter using 100s of LEDs with a FOV of 120^{o} capable of video transmission at 1.5 Mbps at 15 m in a turbid lake water environment [77]. The performance of NLOS UOWC using different modulation techniques was presented in [30] with full details of the work given in chapter four of this thesis. This work was extended to modelling the impulse response in a NLOS link configuration in [32] with details in chapter five.

2.4 UOWC System Components

This section briefly discusses the main components of UOWC systems, i.e. transmitters, receivers, modulation and error correction coding.

2.4.1 Transmitters

Lasers or LEDs are used as sources, with the former preferred in deep clear ocean water and the latter for shallow water [4]. In both cases, the blue-green area of the spectrum is used, where output powers from 10 mW to 10 W are available [4]. Both source types have advantages and disadvantages for UOWC systems. LEDs are simple, cheap, more reliable,

less temperature dependent and less susceptible to underwater effects due to their large viewing angles; however, their link range is very limited due to their omnidirectional coverage and incoherent optical beam. Lasers have high optical power, fast switching times and have been demonstrated for low latencies, long ranges, and high data rates due to their large modulation bandwidth. In [9], the first duplex laser communication between aircraft and submarines was discussed. Giuliano [78] discusses the two technologies further (where LEDs are favoured due to their portability, low cost and versatility) and provides further references for both in UOWC systems.

2.4.2 Receivers

The main devices that have been employed in UOWC receivers are photomultiplier tubes (PMTs), PIN diodes and avalanche photodiodes (APDs) plus biologically inspired quantum photo-sensors. The receiver should have high gain, possess a wide field of view (FOV) and provide a high signal to noise ratio (SNR). A PMT is characterized by low noise, high gain, large collection area and good high-frequency response. However, it is a poor choice for UOWC owing to its large size, fragility and high power consumption. Omnidirectional transmission and reception of optical signals over a 100 m range at 1 Mbps using a PMT was, however, presented in [79]. A PIN photodiode offers low cost and a fast response time with unity gain whereas an APD is potentially even faster with a large internal gain. In [80], three different models (short, hybrid and long propagation ranges) were investigated using APD and PIN receivers. It was shown that APDs are good for long ranges and PIN photodiodes for short and hybrid ranges. Biologically inspired quantum photo-sensors are potential highly efficient candidates for UOWC. Research is underway to develop these devices for underwater operation [81].

2.4.3 Modulation

It is possible to employ direct or external modulation, with the former being simpler but suffering from frequency chirp when using lasers that limits UOWC link range and data rate. In [82], a directly modulated blue laser was

used to demonstrate transmission at 4.8 Gbps over 5.4 m of tap water using 16 QAM orthogonal frequency-division multiplexing (OFDM). External modulation of lasers requires relatively high drive currents and has a limited modulation range. A 1 Gbps underwater optical link was established in [70] using an externally modulated laser operating at 532nm. In UOWC, modulation is classified as per optical communications in general into two broad types: intensity modulation (IM) or coherent modulation (CM) [4].

The IM scheme entails the modulation of light intensity by a direct or external modulator. If the receiver demodulates the intensity modulated signal using direct detection (DD), then the overall scheme is known as IM/DD or non-coherent transmission. IM/DD is the most widely used scheme in UOWC due to its simplicity and low cost as no phase information is required. Common IM schemes are ON/OFF keying (OOK), pulse position modulation (PPM), pulse width modulation (PWM), and digital pulse interval modulation (DPIM). The simplest scheme is OOK, where the presence and absence of light represent bits “1” and “0”. It is the most popular and practical method due to its low power consumption, simplicity and bandwidth efficiency. The UOWC OOK scheme has been theoretically and experimentally studied, inter alia, in [83] and [84]. PPM provides spectral efficiency and power but at the expense of more sophisticated transceiver; it has been studied analytically and experimentally for UOWC in [85] and [86]. PWM has the advantages of spectral efficiency as well as immunity to ISI effects [87]. DPIM provides higher power and spectral efficiency but suffers from error propagation in the demodulation process; its applications in UOWC are studied in [88] and [89].

In CM, a local oscillator down converts the optical carrier to baseband (homodyne detection) or an RF intermediate frequency (as heterodyne detection) at the receiver side. Thus, CM makes use of both amplitude and phase information so may use schemes such as BPSK, QPSK, QAM plus polarization shift keying. It can provide higher spectral efficiency, higher receiver sensitivity, good immunity to noise and is robust but with further complexity and extra cost. Cochenour *et al.* [90] implemented short range

UOWC links in turbid water employing BPSK, QPSK, 8-PSK, 16-QAM, and 32-QAM. Their results show an upgrade from an initial rate of 1 Mbps using BPSK to 5 Mbps by adopting 32-QAM in a 3.6 m water tank. More studies of UOWC using CM can be seen in references [73] and [91]. A comparison of IM and CM techniques was presented in [92], where it was shown that differential PSK (DPSK) was best in terms of BER performance.

2.4.4 UOWC channel coding

The absorption and scattering present in the underwater channel cause considerable degradation of the optical signal as mentioned in the previous chapter. This means that error control coding may be used to improve link performance. The addition of redundant bits to the transmitted signal is well established as a method to enable a receiver to correct a definite number of errors in FEC schemes. FEC channel coding techniques such as turbo, Reed Solomon (RS), low density parity check (LDPC), convolutional, cyclic redundancy check (CRC) and Bose-Chaudhuri-Hockenheim (BCH) can be implemented to reduce the effect of attenuation in UOWC systems [93]. A properly designed FEC coding scheme improves the link range and power efficiency of the UOWC system but at the expense of reducing the bandwidth efficiency.

In general, FEC codes can be divided into block codes and convolutional codes. RS, BCH, and cyclic redundancy (CRC) codes are the block codes implemented in UOWC system. The first block code to be implemented in UOWC was RS (255, 199) [94]. In [93], RS and BCH codes were evaluated for underwater optical communications and it was shown that RS codes gives better performance than BCH codes. The simulated result shows that a (172, 85) coding scheme has a better performance than a (255, 207) coding scheme. It was also shown that an SNR improvement of 4 dB was achieved using RS codes in comparison with uncoded systems but there was a cost in terms of data rate. Block codes are not capable of providing the optimal performance for UOWC links especially in highly turbid water environment where there is strong interference even though they are simple, robust and

easy to implement. Thus, more powerful convolutional codes such as LDPC and Turbo codes are employed which can provide an error performance close to the Shannon limit [87]. The performance of RS, LPDC, and Turbo codes was demonstrated both theoretically and experimentally by Everett [95], whose provides an extremely comprehensive description of FEC coding implementation techniques in UOWC.

2.5 Prototypes and Experimental Work

Several experiments and prototypes have been realized over the years to characterize the underwater wireless optical channel, to study the effect of coding or modulation schemes and to investigate the implementation difficulties of UOWC links. Recently, commercial products have emerged including the 10 Mbps, 40 m system from Ambalux, a tele-submarine built using 70 LEDs per plate holding a 120 degree field of view (FOV) developed by Penguin Automated System Inc. providing data rates of up to 100 Mbps and the 2010 20 Mbps 200 m BlueComm system from Sonardyne referred to in chapter one. The latter has continued to develop the BlueComm range, culminating in the BlueComm5000 link [11]. This has been designed to deliver an upload data rate of 600 Mbps from seabed nodes and 200 Mbps downloads. It is designed to be mounted on ROVs and AUVs autonomously travelling from one node to another in order to harvest large quantities of data as illustrated schematically in Fig. 2.2 [11].

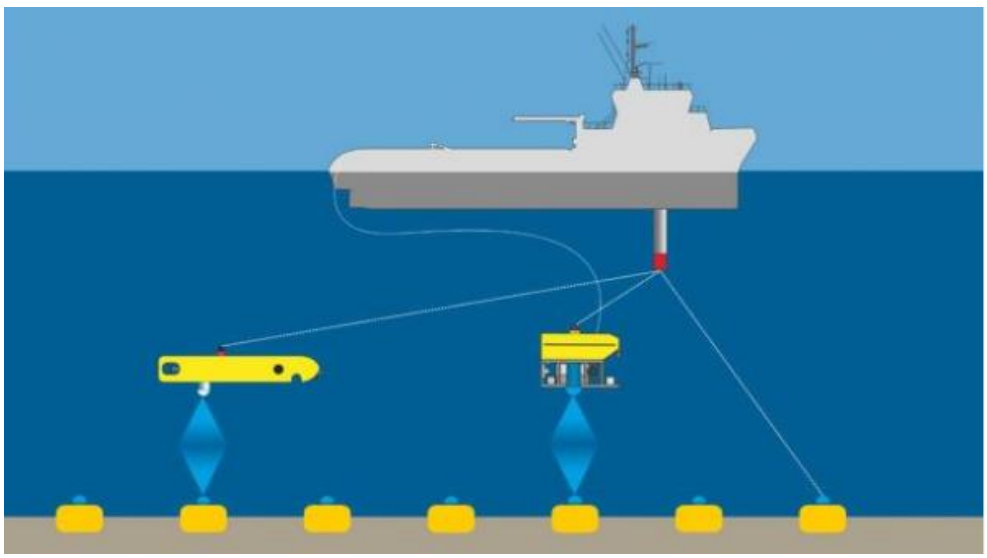

Fig. 2.2: Sonardyne BlueComm5000 Configuration [83]

Snow *et al.* [96] demonstrated the first experimental work using an argon-ion laser diode transmitting at a wavelength of 514-532 nm to send 50 Mbps signals over a 9 m link length. Hanson and Radic [70] used a high-speed transceiver to increase the achievable data rate to 1 Gbps but the distance was limited to a 2 m test tank in one of the first successful laboratory experiments for high rate UOWC. A data rate of 10 Mbps over 100 m laser based links was obtained at Woods Hole Oceanography Institution [97]. The use of a sphere that houses a photomultiplier tube was proposed in [98] to improve the alignment sensitivity achieved in [71]. This delivered a data rate of 5 Mbps over a 200 m link in clear water and 1 Mbps in turbid water. A group of researchers from the University of Yamanashi have transmitted a 1.45 Gbps IM/DD OFDM signals successfully over a 4.8 m range [99]. A series of experimental research was conducted at the University of Genoa, Italy by Anguita and team as demonstrated in [100] where a prototype of UOWC was developed achieving 100 kbps at a range of 1.8 m by adapting the current technology available for UWSNs. Further work was taken by the same research group building an LED omnidirectional transmitter and designing the hardware architecture using HDL (Hardware Description Language). This system was tested for underwater LOS communication paving ways for omnidirectional transmitters [101].

The AquaOptical modem designed and built by Massachusetts Institute of Technology (MIT) was one of the first UOWC prototypes to be realized and comprised three types of the modem (short range, long range and hybrid) to achieve a data rate of 1.2 Mbps in clear water [80]. An improved version (AquaOptical II) offered higher data rates with increased transmission ranges and the capability to control an autonomous underwater robot [88]. The system was also utilized to validate an end-to-end UOWC model [102]. Work at MIT also produced a prototype AUV system referred to as autonomous modular optical underwater robot (AMOUR) to perform tasks such as surveillance, underwater monitoring and exploration [103]. Then, an upgraded version of AMOUR was demonstrated in [89] to achieve real-time control link with higher data rates. The impact of spatial diversity in a

turbid water medium has been investigated using a two transmitter and a two receiver UOWC system [104]. The water turbulence was created by the injection of bubbles and beam splitter was used to generate parallel optical beams. The results showed that spatial diversity helps to mitigate fading-induced errors by a factor of ten. The same team of Simpson *et al.* then developed a novel smart transmitter and receiver [105]. The transmitter can estimate the condition of the water according to the backscattered light captured by the smart receiver and then can take several actions based on the specific water conditions.

Researchers at North Carolina University have conducted experiments in developing Laser/LED based UOWC system, investigating the performance of different links under different conditions. Chancey conducted an initial work building an UOWC system using a transmitter of 1 W LED and a photodetector as the receiver [106]. An UOWC system that can achieve a 1 Mbps capacity using laser-based transmitter and a PMT as the receiver using NRZ OOK modulation was developed in [107]. In [108], a similar data rate was achieved using LED-based transmitter and a photodetector receiver which is cheaper and smaller than the laser based system in [107]. An UOWC system that utilized a high-powered blue LED transmitter and a photodiode receiver was developed by Brundage [109], achieving a 3 Mbps data transmission rate over a 13 m long water tank. Other recent LED-based experimental UOWC systems can be found in [110] and [111]. A non-return-to-zero(NRZ)-OOK system was reported by Oubei *et al.* [112] using a 520 nm laser diode transmitter and APD receiver, operating at a data rate of up to 2.3 Gbps over 7 m. This work was extended by using 16-QAM-OFDM with a laser diode source to deliver a record rate of 4.8 Gbps in a 5.4 m water tank [82]. Research efforts have also focused on the transmission of a laser source to study the temporal and spatial dispersion effects of UOWC over different water conditions, coding schemes and modulation methods [104] [113] [114]. Most recently, a 100 Mbps full duplex UOWC was experimentally demonstrated using two pairs of low-cost laser diode transmitters and PIN diode receivers [115]. The communication

performance of six different types of sea water was quantitatively and qualitatively analyzed in the experiment.

2.6 Conclusion

This chapter started with a brief history of UWC, followed by an introduction to the various physical carriers that can be used for UWC. There are demands for increased UWC capabilities as a result of the increasing numbers of unmanned vehicles such as ROVs and AUVs coupled with a more general need for high speed and high data rates for many underwater applications. The incumbent acoustic transmission methods are well-established but cannot provide the necessary bandwidth and low latency. The absorption spectrum of water is such that RF signals must be at extremely low frequencies to propagate, which again constricts bandwidth. It is undesirable to have optical or copper cables connecting underwater vehicles since they limit both the range and flexibility of underwater operations. Thus, UOWC provides great potential and offers substantial future promise to underwater communications. This chapter also presented the different system configuration that can be implemented in UOWC design followed by a description of the main system components for UOWC. The chapter concluded with a review on the experimental works and prototypes for UOWC. The underwater optical links which is the physical carrier used in this thesis as well as the channel modeling schemes will be discussed in the next chapter.

CHAPTER 3

The Optical Underwater Channel

Understanding hydrological optics, which encompasses how light behaves in natural waters spanning from desert oases to deep oceans containing different particulate and dissolved matter is a key step in the study and design of underwater optical wireless communications. Thus, this chapter discusses in detail the background of the theory of the properties of light under the water; underwater optical beam propagation, important optical ocean constituents, challenges of the underwater channel as well as the channel modelling schemes.

3.1 Light and Energy

UOWC concerns visible light transmission via natural waters, where visible light refers to the radiation between 400 nm to 700 nm in the electromagnetic spectrum to which the human eye is sensitive. Hydrological optics is the science that universally describes the behavior of light in aquatic media. Light is well known for exhibiting properties both as photons (stream of particles) and as a wave [116]. Wave properties of the light such as wavelength and frequency can coexist with that of photon properties through the wave-particle duality of light. The photons travel and the wave propagates at a constant speed v_{vacuum} of value $2.998 \times 10^{8} ms^{-1}$ in a vacuum. This is related to other wave properties by

$$\lambda = v_{vacuum}/f \tag{3.1}$$

where λ is the wavelength while f is the wave frequency. The velocity of the photon decreases by $1/n$ when not in a vacuum, where n is the new medium refractive index through which the beam of light is traversing. In air, n has a value of 1.001 and is approximately 1.333 in water [117]. The wave frequency does not change according to the medium but the wavelength diminishes with the velocity of light by the relation in equation (3.1). Each photon has energy E measured in Joules J, dictated by the

frequency of the wave through the Planck-Einstein relation in the equation below.

$$E = hf = hv_{vacuum}/\lambda \quad (3.2)$$

where $h = 6.63 \times 10^{-34} Js^{-1}$ is Planck's constant.

Light and energy descriptions are explored in section 3.2 in terms of the interaction with the aquatic medium.

3.2 Light properties and the optical beam propagation in water

The underwater environment can be seen as dynamic and complex world consisting of water molecules, impurities such as organic and inorganic matter, suspended particles and dissolved particles [118]. The light interacts with all these underwater particles and is described using the optical properties of seawater. Understanding the propagation of light in water is challenging due to the difference in the fundamental components of the various water bodies and demands fundamental understanding of the physio-chemical underwater environment. For reliable UOWC design, it is necessary to understand the basic properties of the optical beam propagation in the underwater environment. These optical properties vary according to time of day, geographical location, temporal variations as well as organic and inorganic content.

3.2.1 Oceanic Optical Properties

The optical properties of water are divided into two groups [5]: inherent optical properties (IOPs) and apparent optical properties (AOPs). The former depend only on the composition of the medium and the particulate substances within it, whereas the latter depend on both the medium and the geometric illumination structure. The major IOPs are scattering coefficient, absorption coefficient, attenuation coefficient and volume scattering function; the main AOPs are irradiance, radiance, and reflectance. In UOWC, the IOPs have greater effect on the communication link performance and are generally used in determining the communication link budgets. So, they will be the focus of the coverage in this thesis and the details of the AOPs can be found in [5] [119] [120].

3.2.2 Inherent Optical Properties

When a beam of light is sent through a medium, the photon can change its direction and/or change its energy and this is a process known as scattering. The photon can disappear with its energy being converted to another form, such as chemical or heat. This phenomenon is known as Absorption. The IOPs can be derived mathematically as follows.

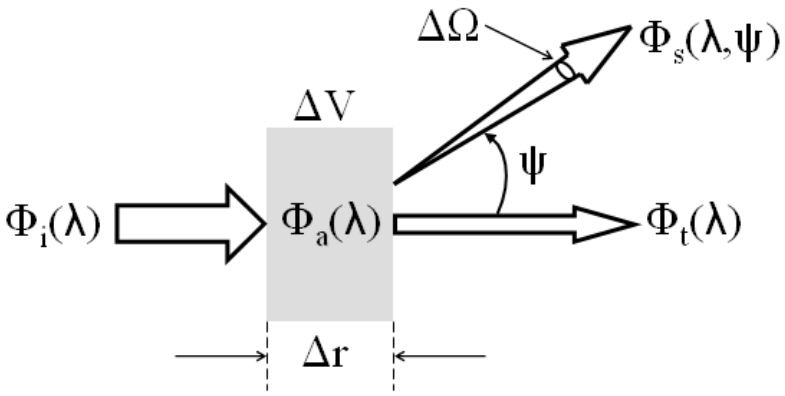

Fig. 3.1: IOP geometry [5]

The procedure begins with consideration of a small volume of water ΔV, thickness Δr, which is illuminated by a collimated beam of monochromatic light at some wavelength λ, of incident spectral radiant power, ϕ_{i}. A fraction of the incident power, ϕ_{a}, is absorbed within the volume of water and some part, ϕ_{s}, will be scattered out of the beam at an angle, ψ. The remaining power, ϕ_{t}, is transmitted through the water unaffected, so by conservation of energy:

$$\phi_i(\lambda) = \phi_a(\lambda) + \phi_s(\lambda) + \phi_t(\lambda) \tag{3.3}$$

The absorptance, $A(\lambda)$, is the ratio of the incident power to the absorbed power within the volume. Similarly, the scatterance, $B(\lambda)$, is the ratio of the incident power to the scattered power.

$$A(\lambda) = \phi_a(\lambda)/\phi_i(\lambda), B(\lambda) = \phi_s(\lambda)/\phi_i(\lambda) \tag{3.4}$$

It is more useful to describe (3.4) per unit distance in the medium by taking the limit as the thickness Δr approaches zero to give (3.5) and (3.6) as the absorption coefficient, $a(\lambda)$,and scattering coefficient, $b(\lambda)$.

$$a(\lambda) = \lim_{\Delta r \to 0} \Delta A(\lambda)/\Delta r = dA(\lambda)/dr \tag{3.5}$$

$$b(\lambda) = \lim_{\Delta r \to 0} \Delta B(\lambda)/\Delta r = dB(\lambda)/dr \tag{3.6}$$

The overall beam attenuation coefficient, $c(\lambda)$, is the combination of absorption and scattering coefficients.

$$c(\lambda) = a(\lambda) + b(\lambda) \tag{3.7}$$

The attenuation coefficient then has units of m^{-1}.

The angular scatterance $\beta(\psi, \lambda)$ per unit distance and unit solid angle is defined as

$$\beta(\psi, \lambda) = \lim_{\Delta r \to 0} \lim_{\Delta \Omega \to 0} \frac{B(\psi,\lambda)}{\Delta r \Delta \Omega} = \lim_{\Delta r \to 0} \lim_{\Delta \Omega \to 0} \frac{\phi_s(\psi,\lambda)}{\phi_i(\lambda) \Delta r \Delta \Omega} \tag{3.8}$$

$B(\psi, \lambda)$ is the fraction of the power scattered out of the beam through an angle ψ as illustrated in fig. 3.1 into a solid angle $\Delta\Omega$ centred on the angle ψ. ϕ_s is defined as $I_s(\psi, \lambda)\Delta\Omega$ which is the spectral power scattered into the solid angle. The incident irradiance $E_i(\lambda)$ is defined as $E_i(\lambda) = \theta_i(\lambda)/\Delta A$. Substituting the volume of the water ΔV, which equals $\Delta A \Delta r$, yields

$$\beta(\psi, \lambda) = \lim_{\Delta V \to 0} \frac{I_s(\psi,\lambda)}{E_i(\lambda) \Delta V} \tag{3.9}$$

The above equation can be interpreted as the scattered intensity per unit incident irradiance per unit volume of the water which is known as the volume scattering function (VSF), more details of which are given later in this chapter.

Integrating the VSF $\beta(\psi, \lambda)$over all directions gives the total scattered power per unit incident irradiance per unit volume of water:

$$b(\lambda) = \int \beta(\psi, \lambda) d\Omega = 2\pi \int_0^{\pi} \beta(\psi, \lambda) \sin\psi \, d\psi \tag{3.10}$$

The forward and backward scattering coefficients b_f and b_b can be defined by the equations below.

$$b_f(\lambda) = 2\pi \int_0^{\frac{\pi}{2}} \beta(\psi, \lambda) \sin\psi \, d\psi \tag{3.11}$$

$$b_b(\lambda) = 2\pi \int_{\frac{\pi}{2}}^{\pi} \beta(\psi, \lambda) \sin\psi \, d\psi \tag{3.12}$$

The scattering phase function (SPF) is found by normalizing the VSF with the scattering coefficient defined as

$$\tilde{\beta}(\psi, \lambda) = \frac{\beta(\psi,\lambda)}{b(\lambda)} \tag{3.13}$$

Physically the SPF can be understood as the probability that the photon will be scattered in the angular direction. More details of the SPF will also be in further sections of this chapter.

3.3 Optically Important Ocean Constituents

Substances contained in the aquatic medium are classified as either dissolved (with particle diameters $<0.4\mu m$) or particulate matter. The main optical components are [5]:

- Sea Water: Comprises of pure water and inorganic dissolved materials which are not surprisingly mostly salts with concentration given by their salinity.
- Particulate Organic Materials: these consists of phytoplankton, zooplankton and bacteria that grow and reproduce. The most optically important is the phytoplankton which are free floating, microscopic, single cell organisms which possesses chlorophyll pigment that allows them to harvest sunlight and produces energy through the process of photosynthesis and hence are primary producers and form the foundation of the oceanic food chain. The optical behaviour of the organic materials is generally approximated to that of chlorophyll since chlorophyll is the primary component of the phytoplankton affecting the optical properties.
- Dissolved Organic Material: this consist of decaying marine matter and broken-down plant tissue. It is a distinct yellow colour and also referred to as Gelbstoff (yellow substance) but more generally known as coloured dissolved organic matter (CDOM). It usually comes from matter within the water or surface run-off from nearby land and is thus mostly found in lakes, rivers and coastal areas. CDOM is a good indicator of biogeochemical processes in the ocean.
- Inorganic Particles: these consists of clays, sands, rocks that have been blown or washed from land into the ocean, as well as metal oxides and minerals. Unfortunately, the optical effect of these is not well documented.

The properties of different water bodies vary with the concentration of dissolved substances and geographical location. Generally, four different water types are considered in UOWC. These are:

- Pure seawater: Absorption is the main restricting factor here and it increases with increase in wavelength. Thus, the red light is attenuated more than the blue wavelength and that is why deep clear ocean water seems a rich blue in colour. The absorption in this kind of water is considered as the sum of the absorption in pure water in the absence of suspended particles and the absorption by salts in pure saltwater.
- Clear ocean: This type of water has a higher concentration of dissolved particles such as mineral components, dissolved salts, CDOM and so on. Based on Jerlov water types [121], they are further classified into type I-III depending on their geographical location and concentration of suspended particles.
- Coastal water: The effect of scattering and absorption is more in coastal ocean water because they have much more concentration of dissolved particles and hence increases the turbidity level.
- Turbid harbour water: This water type limits the propagation of optical beam due to high absorption and scattering because it has the highest concentration of suspended and dissolved particles.

The physical properties of the ocean water not only vary according to geographical location but also according to vertical depth and this is classified in [121] as:

· Euphotic zone: the topmost, near surface layer to a depth of 200 m in clear water.

· Dysphotic zone: the lower layer from a depth of 200 m to 1000 m.

· Aphotic zone: the region of darkness below the dysphotic zone.

Typical values for the absorption, scattering and attenuation coefficients in different locations are shown in Table 3.1 below [70].

Table 3.1: Water attenuation values [70].

Water Type	$a(\lambda)$, m^{-1}	$b(\lambda)$, m^{-1}	$c(\lambda)$, m^{-1}
Pure sea	0.053	0.003	0.056
Clear ocean	0.114	0.037	0.151
Coastal	0.179	0.220	0.399
Turbid	0.366	1.829	2.195

3.4 Challenges of the Channel

The main factors that affect UOWC are attenuation; turbulence; pointing and alignment; multipath interference; physical obstructions. The following sub-sections briefly discuss each of these.

3.4.1 Attenuation

As discussed in section 3.2.2, the two major factors that determine underwater light attenuation are absorption and scattering. Their impact can cause three undesirable effects to UOWC system design. Firstly, the total light propagation energy will diminish continuously due to absorption which will reduce the UOWC link distance. Secondly, scattering will result in a reduction of the number of photons collected by the detector, which degrades the system signal to noise ratio given the finite size of the receiver optical aperture. Thirdly, scattering may cause photons to arrive at the detector plane in different time slots, leading to dispersion.

Absorption

The absorption process is greatly dependent on the composition and concentration of the particles in the water and the coefficient of absorption $a(\lambda)$ is the combination of the coefficient of absorption of the various optical components as shown below [5]:

$$a(\lambda) = a_w(\lambda) + a_{ch}(\lambda) + a_{CDOM}(\lambda) + a(\lambda)_{det} \tag{3.14}$$

where $a_w(\lambda), a_{ch}(\lambda), a_{CDOM}(\lambda), a(\lambda)_{det}$ are the absorption coefficient of pure water, chlorophyll, coloured dissolved organic matter and due to detritus.

Scattering

Scattering occurs when the photon deviates from its original path due to the interaction with the particulate matter in the underwater world. There is a change in the propagation direction with no change in energy. The peak in ocean water scattering is in the forward direction with significant back scattering. The scattering in natural waters is divided into three categories according to Mobley [5] which are molecular scattering, scattering by large particles and turbulent scattering.

The scattering coefficient $b(\lambda)$ can be presented as summation of the scattering coefficients due to pure water, small particles and large particles as shown in the equation below.

$$b(\lambda) = b_w(\lambda) + C_s b_s(\lambda) + C_l b_l(\lambda) \tag{3.15}$$

Where $b_w(\lambda), b_s(\lambda)$ and $b_l(\lambda)$ are the scattering coefficient of pure water, small particles and large particles respectively. C_s and C_l are the total concentrations of small and large particles.

Single scattering albedo ω

This is defined as the ratio of the coefficient of scattering to the extinction (attenuation) coefficient as shown below [5].

$$\omega = \frac{b(\lambda)}{c(\lambda)} \tag{3.16}$$

In water where absorption dominates, the value of the albedo will be near zero and when scattering dominates the value will be near one. The scattering coefficient can be understood as the probability of the photon to be deflected (scattered) rather than being absorbed.

The effect of scattering on UOWC

In UOWC links, the impact of scattering can be explained by three components namely temporal, spatial and angular dispersion [122].

- Temporal dispersion occurs when the beam of light reaches the receiver at different times and this will cause time delay and a path difference which can limit the bandwidth of the communication [122] [123] [124].

- In Spatial dispersion, the photon density decreases at the receiver which is caused by spreading of the beam of light due to the process of multiple scattering. Photons that arrive the receiver are spatially dispersed for a diffuse beam due to the underwater environment and also due to its initial distribution [122] [123].
- Angular dispersion is simply the spread of the photon's angle of arrival due to the underwater scattering events. There is small angular dispersion in seawater because scattering typically occurs at small forward angles whereas the angular dispersion will show significant effects in turbid water where scattering dominates [125].

3.4.2 Turbulence

This is the random fluctuation in the refractive index of water (caused by variations in the salinity, density, and temperature of the ocean water), which greatly affects UOWC [126]. An important criterion used for the description of oceanic turbulence is the scintillation index (which depicts the variance of the wave intensity). This is expressed as the sum of the radial and longitudinal components when a Gaussian beam propagates through weak turbulence without taking into consideration the scattering event as described by Korotkova *et al*. [127].

3.4.3 Alignment

At relatively shallow depths the underwater environment is turbulent and so link misalignment will take place frequently. Pointing errors and misalignment result from two components, boresight and jitter [128]. The former describes the fixed displacement between the transmitter trajectory center and center of the receiver. The latter is the random dislocations of the beam center at the receiver plane. It should be noted that tight pointing specifications are required in pure sea water because of the likely collimated beam trajectory but the increased scattering in coastal and harbor water produces significant optical beam spreading relaxing the pointing and alignment requirements. Sanchez and McCormick [129] discuss the pointing requirements as a function of the light scattering function and the effect of

optical link misalignment in a 3.5 m length pool was analyzed experimentally by Gabriel *et al.* [130]. Serious connectivity loss problems may also be caused by the random movement of the sea surface [131]. To improve the pointing and alignment accuracy of a UOWC system, Simpson *et al.* [105] reported the use of smart transmitters and detectors.

3.4.4 Multipath Interference and dispersion

After an optical signal has encountered multiple scattering objects and/or multiple reflections from underwater bodies, multipath interference occurs in UOWC as in acoustic communications. This leads to waveform time dispersion and decreases the data rate due to inter-symbol interference (ISI). However, unlike acoustic communication, multipath effects are not significant due to the very large speed of light. Multipath interference can be more pronounced in shallow waters due to the reflections of the optical waves from the sea surface or bottom and obstacles in the environment, which can be ignored for deep oceans. To overcome the effect of interference in UOWC, methods such as equalization are used at the receiver [132]. The effects of channel time dispersion leading to ISI in UOWC have been considered in depth [70] [133], whilst the effect of ISI on a 25 m coastal water spatially diverse at 0.5 Gbps and 50 Gbps was conserved by Jamali and Salehi [83]. It was observed that spatial diversity helps in reducing multipath interference effect by providing some compensation for ISI degradation at low data rates but performance degrades for high data rates, especially for high signal to noise ratios.

3.4.5 Physical obstructions

Living organisms such as marine animals and schools of fish will cause temporary losses of signal at the detector since the light beam is very narrow. To ensure re-transmission of data when lost, the use of redundancy measures, signal processing and error correction techniques is required. For example, signal processing has been employed in a 1 Mbps UOWC system using light emitting diodes (LEDs) and photodiodes to improve the propagation range [108]. With respect to error correction, the most widely

used method underwater is forward error correction (FEC), which was discussed in the previous chapter. In error prone underwater networks, the use of hop-to-hop communication approach is also beneficial. In [134], the authors developed a multi-hop underwater optical communication system capable of supporting bandwidth up to 100 kHz over a 1 m communication range.

3.5 UOWC Channel Modelling Schemes

In this section, the channel modelling schemes for UOWC are briefly discussed, which include the Beer-lambert law, volume scattering function, radiative transfer equation, oceanic turbulence model, pointing errors and misalignment modelling.

3.5.1 Beer-Lambert's Law

As discussed earlier in this chapter, both absorption and scattering prevent a photon from reaching a receiver after passing through an underwater channel. These two processes are basically responsible for the decay of the transmitted power as the photon beam propagates through water. The most basic modelling scheme of IOPs encapsulates this power loss and it is combined with the *Beer-Lambert (BL)* law to give an expression for the received Intensity (in Wm^{-2}) in terms of the Intensity at the source (I_0) after a specified distance (z) [47]:

$$I = I_0 \exp[-c(\lambda)z] \tag{3.17}$$

The limitations of the BL law are:

- It only considers absorption and single scattering (in other words, it assumes that photons that undergo scattering are lost and not counted in the received energy).
- It is only valid for LOS links, where the transmitter and receiver are perfectly aligned so it cannot be used for NLOS links or any other geometry [123].

Many UOWC applies this model because of its simplicity and the BL has been used to evaluate the performance of UOWC system in different water types for different communication ranges, for example [49] and [50], where the

impact of environment variability such as refractive index variation with depth were considered.

3.5.2 Volume Scattering Function

The IOPs are not capable of predicting either the temporal or spatial dispersion by themselves and do not consider information about the system configuration such as the receiver field of view (FOV), but they are used as a basis for complex models of the channel. To derive the scattering coefficient, the concept of a volume function (VSF) must first be introduced. The VSF, $\beta(\lambda,\theta)$, describes the angular distribution of light scattered by a suspension of particles at a wavelength λ towards the direction θ. The scattering phase function for typical water types has been measured by Petzold in [135]. However, the angular resolution of the measured data is relatively lower for large scattering angles and thus limits the accuracy of the results. Also, the distribution of the scattering angle must take account of the medium characteristics. In practice it is not easy to measure the VSF [136] and several models have been proposed for it, which will now be described together with Petzold's measurement.

Petzold Scattering Phase function

The Petzold phase function is regarded as the representation of the phase function of typical ocean water which is based on measurements conducted for three water types in the 1970s. the three water types are Clear water, Coastal water and turbid water [135]. It is one of the most cited models for scattering in UOWC. The clear water measurement was conducted at the tongue of the ocean in Bahamas Island, the coastal water in Sandro channel California was used for the coastal water measurement and the turbid water measurement was conducted in California San Diego harbor.

Henyey-Greenstein (HG) Phase function

Historically, the long standing Henyey-Greenstein phase function (HGPF) was originally proposed in 1941 for galactic scattering in describing

scattering angles caused by interstellar dust clouds for astrophysics [137]. It is widely used in approximating the angular scattering in biological tissues due to its simplicity . Many researchers used it in UOWC but highlighting the fact that its accuracy is limited in small angles (less than 20^o) and large angles (greater than 130^o) [138] [27] [32]. The HGPF is defined by (3.18) for a given wavelength and commonly used in ocean optics to model the scattering of light [4].

$$\beta_{\mathrm{HG}}(\theta) = \frac{1-g^2}{4\pi(1+g^2-2g\cos\theta)^{3/2}} \tag{3.18}$$

where $g = \overline{\cos\theta}$ is the average cosine of the scattering angle θ over all scattering directions. It is termed the HG asymmetry parameter and depends on the medium characteristics. It can also be understood as the quantity of light that is scattered in the forward direction [139]. $g = 0$ indicates isotropic scattering and $g = 1$ indicates very forward scattering [140]. A value of $g = 0.924$ [141] is often used for practical situations. The probability distribution of the scattering angle is given by:

$$\rho_{\mathrm{HG}}(\theta, g) = \frac{1-g^2}{2(1+g^2-2g\cos\theta)^{3/2}} \tag{3.19}$$

Two-Term Henyey-Greenstein (TTHG) phase function

The two term HG function (TTHG) is a modified version which is a linear combination of the HG function proposed by Haltrin [142]. It is more accurate than the HGPF model but also not as accurate as the experimental phase function by Petzolds. It has the form:

$$\rho_{\mathrm{TTHG}}(\theta, \alpha, g, k) = \alpha\rho_{\mathrm{HG}}(\theta, g) + (1-\alpha)(\theta, -k) \tag{3.20}$$

where g and k are the asymmetry factors of the forward and backward directed HG phase functions, and α is the weight of the forward-directed

HG phase function. The relationships between these parameters are provided in [142] and are described below.

$$\alpha = \frac{k(1+k)}{(g+k)(1-g+k)} \tag{3.21}$$

The parameter k is given in terms of parameters (c_1, c_2, c_3, c_4) provided by Haltrin thus:

$$k = -c_1 + c_2 g - c_3 g^2 + c_4 g^3 \tag{3.22}$$

where $c_1 = 0.3061446, c_2 = 1.000568, c_3 = 0.01826338,$ and $c_4 = 0.03643748$

He also proposed the empirical expression below for the mean scattering angle:

$$\overline{\cos\theta} = 2\frac{1-2B}{2+B}, B = b_b/b \tag{3.23}$$

Fournier-Forand Phase Function

Another analytic model of the phase function is that of Fournier and Forand [143], which is more realistic but more complicated. The Fournier-Forand phase function (FFPF) assumes that particles have a hyperbolic size distribution and each particle scatters according to the anomalous diffraction approximation to the exact Mie theory. The FFPF can reproduce the shape of the measured phase functions in ocean water and can also reveal the inherent properties of the underwater channel. This phase function is given by:

$$\beta_{\mathrm{FF}}(\theta) = \frac{[\beta_{\mathrm{FF1}}(\theta) + \beta_{\mathrm{FF2}}(\theta)]}{4\pi(1-\delta)^2\delta^v} + \beta_{\mathrm{FF3}}(\theta) \tag{3.24}$$

$$\beta_{\mathrm{FF1}}(\theta) = [v(1-\delta) - (1-\delta^v)] \tag{3.25}$$

$$\beta_{\mathrm{FF2}}(\theta) = \frac{[\delta(1-\delta^v) - v(1-\delta)]}{\sin^2(\theta/2)} \tag{3.26}$$

$$\beta_{\mathrm{FF3}}(\theta) = \frac{(1-\delta_{180}^{v})(3\cos^2(\theta)-1)}{16\pi(\delta_{180}-1)\delta_{180}^{v}} \quad (3.27)$$

The parameters are: $\delta = 4\sin^2(\theta/2)/3(n-1)^2$, where n is the refractive index of the water, and $v = \frac{(3-\mu_{sl})}{2}$, where μ_{sl} is the slope parameter of the best fit hyperbolic function [143]. The value of δ evaluated at θ = 180 degrees is denoted by δ_{180}.

Measurement of the VSF is difficult but it can be determined analytically using Mie's solution to Maxwell's equations for a single photon at a single refractive index boundary [5]. However, this must be extrapolated to millions of photons and for millions of infinitesimally small refractive index changes to form a complete channel model. Hence, most theoretical descriptions choose to begin with the Radiative Transfer Equation (RTE) because it takes both the IOPs and the VSF into consideration.

3.5.3 The Radiative Transfer Equation

This equation, abbreviated to the RTE, expresses the conservation of energy of light that is passing through a medium. It connects the IOPs, boundary conditions and light sources to the radiance. It exists in both scalar and vector form, and for the purpose of optical communications, the vector RTE provides a model of the temporal dispersion and polarization state of light. It is given in [144] as:

$$\left[\frac{1}{v}\frac{\partial}{\partial t} + \boldsymbol{n}.\nabla\right] I(t,\boldsymbol{r},\boldsymbol{n}) = -cI(t,\boldsymbol{r},\boldsymbol{n}) + S(t,\boldsymbol{r},\boldsymbol{n}) + E(t,\boldsymbol{r},\boldsymbol{n}) \quad (3.28)$$

The left hand side of the equation represents a change of intensity over a differential length, where v is the speed of light, $\boldsymbol{n}$ is the direction vector, ∇ is the divergence operator with respect to position vector $\boldsymbol{r}$, $I(t,\boldsymbol{r},\boldsymbol{n})$ is the radiance and t is the time. On the right hand side, c is the attenuation coefficient, so the first term captures the Beer-Lambert law. The second term is contribution of scattered light from other directions, given by:

$$S(t,\boldsymbol{r},\boldsymbol{n}) = \int_{4\pi} \beta(\boldsymbol{r},\boldsymbol{n},\boldsymbol{n}')I(t,\boldsymbol{r},\boldsymbol{n})d\boldsymbol{n}' \tag{3.29}$$

Finally, $E(t,\boldsymbol{r},\boldsymbol{n})$ is the source radiance. Thus, the RTE is an integrodifferential equation of the unknown radiance and known IOPs and is difficult to solve. The nonlinear scattering phase function $\beta(\boldsymbol{r},\boldsymbol{n},\boldsymbol{n}')$ also adds more complexity in solving this equation and the next section summarises the approaches taken to this to date in solving this equation which are the exact analytical solution, approximate analytical solution and numerical solutions.

Exact Analytical Solutions

It is only possible to obtain exact analytical solutions for very simple scenarios such as in the absence of scattering. Even a conceptually simple geometry, for example, an isotopically emitting point light source in an infinite homogeneous body of water does not presently have an exact analytical solution [145]. This is because of the complications of scattering. If there is no scattering, the RTE reduces to a linear, ordinary differential equation which is easily solved but this method is unrealistic as scattering occurs in real ocean environments.

Approximate Analytical Solutions

These solutions can be obtained for an idealised situation such as single scattering in a homogeneous body of water. Although seldom used today, such approaches were very important in the early days of ocean optics and include the single-scattering approximation (SSA) and its further simplification the quasi-scattering approximation (QSSA) [146]. These methods assume that the water is homogeneous, the sea surface is level, the water is infinitely deep and there are no internal sources or inelastic scattering.

These approximate solutions are useful in isolating the main factors affecting underwater radiance but depend on various simplifying assumptions and the predicted radiances are generally accurate to a few tens of percent at best. Beam spread function for laser-based UOWC system

was proposed by Cochenour *et al.* [147], [123] using a small angle approximation method of solving the RTE to simplify the derivation. The relationship between the received optical power versus the link range of transmission was also revealed by this analytical model for various pointing accuracies of the transmitter/detector. It was validated by water tank experiments.

Numerical Solutions

Numerical solutions are generally preferred for accurate solutions to the RTE for realistic oceanic conditions. Mobley *et al*. [148] state that there are three numerical techniques for solving oceanography radiative transfer, namely discrete ordinates, invariant imbedding and Monte Carlo. A summary of these numerical methods is given in Table 3.2 adopted from [145]. The fundamental differences between these methods are the resulting computational time, the treatment of the boundary conditions at the body surface of the water and the mathematical technique implemented in solving the RTE.

The discrete ordinates method gives a solution to the RTE by considering the medium as a series of homogeneous layers. These are divided into a defined number of discrete solid angles and the RTE solved for each of the individual of them. The next layer uses these solutions as boundary conditions to get the next set of solutions. The inability of this method to handle highly peaked scattering phase functions such as those found in oceanic particulate matter makes it a poor choice for UOWC.

Invariant imbedding produces a solution based on analytical estimation. Its main disadvantage is that it is only capable of solving one-dimensional problems because it creates a model by converting the two-boundary value RTE into an ordinary differential equation with an initial condition. It has been employed to calculate the received power of UOWC systems by free Gauss-seidel matrix iteration [149].

The Monte Carlo (MC) method is an accurate, highly flexible, probabilistic technique that finds a solution by sending a single photon at a time through the channel and iterating the process many times (often $\geq 10^6$) until an overall picture of the temporal and spatial distribution of the source at a specified distance is formed. The method thus captures the random interaction of photons with the sea to determine the distribution of photon trajectories at the cost of computational intensity. In UOWC, the MC method was first presented by Hanson and Radic [70]. It is completely general, versatile and can solve 3-dimensional and time-dependent problems but at the expense of a higher computer run time. The US Naval research laboratory designed a robust MC based model in [150]. It has also been used to model the impulse response of an UOWC channel taking into account several receiver parameters such as FOV and aperture size [151]. Recent research efforts using the MC approach to characterize the UOWC channel can be found in [130], [152] and [153]. Agreement between MC simulation and experimental measurements can be found in [154] with MATLAB source code of a MC simulation tool produced by Cox [155]. The MC method has also been used to estimate the performances of NLOS UOWC in [30] and [31].

In summary, it is necessary to solve the RTE in order to fully explore the propagation of light in the underwater environment. Several researchers use different methods such as using approximations or even totally neglecting scattering. The MC method is the foundational technique used in this thesis for modelling the UOWC channel because fewer approximations are required and provide solutions for realistic situations. The MC method is especially beneficial in simulating scattering processes in the underwater environment which is a complex, random and unavoidable process realistically. Most importantly, the MC method is the best choice since the experimental method is difficult, dangerous, time-consuming and too expensive. The parameters can be easily varied according to real scenarios and in UOWC, it can be used to estimate the impulse response which is

difficult to measure. Full details of the MC modelling and mathematical formulas are given in chapter four of this thesis.

An addition, some semi-analytical models have been employed to model UOWC channels. A single gamma function model has been used in [156] to model the impulse response for an UOWC link. Based on MC simulation, Tang *et al*. adopted double gamma functions (DGFs) to produce a model of the UOWC impulse response [157]. This was capable of describing the temporal dispersion of light in turbid water environments and enabled the evaluation of BER and Bandwidth. The DGF approach was modified in [158] to weighted DGFs by adding parameters to model the impulse response of multiple input multiple output (MIMO) UOWC links. Zhang and Dong developed a weighted gamma function polynomial [159] to model the impulse response of a general M by N MIMO UOWC link. Doniec *et al.* [102] presented an end-to-end model to simulate the signal strength and communication distance incorporating all the UOWC system components (light sources, analogue-to-digital converters, amplifiers and detectors).

Table 3.2: Summary of the Advantages and disadvantages of the numerical methods for solving RTE [145]

Numerical Method	Description
Discrete ordinates	➢ Models the medium as a stack of homogeneous layer. ➢ Fast for irradiance calculations and homogeneous water (though it can be slow for radiances or if many layers are needed. ➢ Does not handle highly peaked VSFs well. ➢ Highly mathematical. ➢ Difficult to program.
Invariant Imbedding	➢ Run time increases linearly with optical distance i.e. It is extremely fast. ➢ Includes all orders of multiple scattering. ➢ It can only solve 1D problem. ➢ Highly mathematical. ➢ Difficult to program.
Monte-Carlo	➢ It is based on conceptually simple physics. ➢ Completely general and versatile: can solve time dependent and 3D problems with arbitrary geometry. ➢ Easy to program. ➢ The computer run time can be extremely slow for complex problems.

3.5.4 Modelling Oceanic Turbulence

Most studies in UOWC channel modelling concentrate on obtaining a precise description of the absorption and scattering characterization effects, often ignoring the impact of oceanic optical turbulence on system performance. As mentioned in Section 3.4.2, such turbulence can cause degradation of the performance of the UOWC system and needs further modelling. Consideration of the similarities of the physical mechanisms of oceanic and atmospheric turbulence has led to the extension of traditional

atmospheric turbulence models to the oceans for UOWC channels. For example, Hanson and Lasher [160] adopted the classic model of Kolmogorov for underwater optical turbulence. This led to the proposal of a universal channel model by Liu *et al.* [161] taking into consideration absorption, scattering, and underwater optical turbulence which directly applies the recognized lognormal turbulence model shown in the equation below.

$$f_{\mathrm{I}}(I) = \frac{1}{I\sqrt{2\pi\sigma}} \exp\left\{-\frac{(\ln I - \mu)^2}{2\sigma}\right\} \tag{3.30}$$

where I, μ and σ are the received light intensity, mean logarithmic light intensity and the scintillation index, respectively. The impact of underwater turbulence and depth on underwater imaging has been investigated [162], [163]. Moreover, adaptive optics have been proposed to address the impact of turbulence on underwater imaging and general UOWC [164]. Other studies related to underwater turbulence can be found in [165] [166] [167].

3.5.5 Modelling UOWC Misalignment

Link misalignment is unavoidable in UOWC systems due to limitations of transceivers, variations in refractive index and relative motions caused by ocean current, underwater vehicles and other turbulent sources. It is modelled in terms of the distance between the source and the detector planes (L) and the perpendicular offset between the receiver aperture centre and the beam centre (r) using the beam spread function below [168].

$$BSF(L, r) = E(L, r)\exp(-cL) + F_{\mathrm{s}}(L, r) \tag{3.31}$$

where $BSF(L, r)$ is the irradiance distribution of the detector plane, $E(L, r)$ is the irradiance distribution of the laser source in spatial coordinates and c is the attenuation coefficient. The function $F_{\mathrm{s}}(L, r)$ includes the spatial Fourier transform of $E(L, r)$, $E(L, v_f)$, in which v_f represents the spatial frequency variable. In also includes a zero order Bessel function of the first kind, $J_0(\cdot)$, and other elements, thus:

$$F_{\mathrm{s}}(L, r) = \int_0^{\infty} F_1(L, v_f) F_2(L, v_f) J_0(v_f r) v_f \, dv_f \tag{3.32}$$

$$F_1(L, v_f) = E(L, v_f) \exp(-cL) \tag{3.33}$$

$$F_2(L, v_f) = \exp\left\{\int_0^L bs(v_f[L-z])dz\right\} - 1 \tag{3.34}$$

where b is the scattering coefficient and $s(v_f)$ is the scattering phase function. This model was used to determine the UOWC system BER performance under misalignment conditions. The effects of misalignment of point-to-point UOWC using MC simulations and verified by water tank experiments has been studied by Gabriel *et al.* [130]. Numerical results show that given sufficiently large transmission power, an appropriate amount of misalignment does not yield a significant performance degradation for any water type. Other work on pointing errors and misalignment modelling can be found in [169] and [170].

3.6 Conclusion

This chapter started with a brief introduction of light and energy along with the properties of the optical beam under the water. The background principles and theories of light beam propagation under the water was discussed in detail as this will be the underlying concept for the channel characterization and modelling. The main challenges of the channel were also discussed in this chapter. The existing channel model for UOWC, its applicability and limitations were presented. Numerical results of the RTE give the best description of the light beam state along the channel by including the spatial and temporal distributions of light as it is necessary to solve the RTE in order to fully explore underwater light propagation. Different methods have been used by several researchers such as totally ignoring scattering or using approximations. MC method is the foundational technique used in this thesis for modeling the UOWC channel because it provides solution for realistic situations and fewer approximations are

required. It is especially beneficial in simulating underwater scattering processes which is random, complex, and realistically unavoidable. The MC method is the best choice since experimental method is dangerous, difficult, too expensive and time consuming. The chapter concluded with a brief review of the modelling of link misalignment and oceanic turbulence.

CHAPTER 4

Performance of Non-line-of-sight Underwater Optical Wireless Communication Links

This chapter, first discusses the Monte Carlo (MC) method of modelling light propagation in the underwater domain including its advantages, applications, principles, theories, mechanics along with the mathematical equation and probability theory that are used in modelling the channel. The characteristics of a non-line-of-sight (NLOS) UOWC link with multiple scattering based on Monte Carlo simulation is considered. The channel response of an NLOS-UOWC system is addressed with different channel modulation schemes. The resultant channel impulse (CIR) response varies with the type of water considered and the receiver field of view (FOV). Thus, the CIR for clear ocean, coastal water and turbid water for FOV values of 30° and 60° are obtained. Then, the CIR obtained using different modulation formats is investigated in coastal water since this is a likely application medium. Next, the effect of receiver lens diameter on the performance of the NLOS UOWC system is shown. Finally, the bit error rate (BER) and throughput of the system are evaluated, including variation in the receiver bandwidth. The system provides BER values of 10^{-4} or better and throughput of 2.1 Mbps. This demonstrates that NLOS-UOWC offers a route to transmission at higher speeds than incumbent technologies in areas such as inshore environmental monitoring or oil exploration.

4.1 Overview of Monte Carlo numerical simulation

Taking a historical view, the first report of the MC method was made in 1949 by a group of researchers from Los Amos laboratories [171]. In general, the MC simulation method is a probabilistic technique and uses the known probability of a single individual event to make a prediction of the probability of the entire whole event. As opposed to the analytical models discussed in chapter three, which give an exact answer to an approximate

problem, the MC simulation method uses random sampling to arrive at an approximate solution to an exact problem. The MC method has since been widely used in solving a diverse range of problems in physics, mathematics, finance, biological science, computer graphics, economics and engineering. MC simulation methods are used largely in the field of OWC for solving the RTE. The MC method has been used by several researchers to model the indoor infrared (IR) communication channel [172], various types of outdoor channel environments [173], and also in NLOS ultra-violet (UV) communications [174]. With regards to UOWC, the MC method is used to determine the exact trajectories and distributions of the photons by simulating the interactions of the photons with the water and the random sea surface. The first use of the MC simulation method in this context was by Hanson *et al.* [70].

Generally, the MC simulation method is known for its implementation versatility in either two-dimensional (2D) or three dimensional (3D) scenarios using a computer. It is particularly beneficial in simulating the complex scattering process in the underwater environment. Furthermore, the MC method is the best choice when experiments are difficult, time consuming and too expensive to handle [175]. It can be used specifically in UOWC to estimate the impulse response and temporal effects, which are both difficult to measure. The MC method is considered to be the standard model in the field of light transport in turbid media, having the capability of providing exact solutions to the RTE [176].

Despite the advantages of the MC simulation method described above, it also has some deficiencies. First, a large number of samples must be generated since it is a very demanding method as the accuracy is inversely proportional to the square root of the number of samples N, i.e. $1/\sqrt{N}$ [139]. Secondly, it is slow and inefficient computationally since it has to trace millions of individual photons in order to give a better accuracy, also making it unsuitable for small detector apertures area because few photons will reach the detector [177]. Finally, in some cases the MC model is unsuited where the wave nature of light is examined [151].

In implementing the MC simulation method, several assumptions have been made, these assumptions are outlined below:

- The light is single wavelength i.e. a monochromatic light source.
- The absorption and scattering are uniform throughout the medium i.e. a homogeneous medium, resulting in a constant coefficient of attenuation.
- Scattering events are random and independent, generated by a pseudo random generator.
- The effect of turbulence caused by the difference in the index of refraction is ignored, i.e. the index of refraction is uniform.

4.2 Monte Carlo Simulation algorithm

In the simulation process of the MC method, the light is modelled as the propagation of a large number of photon packets or photons (photons are used throughout this thesis for simplicity). The identification of each photon is by its position, direction and weight. Each photon will move repeatedly once it is emitted until it reaches the receiver or until it is lost. This procedure will be repeated until sufficient photons are received by the receiver. The history of each individual photon will be recorded so that it is used in calculating the impulse response, received power and other parameters. The flowchart of the MC algorithm is shown in figure 4.1 and its details are summarized in the following section.

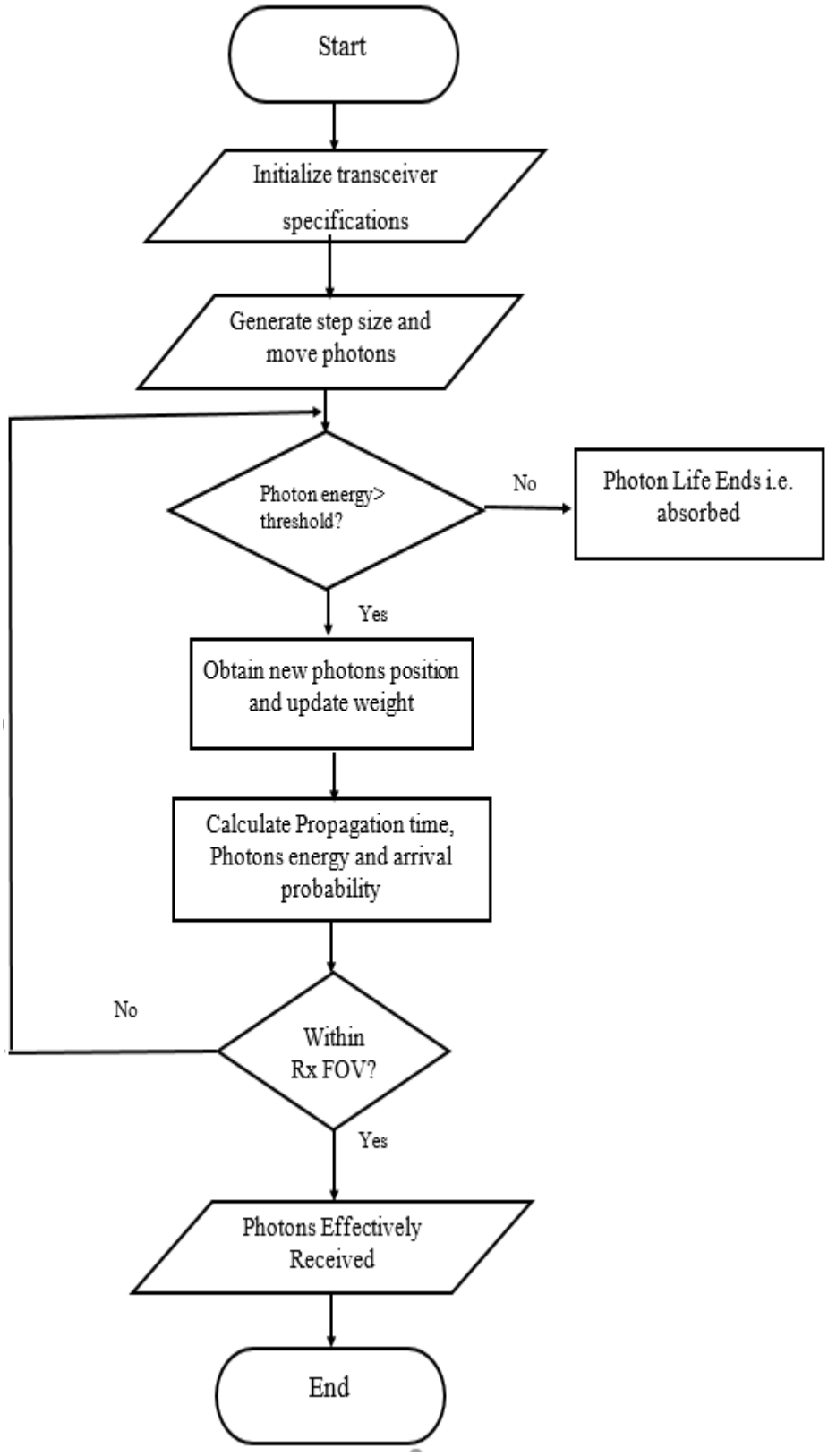

Fig. 4.1: Flowchart for MC simulation algorithm [178]

The simulation starts by initializing all the parameters to the appropriate values. The photon is then launched with its initial x, y, z coordinate position and the projections of the direction vectors μ_x, μ_y, μ_z. Then, the photon will

move by a step size s, where it will be scattered or absorbed. Between successive events, the distance the photons propagate is determined based on the extinction (attenuation) coefficient of the water. The photon is considered lost when it travels out the boundary. Some of the energy of the photon is absorbed while some is deflected or scattered in another direction after every interaction with the water particles determined by the water albedo ω (the probability of photon scattering, i.e. $\omega = b/c$). Then, the new photon directions after scattering can be calculated using the SPF discussed in chapter three. If a photon is received by the receiver, then its weight, location and total distance travelled are recorded and the receiving probability and the impulse response is calculated. The process is repeated for all photons.

4.3 Mechanics of Monte Carlo Simulation

The MC simulation method comprises three main parts which are: the initial conditions, photon propagation and photon reception. The Cartesian coordinate system as well as spherical coordinates are used in the simulation. The transmitter, receiver and the photon propagation direction are located in the x, y, z plane while the polar and scattering angles are modelled in terms of polar and azimuthal angles as θ and ϕ. The position and direction of the photon will be defined locally first for each photon propagation and then transformed to the absolute (global) coordinate system.

4.3.1. Initial Photon Position

Each photon is represented by its x, y, z location coordinate and a projection of a unit vector in the direction of propagation known as direction cosines. These are illustrated in figure 4.2 and are specified as [179]:

$$\mu_x = cos\,\theta_x \tag{4.1}$$

$$\mu_y = cos\,\theta_y \tag{4.2}$$

$$\mu_z = cos\,\theta_z \tag{4.3}$$

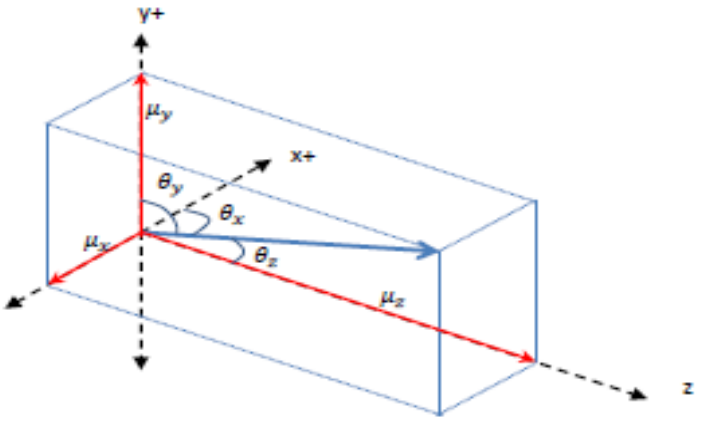

Fig. 4.2: Illustration of direction cosines [179]

The angles between the x, y, z axis and the direction vector are θ_x, θ_y and θ_z respectively. These three direction cosines must satisfy the normalization

$$\mu_x^2 + \mu_y^2 + \mu_z^2 = 1 \tag{4.4}$$

Source Modelling

Lambertian and Gaussian source distributions are used in this thesis as the source emission patterns. Modelling the different sources requires modelling both their polar and azimuthal angles, which can be dealt with separately since they are independent of each other. The azimuthal angle is uniformly distributed between $[0,2\pi]$ so can be easily found while the polar angle must be generated according to the probability density function (pdf) that results from the specific source distribution. The following sections present the sampling rules for the source beam profiles.

Lambertian source

The Lambertian pattern is generally used to model the radiation pattern of LEDs [179]. It is also referred to as a power cosine distribution because the light intensity of the LED is dependent on the cosine of the emission angle from the normal of the surface. The intensity of this source is given by:

$$I(\theta) = I_0 \cos^m \theta \tag{4.5}$$

where θ is the irradiance angle from the normal of the source surface, the intensity at the centre is I_0 and m is the Lambertian order of emission:

$$m = \frac{\ln 2}{\ln(\cos \phi_{1/2})} \tag{4.6}$$

$\phi_{1/2}$ is the semi angle at half illuminance of the LED.

The pdf of the polar angle follows the Lambertian emission pattern of the source and is given by [180], [181]:

$$p(\theta) = (cos\,\theta)^m\, sin\,\theta \tag{4.7}$$

and the cumulative distribution function (cdf) is calculated as:

$$P(\theta) = 1 - (cos\,\theta)^{m+1} \tag{4.8}$$

The polar angle can be calculated by using inversion method, thus:

$$\theta = cos^{-1}\left(\sqrt[m+1]{R}\right) \tag{4.9}$$

where R is a random number that is uniformly distributed on the interval $[0,1]$. The azimuthal angle ϕ_0 is uniformly distributed and randomly chosen on $[0,2\pi]$ From the azimuthal angle, the starting direction cosines of the photon can be calculated:

$$\mu_{x_0} = sin\,\theta_0\, cos\,\phi_0 \tag{4.10}$$

$$\mu_{y_0} = sin\,\theta_0\, cos\,\phi_0 \tag{4.11}$$

$$\mu_{z_0} = cos\,\theta_0 \tag{4.12}$$

Gaussian Beam

For Gaussian beam, the intensity at the origin is given as a function of the radial distance r from the beam center and is given as [180];

$$I(r) = I_0 \exp\left(\frac{-r^2}{b^2}\right) \tag{4.13}$$

where I_0 is the optical intensity of the gaussian beam at the beam centre and b is the waist radius.

The pdf of the Gaussian beam profile as a function r is:

$$I(r) = \frac{\exp\left(\frac{-r^2}{b^2}\right)}{b^2} 2r \tag{4.14}$$

and the cdf is obtained by integrating the pdf as follows:

$$P(r) = \int_0^r p(r)d(r) = 1 - e^{-r^2/b^2} \tag{4.15}$$

The cdf is evaluated to R in order to find r of the beam i.e. $P(r) = R.\ r$, giving:

$$r = b\sqrt{-\ln(1-R)} \tag{4.16}$$

For a Gaussian beam, the initial condition is to create a Gaussian distribution on the transmit plane and then select starting angles to produce a divergent

beam. Cox [179] provides a highly practical method for doing this by approximating the beam as a collimated source that is diverged with a lens. The divergence angle is chosen to match the desired light source and then the distance for this divergence angle is taken as beam waist. Then, the focal length of the lens f_l used for the light divergence is obtained from:

$$f_l = \frac{b_r}{\phi_{div}} \tag{4.17}$$

where ϕ_{div} is the divergence half angle.

The generated photon's polar angle is defined by:

$$\theta_0 = \frac{r}{f_l} \tag{4.18}$$

In a similar fashion to the Lambertian source, the azimuthal angle is randomly chosen based on a $[0,2\pi]$ uniform distribution.

Therefore, the photon starting point is;

$$x_0 = r_0 \, cos \, \phi_0 \tag{4.19}$$

$$y_0 = r_0 \, sin \, \phi_0 \tag{4.20}$$

and the starting direction cosines are as the ones in (4.10), (4.11) and (4.12).

In MC simulation, the environment is defined by the attenuation coefficient c, the volume scattering function and the albedo which defines the contribution of scattering to the overall loss. The albedo determines what percentage of the photon's weight is diminished due to the effect of absorption as the remaining deflected photons are redirected and continue propagation.

4.3.2. Photon Propagation

After generation of the photon, it is then moved governed by its path length, the distance over which it travels before being absorbed or scattered and its scattering angles determined according to the VSF.

Photon step size

The step size of the photon is calculated by sampling the probability of its free path length [140]. It is determined by the attenuation coefficient c of

the water. With respect to the optical propagation distance (l), the pdf for the attenuation of light is given by:

$$p(l) = e^{-l} \tag{4.21}$$

The cdf is thus:

$$P(l) = \int_0^l e^{-l'} dl = 1 - e^{-l} \tag{4.22}$$

The path length l is sampled using inversion sampling by letting $P(l) = R$. Solving for l we have.

$$l = -ln(1 - R) = -ln\, R \tag{4.23}$$

The photon path length is defined as $l = sc$, where c is the attenuation coefficient and s is the geometric distance between optical events found from:

$$s = -\frac{1}{c} \ln R \tag{4.24}$$

Photon weight

Each photon is assigned a weight of 1 as it enters the medium. The photon packet is divided into two after each propagation step. A fraction of the photon packet split is absorbed and the rest scattered [182]. Therefore, the photon's weight will change according to the absorption energy percentage. The albedo, ω, (explained in section 4.2) is used to determine the fraction of the photon packet being absorbed, $1 - \omega$; the fraction being scattered is given by $w' = w\omega$ which represents the new photon weight.

Terminating a Photon

After the photon has gone through the process of scattering and absorption, its energy will diminish to a very small value. This energy is sometimes too small to be calculated at the receiver side during simulation. A minimum energy value is set as a threshold to speed up the simulation time, which determines whether the photon should be terminated or not. If the photon's weight is below the threshold level, it is considered lost. If the threshold value is too small, the simulation time will be too long and if the value is large, then the accuracy will be low. So, there is a need to carefully choose an optimum value of the threshold. Different values of the threshold

have been used by several researchers, namely 10^{-4} [27], 10^{-6} [179], [157] and 10^{-10} [151].

However, to simply terminate the photon would violate the conservation of energy in the simulation so the "roulette" method is employed, which also reduces the simulation time [179]. In this method, an integer parameter α known as the roulette threshold is chosen in conjunction with a random number, R chosen from a uniform distribution on $[0,1]$. The photon is given a chance to survive and continue with a weight of αw. Termination of the photon ($w' = 0$) occurs if $R > \alpha^{-1}$, otherwise it will continue to propagate ($w' = \alpha w$) $R \leq \alpha^{-1}$.

Scattering.

The angle of scattering is chosen from the VSF, which is customarily one of those that are widely used and discussed in chapter three; in this thesis, the well-known VSFs were used . The azimuthal or radial scattering angle ϕ' is chosen from the equation below.

$$\phi' = 2\pi R \tag{4.25}$$

R is a random number in the interval $[0,1]$. Note that the random number used to choose θ' and ϕ' should be different in order that they both be independent random variables.

Updating the direction cosines

The local direction of scattering will be transformed to the global direction of scattering where the new direction cosines must be updated with the chosen azimuth ϕ' and polar θ' scattering angles. When rotated by θ' and ϕ', the new direction cosines are defined as [150]:

$$\begin{bmatrix} \mu_x' \\ \mu_y' \\ \mu_z' \end{bmatrix} = \begin{bmatrix} \mu_x\mu_z/\sqrt{1-\mu_z^2} & -\mu_{xy}/\sqrt{1-\mu_z^2} & \mu_x \\ \mu_y\mu_z/\sqrt{1-\mu_z^2} & \mu_x/\sqrt{1-\mu_z^2} & \mu_y \\ -\sqrt{1-\mu_z^2} & 0 & \mu_z \end{bmatrix} \begin{bmatrix} \sqrt{1-\mu_s^2 s}\, cos\, \phi' \\ \sqrt{1-\mu_s^2 s}\, sin\, \phi' \\ \mu_s \end{bmatrix} \tag{4.26}$$

where μ_z is very close to 1 and $\mu_s = cos\, \theta'$.

Updating the photon propagation

The position as well as the direction cosines of the photon must be updated after the scattering process. The new photon's position is defined as:

$$x' = x_0 + \mu_x' s \tag{4.27}$$

$$y' = y_0 + \mu_y' s \tag{4.28}$$

$$z' = z_0 + \mu_z' s \tag{4.29}$$

where s is the step size, and μ_x', μ_y', μ_z' are the current direction cosines.

4.3.3 Photon reception

The receiver will select the photon that reaches it based on its FOV and aperture characteristics. When the angle of arrival of a photon received outside the aperture is greater than the FOV, it is considered lost. The received photon has important parameters such as its final cartesian coordinates, its weight, direction cosines and distance travelled which are all recorded for further analysis.

Power calculation

In MC simulation, the received power is acquired by summing the weight of all received photons and then normalizing it by the total weight transmitted as shown below

$$P_r = \frac{N_R}{N_T} \tag{4.30}$$

where P_r is the received power, N_R and N_T are the number of received and transmitted photons respectively.

Impulse Response Calculation

In the underwater environment, the effect of multiple scattering on the pulses of light is shown in Fig. 4.3. As can be seen from the figure, the photon propagation paths will change due to the multiple scattering effect, making the propagation longer than the distance between the source transmitter and detector. These photons will then reach with a particular time delay after the first received photons. The total propagation distance of individual photons in MC simulation can be measured, enabling calculation of each photon's total transmit time. Details of the impulse response calculation are explained below.

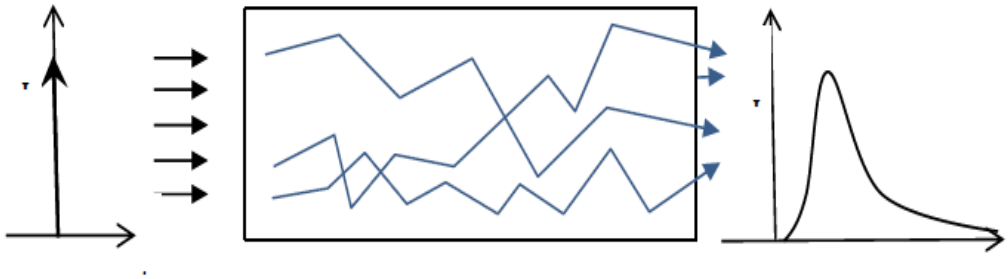

Fig. 4.3: multiple scattering effect to the impulse response [183]

The difference in path length is computed firstly as:

$$\Delta d = d_{photon} - d \tag{4.31}$$

where d_{photon} is the distance travelled by the photon and d is the distance from the transmitter to the receiver.

The time delay Δt can be computed using the speed of light in water v_{water}, thus:

$$\Delta t = \Delta d / n_{\text{water}} \tag{4.32}$$

Where $v_{water} = v_{vacuum}/n_{water}$, with v_{vacuum} being the speed of light in vacuum and n_{water} the refractive index of water.

The histogram of the time delay is then plotted from this information. The normalized histogram (which is regarded as the pdf of the discrete impulse response [179] [177]) is computed by dividing the total histogram by the weight of the received photons [179].

4.4 Simulation of NLOS UOWC Links

Despite the wide range of potential applications that could benefit significantly from UOWC (discussed in chapter one), such systems suffer from significant channel absorption and scattering (discussed in chapter three), and may experience blocking by underwater obstructions. The majority of UOWC work to date has concentrated on when there is a clear path between the transmitter and the detector, the LOS configuration [27], [168]. The work of Hanson and Radic [70] considered single scattering in a LOS configuration to attain a data rate of 1 Gbps, extended to LOS multiple scattering by Gabriel *et al.* [27] utilizing 100 Mbps. In practical scenarios, LOS communication links are not always possible due to obstructions from sea creatures, bubbles, large suspended particles and features of the

seabed, especially in coastal and turbid water environments. LOS links are also unsuitable when the transmitter and receiver are nonstationary nodes [28]. The LOS arrangement has strict pointing and alignment problems as discussed in chapter three. Thus, NLOS UOWC techniques are needed to fully explore the underwater channel but very little work has been reported so far regarding it. Arnon and Kedar [76] proposed a NLOS UOWC link with single scattering and analyzed the bit error rate (BER) performance. Choudhary *et al.* [184] reported the determination of impulse responses based on MC simulation for NLOS UOWC. The same group also carried out a path loss performance analysis [185] for NLOS UOWC with different fields of view for clear ocean water using just on-off keying (OOK) modulation and neglecting receiver noise.

So, to overcome the shortfalls in existing designs this work concentrates on a three-dimensional multiple scattering NLOS UOWC channel, investigating the channel impulse response (CIR) and system performance in different water types using a variable field of view (FOV). The simulation considers the trajectories of a large number of photons using the MC approach for a variety of modulation schemes in the presence of receiver noise. Thus, the contributions of this part of the chapter for characterization of NLOS-UOWC are as follows:

I. The established Henyey-Greenstein (HG) phase function is employed in the impulse response model with tracking of photons and scattering that fit well with the MC simulation.
II. Clear ocean water, coastal water and turbid water are considered.
III. The CIR characteristics of the channel modulation schemes quadrature phase shift keying (QPSK), 8-PSK 16-quadrature amplitude modulation (16-QAM) and 64-QAM are investigated.
IV. The BER and throughput of the underwater optical NLOS channel are evaluated.

The remainder of this chapter is organized as follows. In Section 4.5, the model is introduced with a block diagram and description of each block. Section 4.6 presents the details of the model from the implementation methodology to the mathematical framework that shows the effect of seawater on beam pulse propagation and the basic rules of our MC approach. Section 4.7 covers simulation results and their discussion, with conclusions presented in Section 4.8.

4.5 NLOS-UOWC System

Characterizing light-water interaction is a highly complicated procedure encompassing the effects when photons meet matter. Fig.4.4 presents an abstract picture, illustrating the process when light meets a particle within the water causing some photons to be absorbed, some to be transmitted and the trajectory of some others to be altered (scattering). Such of interactions are part of radiative transfer function (RTF) theory and are called the IOPs of the water discussed in chapter three [186]. In turbid and coastal waters, suspended particles mean that photons will undergo multiple scattering which is covered in this research. The attenuation coefficient (also known as the extinction coefficient) $c(\lambda)$ defines the total loss of energy as a sum of the absorption coefficient, $a(\lambda)$, and the scattering coefficient $b(\lambda)$.

Here, the focus is on clear ocean, coastal and turbid water with channel parameters as given in Table 4.1 [185].

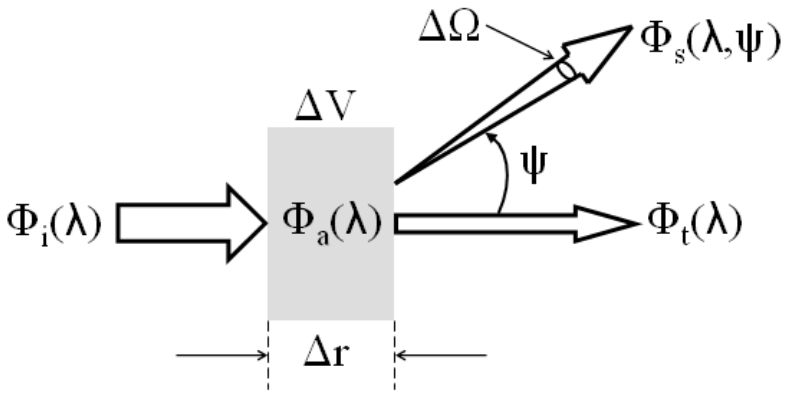

Fig. 4.4: Underwater optical light-particle interaction

Table 4.1: Absorption, Scattering and Attenuation Coefficient for the Water Types [185]

Water type	$\boldsymbol{a(\lambda)(m^{-1})}$	$\boldsymbol{b(\lambda)(m^{-1})}$	$\boldsymbol{c(\lambda)(m^{-1})}$
Clear Ocean	0.069	0.08	0.15
Coastal	0.088	0.216	0.305
Turbid	0.295	1.875	2.17

Understanding the statistical distribution of optical signal fluctuations for reliable, efficient, and robust UOWC system design requires detailed modelling and characterization of the underwater wireless optical channel. Here, an NLOS–UOWC system with transmitter (TX), receiver (RX), and NLOS channel shown schematically in Fig. 4.5 is considered. In the transmitter section, a light pulse is modulated and enters the medium after passing through appropriate projection optics. The underwater channel is considered to be homogeneous and time-invariant given the very high propagation speed of light and small propagation distance. The receiver section consists of a collecting lens which focuses the light incident on it to a photodetector placed at its focal point followed by post-detection signal processing and demodulation.

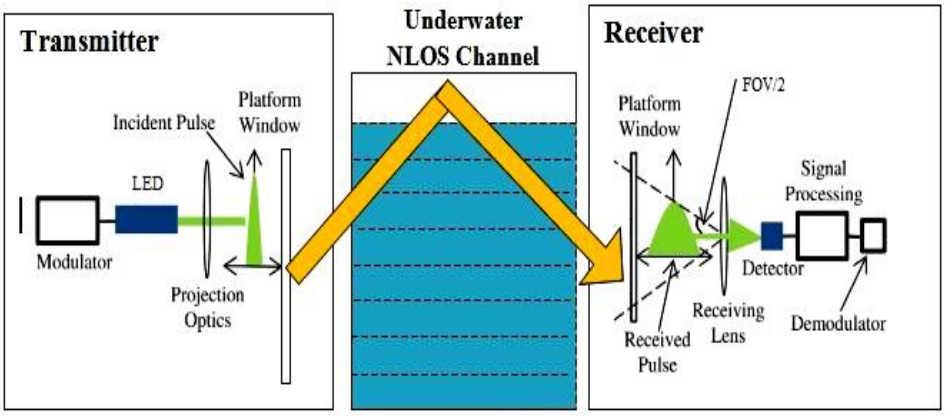

Fig. 4.5: Schematic block diagram of UWOC-NLOS system

In UOWC, the noise is a combination of background noise, thermal noise, shot noise and dark current noise, which can be approximated and modelled as additive white Gaussian noise (AWGN) [112]. Based on the parameters used here and in [112], the background noise is negligible compared to receiver noise because of the substantial attenuation of the sun underwater. Hence the model includes only receiver AWGN noise, namely thermal, shot and dark current noise; i.e. it is assumed that AWGN is the dominant noise.

4.6 Details of the Model

The process flow of the NLOS-UOWC model is shown in Fig. 4.6. This begins with the generation of a sequence binary data using a random generator, which is then mapped to the appropriate QAM or PSK constellation points to enable performance investigations using different modulation schemes. Following modulation, binary streams become symbols corresponding to the Fourier transform size with auxiliary information inserted using additional pilot symbols. The useful data and the auxiliary data are transformed using the inverse fast Fourier transform (IFFT) before addition of the header and cyclic prefix (CP). Finally, after digital/analogue (D/A) conversion the signals generated are used to drive the LED transmit filter. The photon beam combiner (PBC) collimates the parallel optical signals and combines them into a single beam for transmission through the channel.

This signal propagates through the NLOS underwater optical channel. In the receiver section, the optical signals that have passed through the underwater channel are converted to parallel signals using the photon beam splitter (PBS) for photodetection. After analogue/digital (A/D) processing, symbol synchronization is required. Then, the CP is removed and the signal converted using the fast Fourier transform (FFT) prior to auxiliary symbol removal and demodulation, followed by signal reconstruction for error counting.

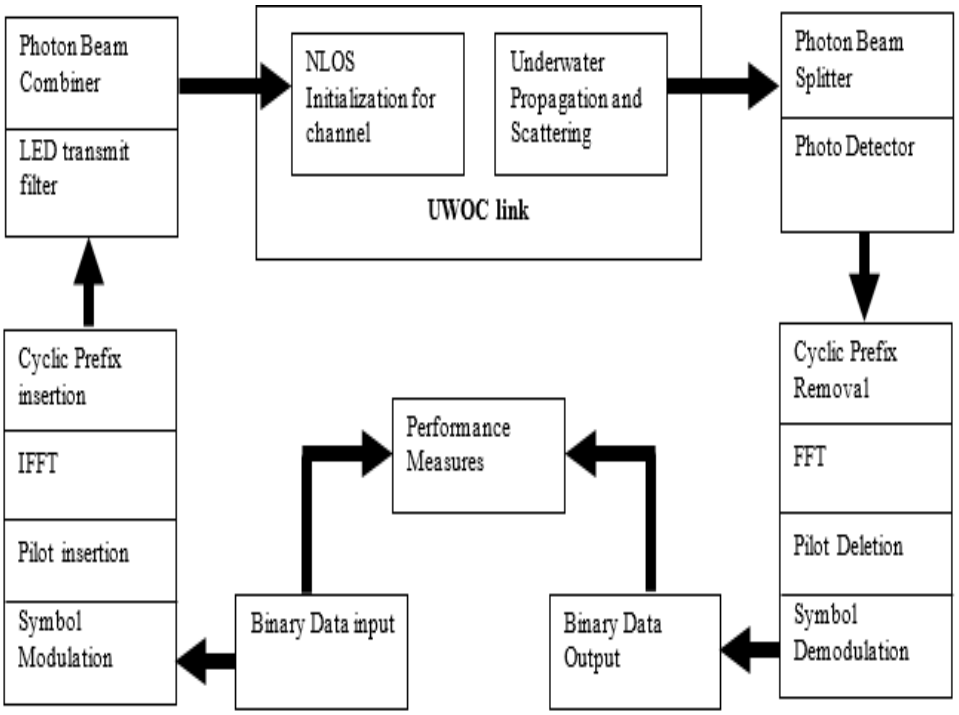

Fig. 4.6: Process flow of NLOS-UOWC model

Photon Angle Scattering

As seen in Section 4.5, after interaction with a particle, the photon deviates from its incoming direction. The new propagation direction is determined by regenerating randomly the azimuth angle ϕ and the scattering angle θ [187]. The angle ϕ is considered as a random variable (RV) uniformly distributed over [0, 2π]. However, the distribution of the scattering angle, θ, has to take account of the medium characteristics, which is achieved via

a phase function. Here the Henyey-Greenstein (HG) phase function [188] that is commonly employed in ocean optics to model light scattering [189] is used. This has the form:

$$\beta(\theta) = \frac{1 - g^2}{4\pi(1 + g^2 - 2g\cos\theta)^{3/2}} \tag{4.33}$$

where g is the HG asymmetry parameter that depends on the medium characteristics. To determine g, the average of the cosine of the scattering angle over all scattering directions is determined. That is to say $g = \overline{cos\theta}$, where here $g = 0.924$ is taken [27] . The probability density function PDF of the scattering phase function is then given by:

$$\rho_{HG}(cos\,\theta\,, g) = \frac{1 - g^2}{2(1 + g^2 - 2g\,cos\,\theta)^{3/2}} \tag{4.34}$$

This is employed in the NLOS UOWC simulation model that is now described.

MC Channel Modelling

A method describing the photon propagation via a probability distribution that defines the path length of the photon movement before a photon-particle interaction, and the angles of scattering after a scattering event occurs is adopted. Since MC is a statistical approach, the angles and directions for many photons producing an RTE solution method are calculated using three steps [185]: (a) initialization of photon properties; (b) photon-particle interaction; (c) photon reception.

Prior to describing the MC steps in detail, the link configuration used is first presented, which is shown schematically in in Fig. 4. The transmitter (Tx) and receiver (Rx) are separated by a distance d, and Rx has aperture area A_r. The Tx and Rx are located at (0, 0, 0) and (0, d, 0) respectively, with respective elevation angles θ_{tx} and θ_{rx}. The angle ϕ_{tx} is the transmitter divergence angle and ϕ_{rx} is the FOV; to locate the beam, initial azimuth angles ψ_t and ψ_r respectively are taken; MC simulation described in section 4.3 captures the life of the photons generated. This begins with generating photons, which are then scattered and positioned with new directional coordinates (ψ, θ) referenced to the current direction after every interaction with water particles until they are lost or received. Losses occur

because of every interaction produces some energy reduction. If a photon is received by the Rx, then the receiving probability and the impulse response are calculated, and the process is repeated for all photons.

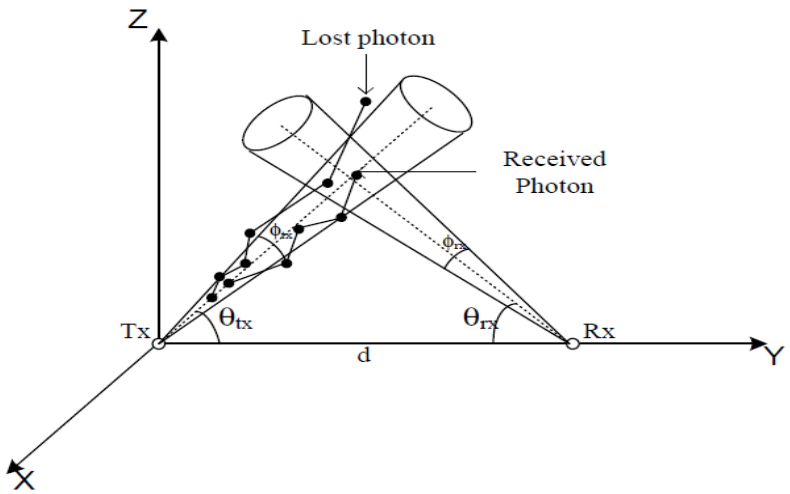

Fig. 4.7: NLOS UOWC channel link [185]

(i) Initialization of Photon Properties

The initial simulation conditions determine: the starting location in Cartesian coordinates; photon direction using directional cosines of the photons; type of environment to be simulated; nature of the photon source. The projections are defined as:

$$\mu_x = cos\,\psi_{\text{ini}}\,sin\,\theta_{\text{ini}} \tag{4.35}$$

$$\mu_y = sin\,\psi_{\text{ini}}\,sin\,\theta_{\text{ini}} \tag{4.36}$$

$$\mu_z = cos\,\theta_{\text{ini}} \tag{4.37}$$

Then the scattering azimuth angle, ψ, can be computed using:

$$\psi = 2\pi R \tag{4.38}$$

where, R is a uniform RV variable in [0,1].

(ii) Photon-Particle Interaction

The photon travels a random distance, or *step size*, Δs, before interaction with a scattering particle that is given by:

$$\Delta s = -\frac{\log(R)}{c(\lambda)} \tag{4.39}$$

with R being a uniform random RV also drawn from $[0,1]$. When interacting with the particle, the photon loses a fraction of its initial weight (hereafter referred to as the weight drop) and deviates from its initial direction (photon scattering) [27]. The photon weights before and after the interaction are denoted by W_{bf} andW_{af}, respectively. Their relationship is:

$$W_{af} = (1 - a/c)W_{bf} \tag{4.40}$$

The trajectory direction of a photon is also randomly changed with the scattering zenith angle θ as a result of the scattering effect. So, to produce a random θ, another uniform RV in [0,1], χ_{HG} is produced initially. This provides an implicit relationship:

$$\chi_{\mathrm{HG}} = \int_0^{\theta} \rho_{HG}(\Theta, g) \sin\Theta \, d\Theta \tag{4.41}$$

in terms of the dummy variable Θ, from which θ is obtained [27].

$$cos\,\theta = \frac{1}{2g}\left[1 + g^2 - \left(\frac{1 - g^2}{1 - g + 2g\chi_{HG}}\right)^2\right] \tag{4.42}$$

The interaction then produces photon coordinates and direction cosines thus:

$$x' = x + \mu_x * \Delta s \tag{4.43}$$

$$y' = y + \mu_y * \Delta s \tag{4.44}$$

$$z' = z + \mu_z * \Delta s \tag{4.45}$$

$$\mu_x' = \mu_x\, cos\,\theta + \frac{sin\,\theta}{\sqrt{1 - (\mu_z)^2}}\left(\mu_x\mu_z\, cos\,\psi - \mu_y\, sin\,\psi\right) \tag{4.46}$$

$$\mu_y' = \mu_y\, cos\,\theta + \frac{sin\,\theta}{\sqrt{1 - (\mu_z)^2}}\left(\mu_y\mu_z\, cos\,\psi + \mu_x\, sin\,\psi\right) \tag{4.47}$$

$$\mu_z' = \mu_z\, cos\,\theta - sin\,\theta\sqrt{1 - (\mu_z)^2}\, cos\,\psi \tag{4.48}$$

(iii) Photon Reception

The process "step size generation, weight drop and angle scattering" described above is repeated until one of the following events happens:

a) The photon weight becomes negligible and it is considered to have been absorbed; the threshold limit is set to 10^{-4} here [27].

b) The photon reaches the receiver plane; if it is within the receiver aperture, it is considered to have been effectively received or else it is considered lost.

4.7 Results and Discussion

The model described above for the NLOS UOWC system with channel characteristics utilizing the HG model was run using the MATLAB package with the parameters given in Table 4.2 [185]. No receiver spatial filtering was included since in deep-sea waters, background radiation is negligible, so the system was subject to AWGN at the receiver. First, the channel impulse response (CIR) for the three water types specified in Table 4.1 using a 30° FOV was determined, shown in Fig. 4.8.

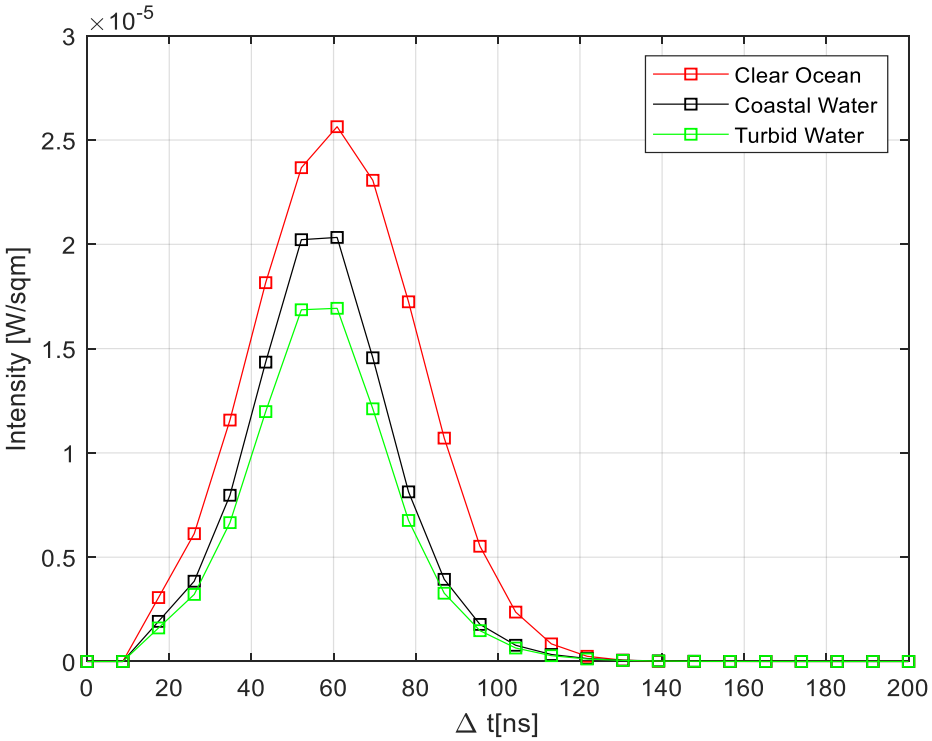

Fig. 4.8: CIR for the water types in Table 1.

The intensity is determined by summing the weight of the photons that arrive in a particular time window and normalizing using the total transmitted weight (here 10^6 photons). The impact of attenuation and scattering may be observed, improved performance is seen for clear ocean

water in contrast to coastal and turbid water since scattering is more pronounced.

Table 4.2: Simulation parameters and corresponding values [185]

	Parameter	**Value**
	Transmission wavelength	532 nm
	Elevation angle (θ_t)	π/4
	Elevation angle (θ_{r})	π/2
	Divergence angle (ϕ_{t})	π/3
	Aperture diameter	20 cm
	Range sensitivity	20 m
	FOV	$30^{\circ}, 60^{\circ}$
	Bitrate	100Mbps
	Modulation schemes	QPSK, 8-PSK, 16 QAM, 64 QAM

Having established the impact of the type of water, attention is now turned to coastal water, since this is the most likely application scenario of NLOS transmission. Fig. 4.9 shows the CIR at FOV values of 30° and 60° when employing QPSK, 8-PSK, 16-QAM and 64-QAM. Although these are similar, the highest intensity achieved in our design was when using 64-QAM. Compared with other three modulation schemes, this provided the best receiver CIR performance as it has a higher spectral efficiency and less susceptibility to noise.

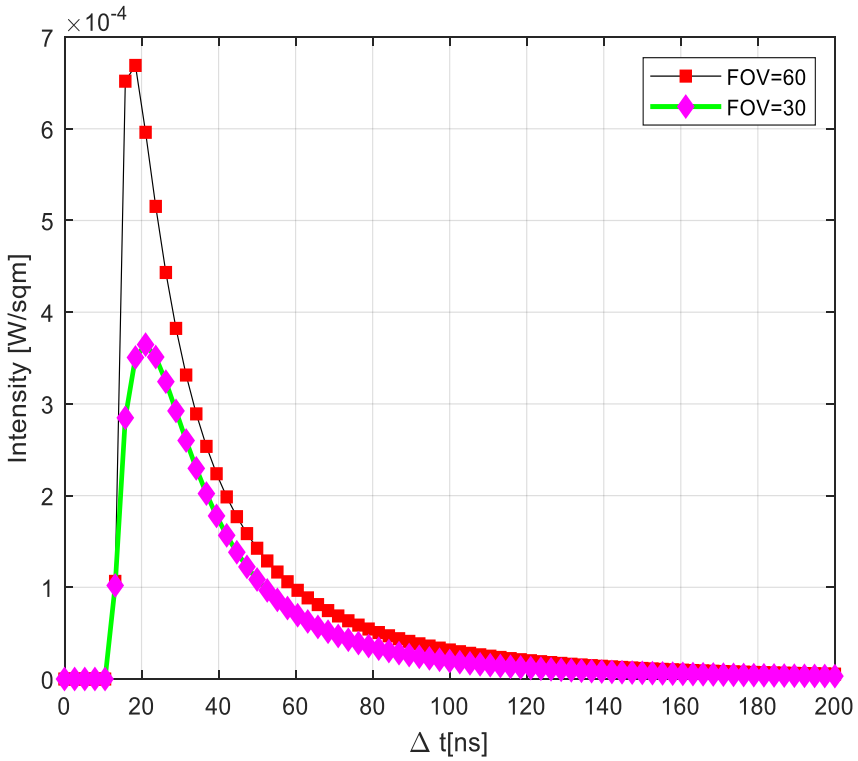
×10^-4
FOV=60
FOV=30
Intensity [W/sqm]
Δ t[ns]

(a) QPSK

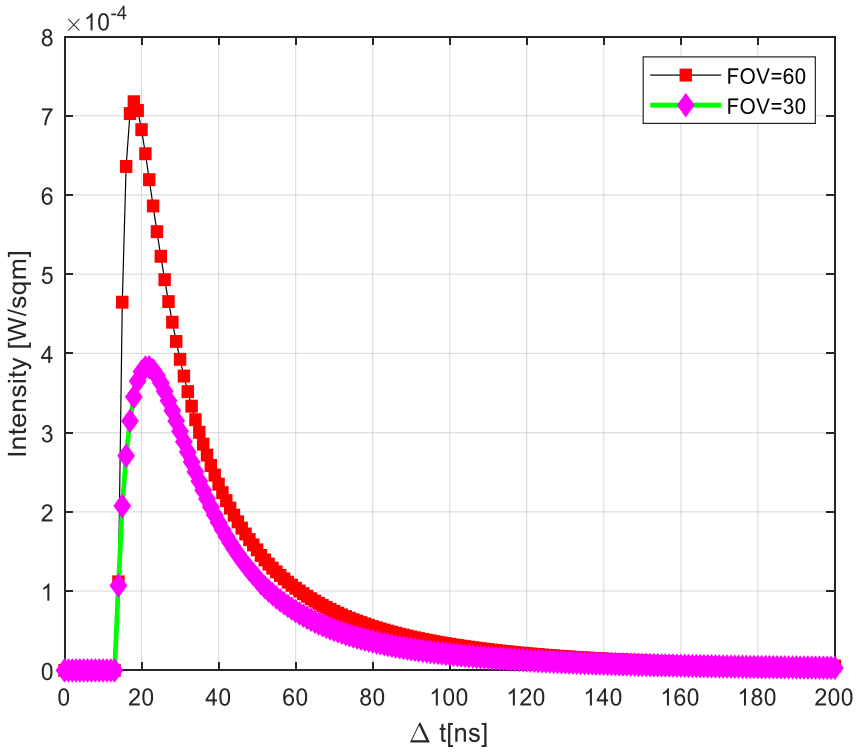
×10^-4
FOV=60
FOV=30
Intensity [W/sqm]
Δ t[ns]

(b) 8-PSK

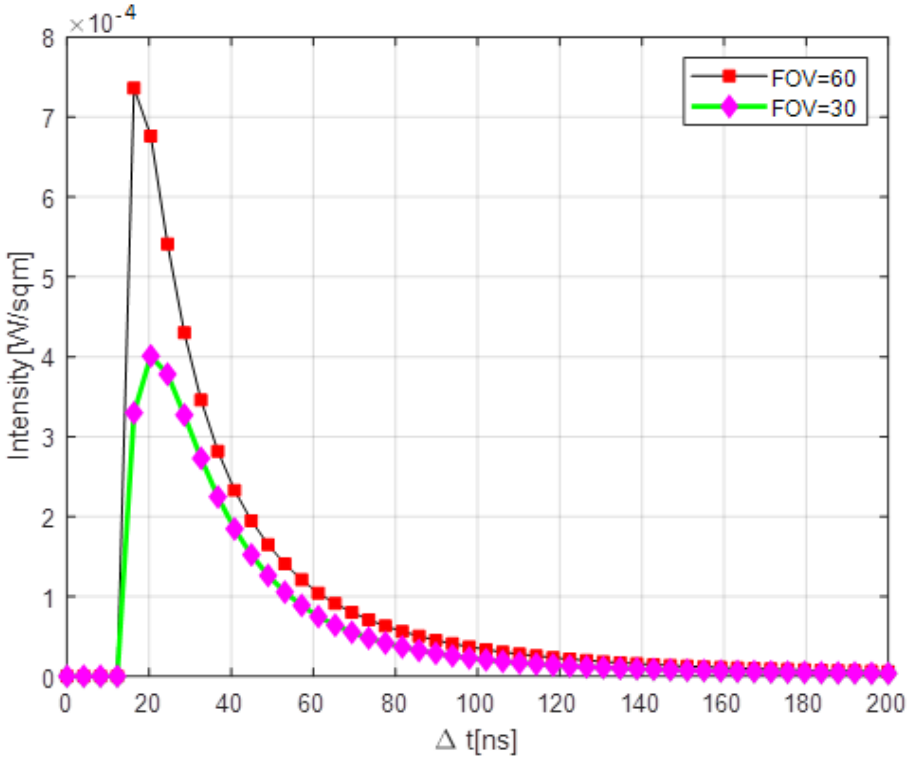

(c) 16-QAM

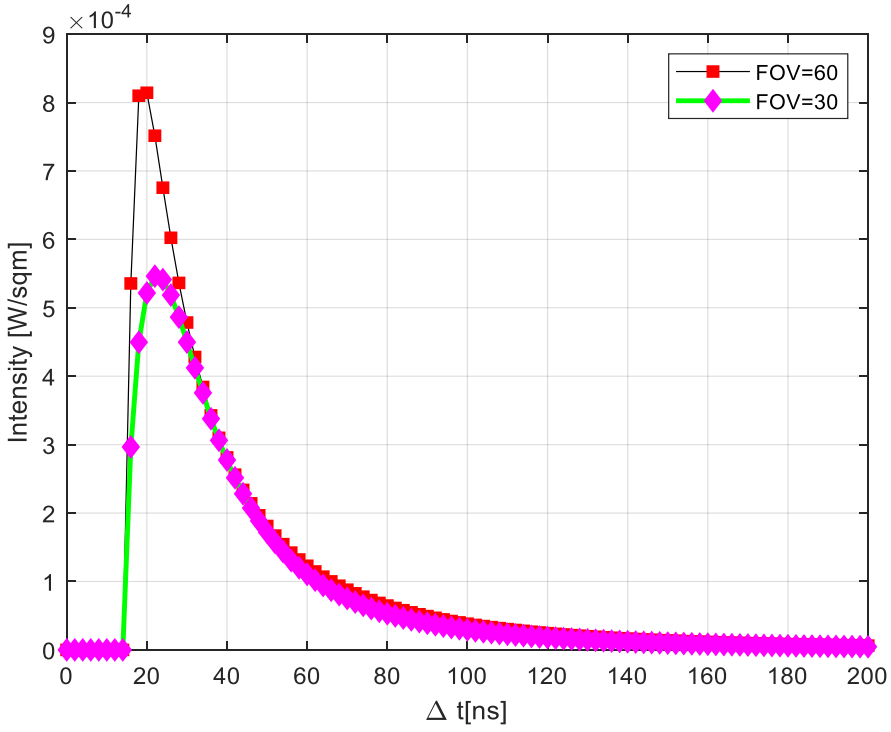

(d) 64-QAM

Fig. 4.9: Coastal water CIR curves for various modulation schemes using 30° and 60° FOV values

The results for the received intensity for each modulation scheme with 30° and 60° FOV values are listed in Table 4.3.

Table 4.3: Intensity for different modulation schemes

Modulation Type	Intensity (W/sqm)	
	FOV= 30°	**FOV= 60°**
QPSK	3.7×10^{-4}	6.8×10^{-4}
8-PSK	3.9×10^{-4}	7.2×10^{-4}
16-QAM	4.1×10^{-4}	7.4×10^{-4}
64-QAM	5.6×10^{-4}	8.2×10^{-4}

The whole concept here is that performance increases with wider FOV and higher modulation order. This is shown by the results.

The effect of the receiver's lens diameter on the impulse response is also shown Fig. 4.10. Two extreme cases are examined, too small a diameter (1 cm) and too large a diameter (45 cm) to clearly see the impact on the CIR. It can be clearly seen from the figure that the use of larger lens diameter allows significantly more photons to be more collected. This produces a 22 dB increase in the Impulse response when the receiver lens diameter increases from 1 cm to 45 cm (note that the received intensity I_r in dB corresponds to $10\,log_{10}\,I_r$ and it is used for convenience as the intensity is considered as the optical power). Enlarging the lens diameter also results in more scattered photons being collected, thus widening the channel impulse response.

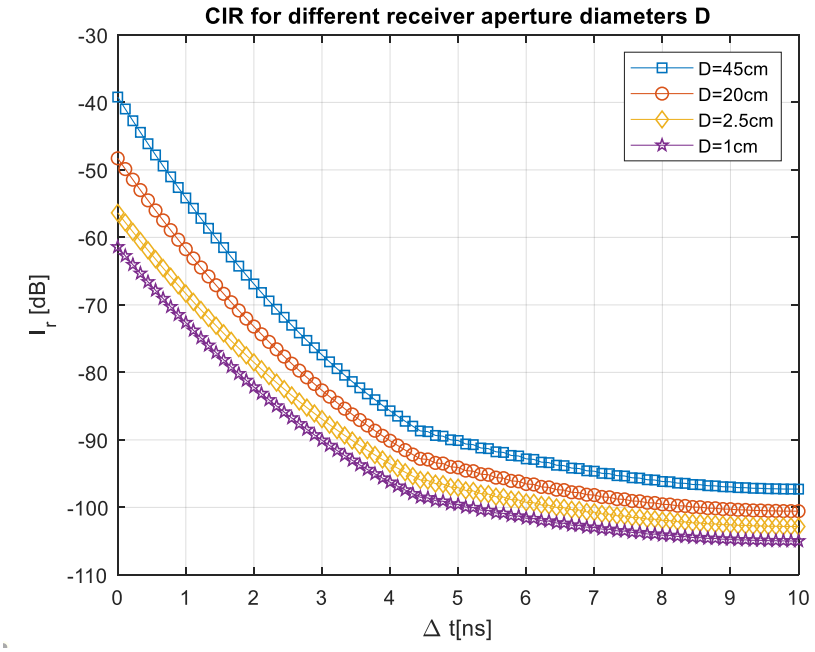

Fig. 4.10. CIR for different receiver aperture diameters.

Thus, based on the CIR results, 64-QAM was adopted to investigate BER and throughput of a complete communication system as a function of the customary ratio of the energy per bit to the noise power spectral density (E_b/N_0) at the receiver. The analysis was performed for a range of receiver bandwidths from 20 MHz and 420 MHz.

As shown in Fig. 4.11, the lowest BER is obtained by using a bandwidth of 20 MHz and the BER increased with bandwidth since the thermal noise at the receiver was proportional to the bandwidth. For a BER of 10^{-4}, at 20 MHz the sensitivity was 23.2 dB whereas this increased to 24.3 dB when using a 420 MHz bandwidth.

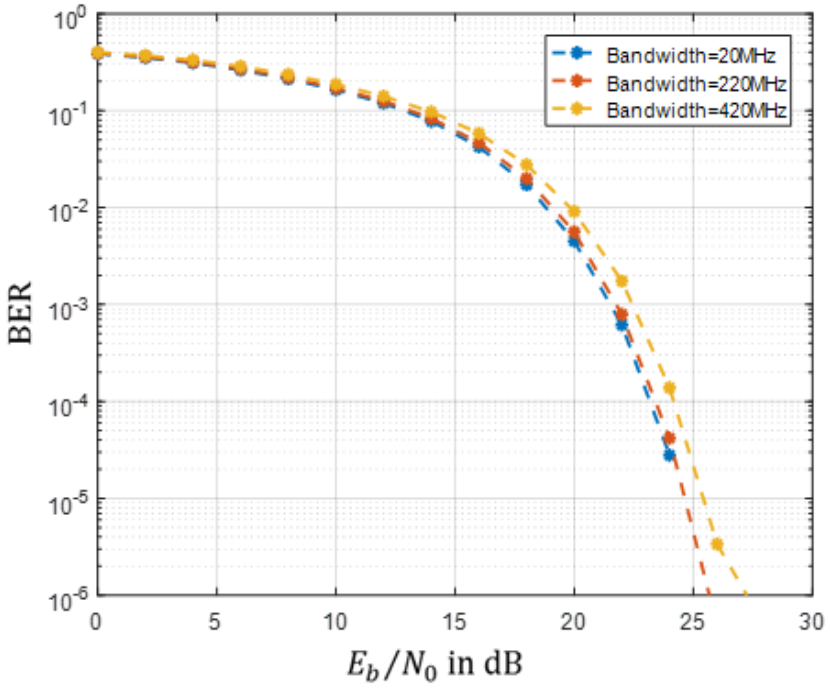

Fig. 4.11: BER of NLOS UOWC using 64-QAM.

Fig. 4.12, shows the system throughput results as a function of E_b/N_0. As would be expected, this increases with E_b/N_0 as the level of the signal relative to the noise improves. The bandwidth has only a small effect, becoming negligible for E_b/N_0 greater than approximately 20 dB. At this point, the throughput tends to the maximum value of 2.1 Mbps observed at $E_b/N_0 = 30$ dB.

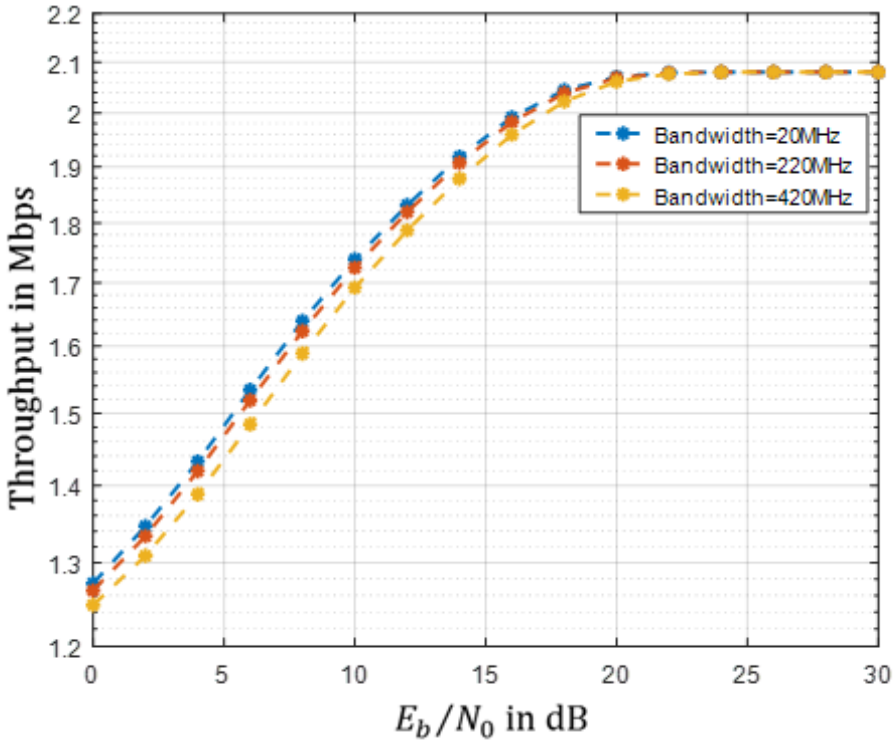

Fig. 4.12: Throughput of NLOS UOWC using 64-QAM.

4.8 CONCLUSION

The principles of MC modelling for UOWC were presented in this chapter. MC is a powerful tool in problem solving and equations that are difficult to solve using analytical methods due to many variables. The chapter also highlights the advantages and disadvantages of the MC simulation method. The mechanics and mathematically modelling of the MC simulation were also explained in detail. The details of and results from a simulation of the characteristics of a NLOS-UOWC transmission system have being presented. Using MC simulation based on the RTE, the effects of losses due to absorption, scattering, and attenuation in NLOS-UOWC links have been incorporated. The scattering is accommodated utilizing the commonly employed HG function. Initially, the CIR has been for clear ocean, coastal water and turbid water to ensure that the simulation was producing realistic results. Attention was then focused on the impact of the FOV for different modulation schemes in coastal waters, since these represent a likely environment for NLOS-UOWC applications as it must be acknowledged that

clear ocean admits the use of LOS systems, with turbid water offering similar but inferior performance to coastal water. The results demonstrate that the performance is better with 60° FOV and a higher modulation order. Thus, 64-QAM gives the best performance. The effect of the receiver lens diameter based on the simulation was also demonstrated and it was found, as may be expected, that a receiver with a large aperture diameter increases the CIR performance. The receiver bandwidth was found to have a relatively modest impact when varied from 20 MHz to 420 MHz, producing a maximum power penalty of 1.1 dB for the largest value. In terms of throughput, using a 100 Mbps transmission rate produced 2.1 Mbps over the channel because of its highly lossy nature. Nevertheless, it is possible to communicate at BER values that would enable the use of forward error correction to deliver highly reliable communication over useful distances.

CHAPTER 5

Modelling Impulse Response for NLOS Underwater Optical Wireless Communications

In turbid water environments (coastal and harbor), the presence of multiple scattering causes temporal spread of the beam pulse, characterized by the impulse response. This results in inter-symbol interference (ISI) and therefore limits the error performance of the system. UOWC requires efficient channel modelling to study the propagation properties of the light beam and evaluate the overall performance of the system. In this chapter, the characteristics of an NLOS UOWC link with multiple scattering is considered, different models of the phase scattering from underwater propagation are considered. The double gamma function (DGF) and weighted double gamma function (WDGF) are used to determine the impulse response of the channel for various link ranges, FOV and water type. MC numerical results validate the DGF and WDGF that are used to obtain temporal dispersion results for NLOS UOWC links in coastal and harbor water environments. Curve fitting using the analytical models shows correlation coefficients of between 0.98 and 0.99, demonstrating the utility of the models employed.

5.1 Introduction

As discussed in chapter three, Mobley's in-depth theoretical and experimental study of the interaction of light propagation in water with particles [186] showed that the scattering and absorption of the optical beam can be described by the IOPs of water. The absorption will cause an irreversible energy loss, so the blue-green spectral region of minimum absorption by seawater is used. Scattering introduces directional changes into the transmitted optical beams. In turbid harbour and coastal waters, there is multiple scattering, where photons change directions many times

during their propagation [147]. This causes temporal dispersion of the beam pulse and thus distortion of the received signal. The effect of multiple scattering is studied in [147].

So, in this work, the focus is on the temporal dispersion of NLOS UOWC channels and investigate the effect of the corresponding channel impulse response in turbid water environments. Recently, the impulse response of UOWC has been studied theoretically and experimentally. Most prior work has used MC simulations to model the impulse response [179] [190]; experimental work has validated the efficacy of this approach [124]. Jaruwatanadilok [133] developed an analytical model solution of the impulse response based on radiative transfer function theory. Inspired by the work in [122] on modelling the impulse response in clouds, Tang *et al.* [157] applied Double Gamma functions (DGF) to model the impulse response in line-of-sight (LOS) links. In [158], the DGF was modified by adding two parameters to model the impulse response. In previous work, the HG phase function [145] was used for scattering but here, a more realistic NLOS UOWC model was designed. Different scattering phase function models (the HG function, the Two Term HG function (TTHG), the Fournier-Forand phase function) and analytical impulse response models were used. The rest of the chapter is organized as follow. Section 5.2 describes the optical characterization of seawater and the NLOS channel model. In section 5.3 describes the different scattering phase function models of seawater. Section 5.4 describes the MC simulation, DGF and WDGF models of the impulse response. Results and discussion are presented in section 5.5 and finally section 5.6 concludes the chapter.

5.2 System Model

5.2.1 Optical Characteristics of Seawater

As introduced above, absorption and scattering influence photon propagation, resulting in direct loss and failure to capture photons at the receiver aperture (and hence loss), respectively. The energy loss generated

by these two processes can be evaluated by the absorption coefficient $a(\lambda)$, and scattering coefficient $b(\lambda)$, respectively. Moreover, the extinction coefficient (also known as attenuation coefficient) describes the overall energy loss in the channel which is the total effects of absorption and scattering processes.

It is worth mentioning that the values of these coefficients vary with the water type and the source wavelength of the light. In this chapter the focus is on the temporal spread in turbid water environments (coastal and harbour) with channel parameters with typical values taken from Mobley [186] summarized in table 5.1.

Table 5.1: Parameters in coastal and harbour water for blue/green light [5]

Water Types	$\boldsymbol{a}\{\boldsymbol{m^{-1}}\}$	$\boldsymbol{b}\{\boldsymbol{m^{-1}}\}$	$\boldsymbol{c}\{\boldsymbol{m^{-1}}\}$
Coastal	0.179	0.219	0.398
Harbor	0.366	1.824	2.190

5.2.2 NLOS Channel

An UOWC system with a NLOS link configuration is considered (similar to the NLOS system in chapter four) because the NLOS is more feasible in practical situations, not suffering from blocking by obstructions or alignment issues. The underwater channel in this analysis is assumed to be a homogenous medium without turbulence. The light pulse emitted from the transmitter section is temporally deteriorated through the underwater channel due to absorption and multiple scattering and then corrupted by the noise in the detector. AWGN is assumed at the receiver as explained in chapter four and the UOWC system can be modelled as

$$y(t) = h(t) * x(t) + n(t) \tag{5.1}$$

where $y(t)$ and $x(t)$ are the received and the transmit signal respectively, $h(t)$ is the impulse response for the UOWC links, $*$ is the convolution operator and $n(t)$ is the AWGN.

5.3 Scattering Phase function models of seawater

Unlike atmospheric free space optical links, light in the UOWC channel will encounter a large number of suspended particles such as mineral components, dissolved salts and organic matter. This produces more scattering, especially in harbor and coastal water. To study the effect of this multiple scattering, the scattering phase function (SPF) $\beta(\lambda,\theta)$ captures the energy distribution of the scattering effect versus the scattering angle θ. it is constrained so that:

$$2\pi \int_0^{\pi} \beta(\lambda,\theta)\, sin\,\theta\, d\theta = 1 \tag{5.2}$$

Petzold [135] measured the SPF for typical water types and several models have been proposed for it, which will now be described.

5.3.1 Henyey-Greenstein model

The long standing Henyey-Greenstein phase function (HGPF) was originally proposed by Henyey and Greenstein for galactic scattering in astrophysics [191]. The HGPF, defined by Eq. (5.3), is commonly used in ocean optics to model scattering of light [186].

$$\beta_{HG}(\theta) = \frac{1-g^2}{4\pi(1+g^2-2g\,cos\,\theta)^{3/2}} \tag{5.3}$$

where g is the average cosine of the scattering angle θ over all scattering directions and is termed the HG asymmetry parameter which depends on the medium characteristics. The best estimate is to set $g = 0.924$ as proposed in [141] for most practical situations.

5.3.2 The two term Henyey-Greenstein model

The HG function is simple and allows easy computation of the RTE. The two term HG function (TTHG) is a modified version which is a linear combination of the HG function proposed in literature [192] [193]. It has the form:

$$\rho_{TTHG}(\theta,\alpha,g_{FWD},g_{BKWD}) = \alpha\rho_{HG}(g_{FWD},\theta) + (1-\alpha)\rho_{HG}(-g_{BKWD},\theta) \tag{5.4}$$

where g_{FWD} and g_{BKWD} are the asymmetry factors of the forward and backward directed HG phase functions, and α is the weight of the forward-

directed HG phase function. The relationships between these parameters are provided in [142] and are described below.

$$\alpha = g_{BKWD}(1 + g_{BKWD})/(g_{BKWD} + g_{FWD})(1 - g_{FWD} + g_{BKWD}) \quad (5.5)$$

$$\overline{cos\,\theta} = \alpha(g_{BKWD} + g_{FWD}) - g_{BKWD} \quad (5.6)$$

$$g_{BKWD} = -0.3061446 + 1.000568 g_{FWD} - 0.01826338 {g^2}_{FWD} + 0.03643748 {g^3}_{FWD} \quad (5.7)$$

An approximate equation obtained via regression based on experimental data was proposed in [142]:

$$\overline{cos\,\theta} = 2\frac{1-2B}{2+B} \quad (5.8)$$

$$B = b_b/b \quad (5.9)$$

where b_b is the back-scattering coefficient.

5.3.3 Fournier-Forand phase function Model

Another analytic model of the phase function is the more realistic but more complicated Fournier-Forand phase function (FFPF) developed by Fournier and Forand under the assumptions that the particles have a hyperbolic size distribution and each particle scattering is according to the anomalous diffraction approximation to the exact Mie theory [143]. The FFPF can reproduce the shape of the measured phase functions in ocean water and can also reveal the inherent properties of the underwater channel. This phase function is given by:

$$\beta_{FF}(\theta) = \frac{1}{4\pi(1-\delta)^2\delta^v}\Big[v(1-\delta) - (1-\delta^v) + [\delta(1-\delta^v) - v(1-\delta)]\,sin^{-2}\left(\frac{\theta}{2}\right)\Big] + \frac{1-{\delta^v}_{180}}{16\pi(\delta_{180}-1){\delta^v}_{180}}(3\,cos^2(\theta) - 1) \quad (5.10)$$

Where $\delta = \frac{4}{3(n-1)^2} sin^2\left(\frac{\theta}{2}\right)$ and $v = \frac{3-\mu}{2}$,

Here n is the refractive index of the water, μ_{sl} is the slope parameter of the hyperbolic distribution (best fit of μ_{sl} = 3.5835 [145]), and finally, δ_{180} is δ evaluated at θ equal to 180 degrees.

A MC simulation approach that is described in the next section is used to evaluate the impulse response in NLOS configuration using the three scattering phase functions above with results as shown in Fig. 5.2. The FFPF gives the best performance because the HG function differs from Petzold's long established measurements in both small- (< 20°) and large-angles (> 130°); the TTHG function also underestimates Petzold's measurement for scattering angles < 1° [142]. Therefore, the FFPF is more realistic and more accurate as it does a far better job of reproducing the shape of phase functions in the underwater environment especially at smaller angles. Thus, the FFPF is applied to model the scattering in the rest of the chapter.

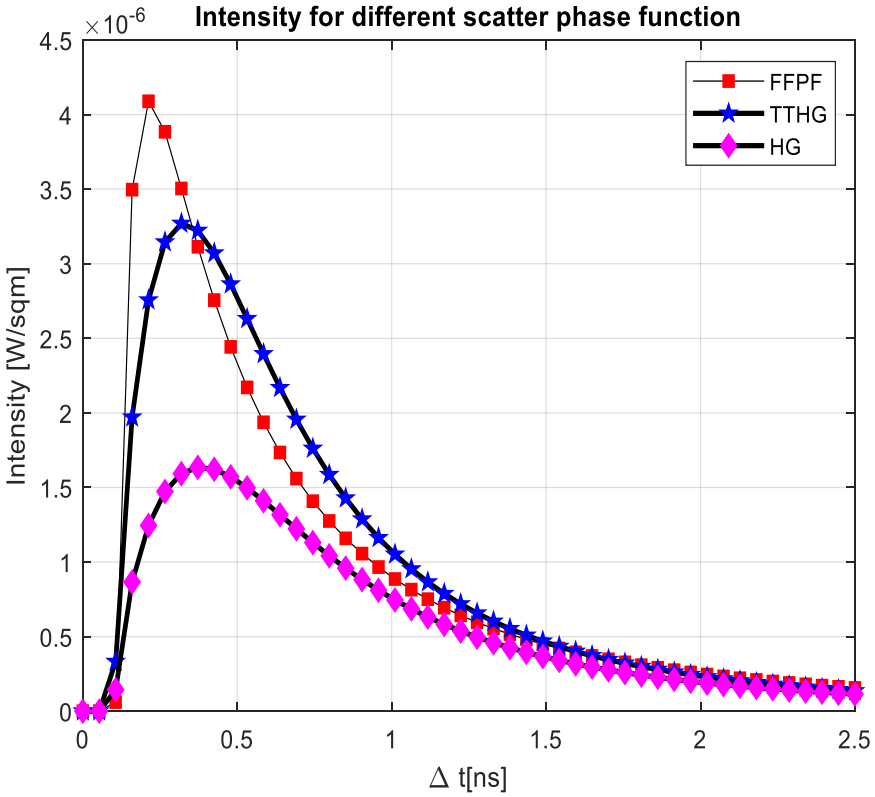

Fig. 5.1: Intensity for different scattering phase function

5.4 Impulse response modeling

A description of the MC, DGF and WDGF for modeling the impulse response is described in this section.

5.4.1 MC simulation model

To fully analyze the propagation of light underwater, it is necessary to solve the RTE [186]. The MC method is a numerical RTE solution, which applies statistics to evaluate the characteristics of the underwater channel by generating many photons and then simulating the interaction of these with the underwater medium. The MC method is much more flexible for various geometries without constraints on the scattering angles as compared to the analytical solutions of the RTE which are only available for a confined range of geometries. It is thus widely applied to simulate the propagation of light in dispersive media.

A MC approach similar to that of chapter four and the work in [30] and [31] was adopted. Here, a set of photons was emitted by the transmitter with specific divergence angle. Each photon's interaction with the underwater medium comprised absorption and multiple scattering and could be modelled by altering the basic characteristics of each photon (photon position, transmit direction, weight and propagation time) during the propagation. These attributes were then recorded when the photon reached the detector. The channel characteristics such as path loss and impulse response were obtained by collecting and analysing the primary attributes of all received photons. These included the position of the photon in Cartesian coordinates (x_0,,y_0, z_0), the transmission direction which was described by the zenith and azimuthal angle (θ, ϕ), weight W and the propagation time t. Each individual photon was initialized at (0,0,0) with unity weight and zero start time; the emission direction depended on the divergence angle [133]. Each individual photon may interact with the underwater medium when travelling a distance Δs, which could be determined by (5.11) below.

$$\Delta s = -\frac{log(\xi^s)}{c(\lambda)} \tag{5.11}$$

with ξ^s being a uniform random variable (RV) between [0, 1] (denoted by $R[0,1]$). The spatial position and propagation time could be updated

subsequently after Δs was determined. The photon weight could also be updated as below:

$$W^{n+1} = W^n(1 - a/c) \tag{5.12}$$

with W^n being the weight of the photon after the n^{th} interaction with the underwater medium. The scattering processes also affected the direction of the photon trajectory and thus, the zenith angle is generated by applying the equation below [194]:

$$\theta = F_{FF}^{-1}(X) \tag{5.13}$$

where, again $R \sim U[0,1]$. The azimuthal angle could also be obtained by:

$$\phi = 2\pi . R[0,1] \tag{5.14}$$

The next step was to transfer the zenith and azimuthal angles in (5.13) and (5.14) into the absolute Cartesian coordinate system since the scattering angles before interactions were relative rotation angles.

Then, the cycle of step size, weight reduction and photon scattering was repeated and the tracking of each individual photon stopped when its weight was lower than a certain threshold or when it got to the receiver plane. In the former case, a photon of negligible weight was considered absorbed. This threshold was set to 10^{-4} here to avoid overly long simulations and it is verified that this was sufficient for the results presented in this chapter. In the latter case, the photon was considered received if it was in the receiver aperture and field of view FOV; otherwise, it was considered lost. The steps above were repeated for each photon and the attributes for all the detected photons recorded. The channel impulse response was then estimated by summing the weights of the photons with the same propagation time and then normalizing this using the total transmitted weight.

5.4.2 Double Gamma Function

The transportation of energy in UOWC channels can be divided into two regions according to the measurement in [141], where multiple and non-scattering light dominate, respectively. For small values of the optical thickness (attenuation length), $\tau = c(\lambda)L$, where L is the physical link range,

the path loss follows Beer's law [147] because non-scattered light dominates. However, as τ increases multiple scattering becomes more pronounced and the path loss deviates from Beer's law. In the non-scattering region, there is negligible dispersion as verified by Gabriel *et. al* in [27], so here the focus has been on the NLOS UOWC links in harbor and coastal waters where τ is relatively large.

A single gamma function model has been used in [156] to model the impulse response for a NLOS link geometry. The DGF was initially adopted by Mooradian and Geller in [122] to model the impulse response in clouds and inspired by the dispersive nature of both cloud and the underwater environment, modelling was then performed of the impulse response in NLOS UOWC for different link ranges using the DGF in coastal and harbor water environment where multiple scattering dominates. Such a function can be written as:

$$h_{DGF}(t) = C_1 \Delta t e^{-C_2 \Delta t} + C_3 \Delta t e^{-C_4 \Delta t} \tag{5.15}$$

where $\Delta t = t - t_0$, in which t is the time scale, $t_0 = L/v$ (the ratio of the link range over the speed of light in water) also known as the non-scattering propagation time . C_1, C_2, C_3, C_4 are parameters to be found, which can be computed from MC simulation using a non-linear least square criterion in a scientific computing software, for example, MATLAB:

$$(C_1, C_2, C_3, C_4) = argmin(\int [h_{DGF}(t) - h_{mc}(t)]^2 dt) \tag{5.16}$$

where $argmin(.)$ is the operator to return the argument of the minimum, $h_{DGF}(t)$ is the model of the DGF and $h_{mc}(t)$ is the impulse response results of the MC simulation.

5.4.3 Weighted Double Gamma functions

The DGF is only applicable where the multiple scattered light is dominant and with a relatively large values of the attenuation length. In [158], two parameters were added to the DGF in order to generalize the functions known as the weighted double gamma functions (WDGF) which is applicable for both small and large values of τ . The WDGF has the form:

$$h_{WDGF}(t) = C_1 \Delta t^{\alpha} e^{-C_2 \Delta t} + C_3 \Delta t^{\beta} e^{-C_4 \Delta t} \tag{5.17}$$

where α,β are the two added parameters to be determined using a similar criterion to section 5.4.2 using $h_{WDGF}(t)$ instead of $h_{DGF}(t)$. Thus, The values of the set of parameters$\{C_1, C_2, C_3, C_4, \alpha, \beta\}$ can be computed in scientific software like MATLAB using non-linear least square criterion given by:

$$\{C_1, C_2, C_3, C_4, \alpha, \beta\} = argmin \int [h_{WDGF}(t) - h_{MC}(t)]^2 \, dt \qquad (5.18)$$

The WDGF is also applied to model the impulse response in our NLOS UOWC channel in coastal and harbour water environment. Results are discussed in next section.

5.5 Results and Discussion

The NLOS UOWC system with a 532nm source wavelength and a photodetector with a 20cm aperture were considered. A divergent source over a collimated one was chosen aimed at increasing the temporal dispersion. The speed of light in water is kept at a typical value of $v_{water} = 2.237 \times 10^8 \ \mathrm{m\ s^{-1}}$. Based on the above settings, MATLAB was used to simulate the beam propagation using MC method for various link lengths and FOVs in coastal and harbor water using 10^9 transmission photons for each scenario. The MC impulse response was then obtained and a fit to it produced using the DGF and the WDGF separately. The results of four link ranges are presented, reflecting coastal and harbor waters for both the DGF and WDGF, in Figs 5.3 and 5.4 respectively for a range of FOV values.

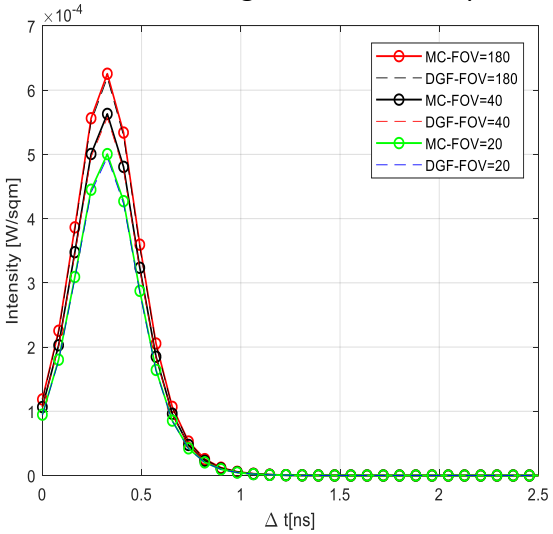

(a) 40m Coastal water

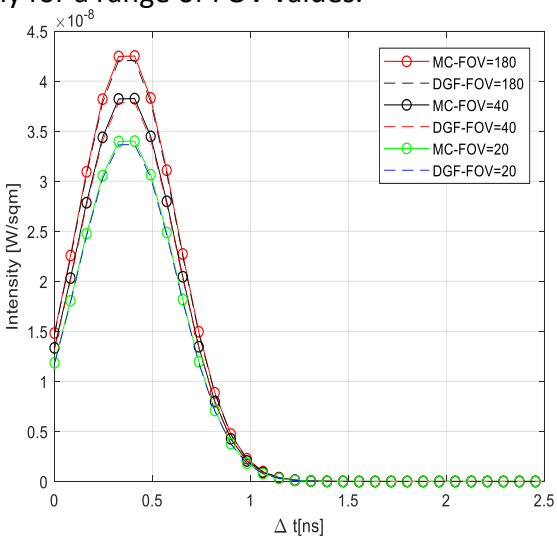

(b) 8m harbor water

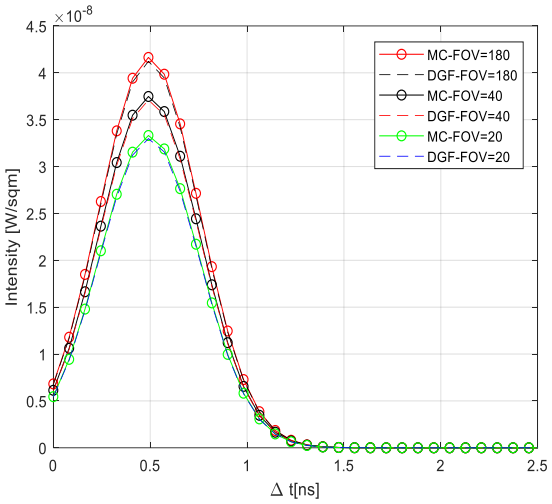

(c) 60m coastal water

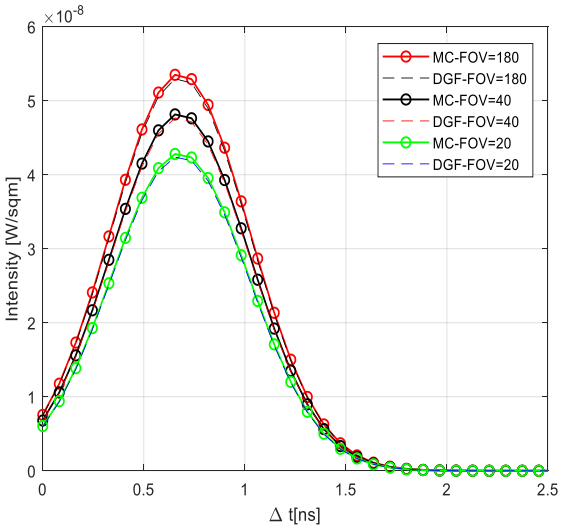

(d) 12m harbour water

Fig. 5.2: MC and DGF Impulse response for coastal and harbour waters in various link ranges

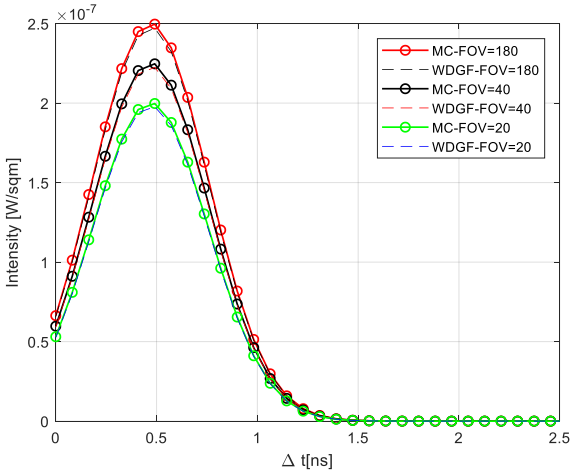

(a) 40m Coastal water

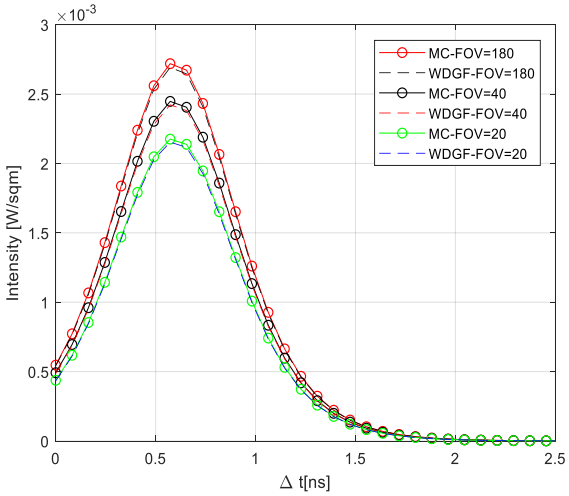

(b) 60m Coastal water

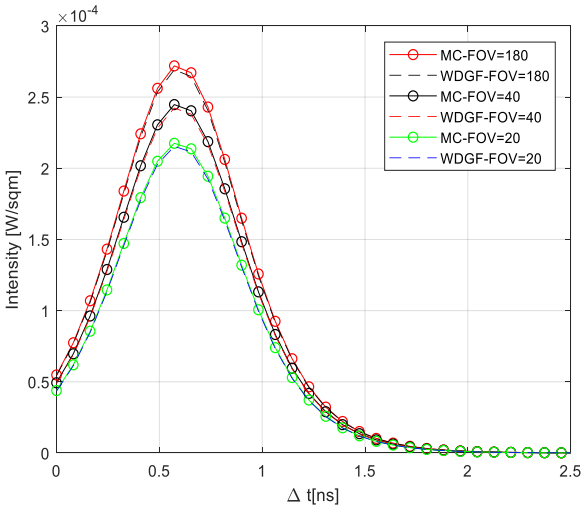

(c) 8m harbour water

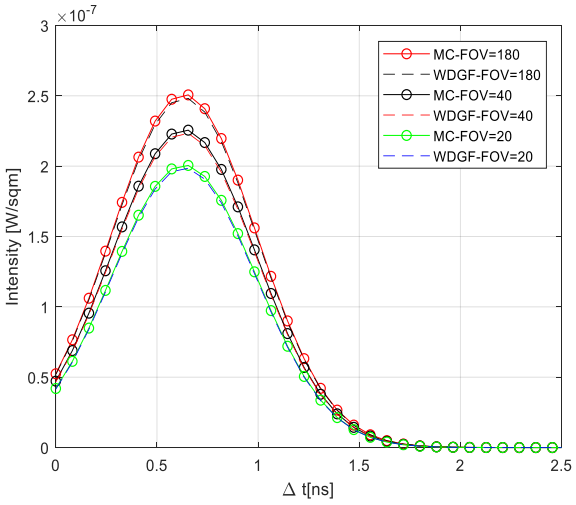

(d) 12m harbour water

Fig. 5.3: MC and WDGF Impulse response for coastal and harbour water in different link ranges

Both figures show that the DGF and WDGF fit well with the NLOS simulated impulse response regardless of the field of view, link range and water type. The increased dispersal with τ is clear there is more scattering with the greater effective distance travelled.

Furthermore, the R-square coefficient of determination was used to quantify the fits [195]. This ranges from zero to one, with higher values being better. Table 5.2 shows the values of R-squared for both DGF and WDGF models in different link ranges of coastal and turbid harbor water. It may be seen that the WDGF gives a little better numerical performance than the DGF but both have R-squared values approaching 0.99. Therefore, utilizing FFPF as scattering phase function and WDGF for modelling the impulse response provides a plausible and more convenient way to evaluate UOWC system performances for different link configurations.

Table 5.2: Curve fitting results for Coastal and Harbor water.

Link Range	**R-square value for DGF**	**R-square value for WDGF**
40 m Coastal	0.986	0.988
60 m Coastal	0.987	0.989
8 m Harbor	0.987	0.988
12 m Harbor	0.989	0.990

5.6 Conclusion

In this chapter, the temporal dispersion of NLOS UOWC links resulting from multiple scattering in coastal and harbor water environments has been investigated. Different scattering phase function models, namely the HG function, TTHG function and the FFP function were considered with the FFP function given the better performance as illustrated in fig 5.2. Then modelling was performed on the channel impulse response using DGF and WDGF for NLOS UOWC links in coastal and harbor water. Results show that both the DGF and WDGF models fit MC simulation results well for NLOS UOWC channels regardless of the link range, FOV, and water type. The R-squared coefficient of determination applied in the system shows that the

WDGF gives a little better numerical performance than the DGF in terms of modelling the NLOS UOWC channel for example 60 m coastal water gives R-square value of 0.989 utilizing WDGF and 0.987 using DGF. This value reaches 0.990 at best. Therefore, utilizing FFPF as scattering phase function and WDGF for modelling the impulse response provides a plausible and more convenient way to evaluate UOWC system performances for different link configurations.

CHAPTER 6

Performance of Non-Line of Sight Underwater Optical Wireless Communication Links with Spatial Diversity

This chapter presents the performance of a spatially diverse NLOS UOWC system employing continuous phase modulation (CPM), which is shown to offer sensitivity benefits of several dBs over OOK without coherent reception. The channel impulse response (CIR) is obtained by using Monte Carlo (MC) simulation, including absorption and multiple scattering. Turbulence is included by conditioning the CIR on log-normal statistics. To mitigate the resultant fading, the chapter exploits spatial diversity with equal gain combining at the receiver side. Photon counting at the receiver is employed to accommodate shot noise. The Saddlepoint and Gaussian approximations are compared for bit error rate (BER) calculations, using the latter for later calculations as it delivers excellent results and is simpler. The results show that spatial diversity offers performance improvements, for example an 8 dB sensitivity gain at 10^{-9} BER using 1 Gbps 3×1 multiple-input single-output (MISO) transmission over a 20 m link with 0.16 log-amplitude variance. This chapter also determines using an upper bound that Inter-symbol Interference (ISI) has a significant impact at high bit rates, producing error floors for multiple-output arrangements.

6.1 Introduction

Underwater, absorption and multiple scattering are the two main factors that induce power loss and degrade the performance of UOWC systems [154]. Thus, a considerable amount of effort in prior chapters has gone into channel absorption and scattering effects. Optical turbulence is another

impairment which has a significant impact on the performance of UOWC systems. It results from random variations in the refractive index in water arising from ocean temperature and salinity fluctuations leading to fading or received intensity fluctuations, hence degrading UOWC system performance [166]. This contrasts with acoustic links, where multipath reflections are the major source of fading [52]. The study of the impact of turbulence on UOWC systems has received relatively little attention compared to turbulence-induced fading in free space optical communications, where the results of many valuable studies on fading characterization and mitigation have been reported [4]. However, this has begun to change recently with the study of the statistical properties of a gaussian beam travelling through turbulent water [127], [196] Furthermore, the Rytov method has been used to determine the scintillation index of plane and spherical optical wave propagating in the turbulent underwater medium [167]. Vali *et al.* [197] used MC simulation to model UOWC turbulence. They successfully reproduced the lognormal probability density function (PDF) of the received intensity in weak and moderate oceanic turbulence, and their results were in accordance with previous experimental studies.

One of the favorable solutions to resolve the turbulence problem in UOWC is spatial diversity, often using multiple-input-multiple-output (MIMO) transmission that has been extensively studied in visible light and optical fibre communications [198] [199] [200]. MIMO is also essential for large scale implementation of UWSNs [14]. MIMO offers spatial diversity gain and performance improvements compared with employing single-input single-output (SISO) transmission. The performance of MIMO-UOWC has been investigated by Jamali and Salehi [201], whose simulation results showed that MIMO can enhance the communication range and alleviate the turbulence-induced fading of the channel. Previously, Simpson [108] used two light emitting diode (LED) transmitters and two pin photodiode receivers to obtain the advantage of spatial diversity in UOWC.

So, this chapter uses a NLOS link and take all the channel impairments (absorption, scattering and turbulence) into account. The performance of spatial diversity employing continuous phase modulation (CPM) is investigated. An equal gain combiner (EGC) is assumed at the receiver side and the BER performance is evaluated using the Gaussian approximation (GA) and the Saddlepoint approximation (SPA) [202]. The chapter also employs a photon-counting approach to include the impact of shot noise. The channel free-fading impulse response is obtained using MC simulation by taking absorption and scattering into account. This is multiplied by the square of a fading coefficient modelled as a lognormal random variable for oceanic turbulence.

The remainder of this chapter is organized as follows. Section II describes channel modelling employed, including the fading induced by turbulence. Section III presents the principles of the proposed MIMO UOWC system, including a description of CPM. Section IV introduces the BER expressions with EGC at the receiver. In Section V, the results for various system configurations is presented followed by a discussion of the performance. Finally, Section VI concludes the chapter.

6.2 Channel Modelling

This section describes the model of the NLOS underwater channel used. This includes the underwater impairments of absorption, scattering and turbulence.

6.2.1 A*bsorption and scattering*

As discussed in prior chapters, the interaction between a photon and a water particle in the propagation of the optical beam under the water induces either absorption or scattering. The former causes the translation of photon energy into other forms such as thermal energy, which is irreversible. The latter deflects the photon's direction of travel, which also appears as a transmission energy loss because receiver has a finite sized aperture that will capture fewer photons. The extinction (attenuation)

coefficient $c(\lambda)$ describes the total loss of energy; it is the sum of the absorption coefficient $a(\lambda)$ and the scattering coefficient $b(\lambda)$ i.e. $c(\lambda) = a(\lambda) + b(\lambda)$. There is considerable variation in $a(\lambda)$ and $b(\lambda)$ (hence in $c(\lambda)$) with water types and source wavelength [203]. As mentioned in chapter one, it has been shown in the literature that absorption and scattering have the lowest impact in the blue-green wavelength interval $450nm \leq \lambda \leq 550nm$ and therefore UOWC systems apply this region of the visible light spectrum for data communications [28].

In this chapter, the free fading impulse response between the ith transmitter (Tx) in the system and the jth receiver (Rx) is denoted by $h_{0,ij}(t)$. This is found by using MC simulation including both absorption and scattering in the NLOS UOWC link similar to the previous work in chapter four. To derive the scattering coefficient, the volume scattering function (VSF) is needed. This describes the angular distribution of light scattered by a suspension of particles at a given wavelength, making use of a phase function [204]. There are several choices for this as described in chapter three but here, the Fournier-Forand function is employed as it provides better performance compared to the more common Henyey-Greenstein (HG) and two-term HG functions [32].

6.2.2 Turbulence

The most commonly occurring natural examples of optical turbulence are the Earth's atmosphere and the ocean. The physical mechanism of underwater optical turbulence is similar to that of atmospheric optical turbulence since both are mainly caused by the random fluctuations of pressure and temperature of the medium. Description of the absorption and scattering factors was presented in the previous subsection. To capture the turbulence effects, the free fading impulse response $h_{0,ij}(t)$ is multiplied by the square of a fading coefficient ${\alpha^2}_{ij}$ with a log-normal distribution for oceanic weak turbulence [83]. To model the fading presented by turbulence, let $\alpha = \exp(X)$ so that this has a log-normal fading probability density function (PDF) [83]:

$$f(\alpha) = \frac{1}{\alpha\sqrt{2\pi\sigma_X^2}} \exp\left(-\frac{(\ln(\alpha) - \mu_X)^2}{2\sigma_X^2}\right) \tag{6.1}$$

Thus, μ_X and σ_X^2 are the mean and variance of the Gaussian distributed fading log-amplitude$X$. Normalizing the fading amplitude ensures that the fading does not attenuate or amplify the average power, i.e. $E[\alpha^2] = 1$ implying that $\mu_X = -\sigma_X^2$ [83].

Therefore, to describe the fading statistics there is a need to determine the relationship between this variance to the turbulence parameters of the ocean. The scintillation index of a light wave with instantaneous point intensity, I, is denoted by σ_I^2 and defined by Korotkova *et al.* [127] as:

$$\sigma_I^2 = \frac{\langle I^2 \rangle - \langle I \rangle^2}{\langle I \rangle^2} \tag{6.2}$$

The scintillation index of light in the turbulent underwater medium can be expressed using the Rytov approximation as [205]:

$$\sigma_I^2 = \exp\left[\frac{0.49\sigma_r^2}{\left(1 + 1.11\sigma_r^{12/5}\right)^{\frac{7}{6}}} + \frac{0.51\sigma_r^2}{\left(1 + 0.69\sigma_r^{12/5}\right)^{\frac{5}{6}}}\right] - 1. \tag{6.3}$$

In (3), σ_r^2 is the Rytov variance [204].

$$\sigma_r^2 = 37.3K(2\pi/\lambda)^{7/6}L^{11/6} \tag{6.4}$$

where L is the migration length of the light beam and K is a constant that determines the strength of the turbulence [161]. The value of K ranges from 10^{-14} to 10^{-8} $\mathrm{m}^{-2/3}$ which is several orders of magnitude greater than the values of the corresponding constant in atmospheric optical turbulence [161].

6.3 System model

The system considered is based on LEDs, which are more suitable than lasers because their wider divergence angles make alignment less critical in turbid

water [14]. Although LEDs historically offered modest bit rates, recent developments have removed this drawback [206].

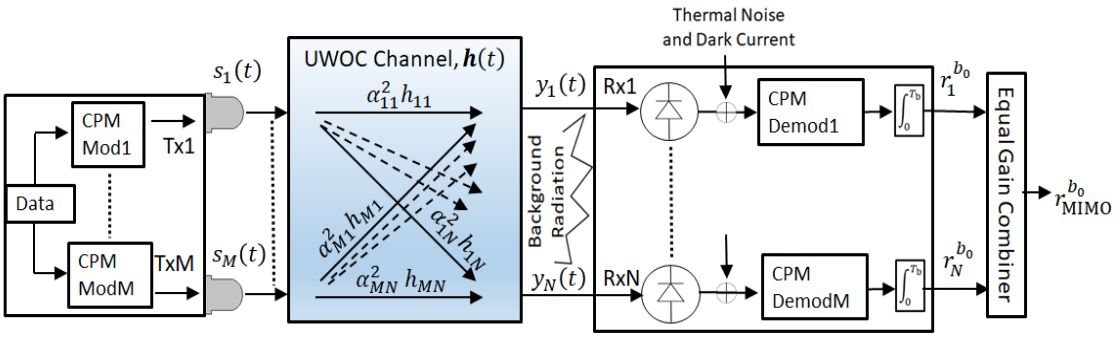

Fig. 6.1: Proposed Architecture of NLOS-MIMO-UOWC System(adapted from [83])

6.3.1 MIMO UOWC Model

A MIMO UOWC system abstracted as in Fig. 6.1 is considered, which employs a Tx array of M LEDs that can provide high data rate communications to an array of N Rx photodetectors followed by an equal gain combiner (EGC). The EGC is employed because it has been shown to offer performance close to optimal combining but with considerably reduced complexity [83].

The LEDs are modulated by the electrical inputs after these have been converted to either OOK or the CPM scheme described in Section 6.3.2. The received optical signal $\boldsymbol{y}(t)$ in a $M \times N$ MIMO system may be described in terms of the transmitted signal $\boldsymbol{s}(t)$ convolved with a $M \times N$ channel impulse response matrix $\boldsymbol{h}(t)$ and multiplied by a matrix $\boldsymbol{A2}(t)$ that contains the squares of the fading coefficients α_{ij} between transmitter i and receiver j, whose amplitude PDF was defined in Section 6.2.2 above [83]:

$$\boldsymbol{y}(t) = \boldsymbol{A2}(\boldsymbol{t}).\boldsymbol{h}(t) * \boldsymbol{s}(t) \tag{6.5}$$

This then experiences various sources of noise that must be included in the analysis, namely background optical radiation, dark current and additive white Gaussian noise (AWGN).

6.3.2 Continuous Phase Modulation (CPM)

The term Continuous-Phase-Modulation (CPM) refers to a class of coded modulation schemes possessing desirable power and bandwidth efficiency [207]. Although CPM has been shown to achieve near capacity performance in optical communications [208], this has been based on coherent detection with the need for perfect receiver channel state information. When performing hard signal detection at the receiver, CPM also has the advantage that it does not require dynamic thresholding for optimal detection.

CPM presents a constant signal envelope with a continuous phase and constant transmitted carrier power. It is a multi-level scheme and in classical m-ary CPM, a symbol corresponds to $M = \log_2 m$ bits. The discrete CPM modulator shown in Fig. 6.2 produces a signal with symbol duration T described by, for the time interval $lT < t < (l+1)T$, using an arbitrary phase offset φ_0 and instantaneous phase $\varphi(t)$ [209]:

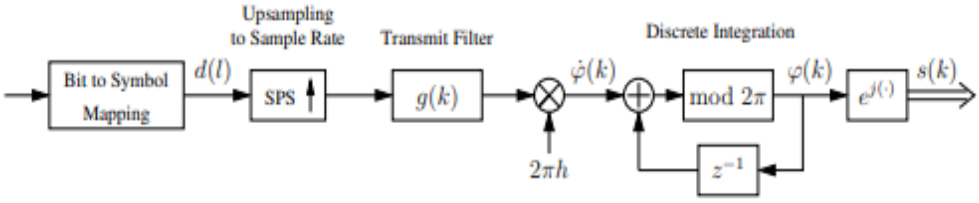

Fig. 6.2: Discrete CPM modulator [27]

$$s(t) = e^{j(\varphi(t)+\varphi_0)} \tag{6.6}$$

$$\varphi(t) = 2\pi h \int_0^t \sum_{i=0}^{l} d(i)g(\tau - iT)d\tau \tag{6.7}$$

where h is the modulation index, $g(t)$ is the transmit filter with the symbols $d(i)$ taken from an M-ary alphabet, where M is even. Fig. 6.2 also shows the

process of symbol upsampling by a factor SPS, where $SPS-1$ zeros are inserted between two successive symbols. The transmit filter has a raised cosine impulse response:

$$g(k)=\begin{cases}\frac{1}{2L\,.SPS}\left(1-\cos\left(\frac{2\pi k}{L.SPS}\right)\right) & 0\le k\le L.SPS\\ 0 & otherwise\end{cases} \tag{6.8}$$

L is the length of the impulse response in symbol intervals. Using $L=1$ produces full response CPM, whereas using L > 1 results in a partial response, where intersymbol interference (ISI) is introduced for increased spectral efficiency [209]. The response $g(k)$ also fulfils the normalization condition:

$$\sum_{k=0}^{L.SPS} g(k)=\frac{1}{2} \tag{6.9}$$

6.4 Photon-Counting BER Analysis

In this section, the system BER is expressed analytically using a photon-counting method and then applying either the GA or the SPA. Assuming OOK signalling, each bit '1' (ON-state) will be transmitted with a pulse shape $P(t)$ and it is off when sending data bit '0'. For simplicity, the consideration is the case when $P(t)$ can be expressed as in terms of a unit rectangular pulse $\prod(t)$ in the interval [-1/2, 1/2] and the bit duration time T_{b} as $P(t)=\prod(\{t-0.5T_{\mathrm{b}}\}/T_{\mathrm{b}})$. Hence, the transmitted signal can be expressed as:

$$S(t)=\sum_{k=-\infty}^{\infty} b_k P(t-kT_{\mathrm{b}}) \tag{6.10}$$

for bit $b_k \in \{0,1\}$ in the k^{th} time slot. In the case of SISO, the free-fading impulse response is denoted by $h_0(t)$ and the fading coefficient by α. Therefore, after propagating through the channel, the received optical SISO signal becomes:

$$y(t)=S(t)*\alpha^2 h_0(t)=\alpha^2\sum_{k=-\infty}^{\infty} b_k \Gamma(t-kT_{\mathrm{b}}) \tag{6.11}$$

where $\Gamma(t) = h_0(t) * P(t)$ and $*$ denotes the convolution operator.

In the case of MIMO, to make a fair comparison with SISO, using *M* transmitters the total transmitted power for the ON-state is $P = \sum_{i=1}^{M} P_i$, where P_i is the power transmitted by $\mathrm{Tx_i}$. So, the transmitted signal hereon from $\mathrm{Tx_i}$ is:

$$S_i(t) = \sum_{k=-\infty}^{\infty} b_k P_i(t - kT_b) \tag{6.12}$$

Thus, the received optical signal after the signal passes from $\mathrm{Tx_i}$ through the channel impulse response $\alpha_{ij}^2 h_{0,ij}(t)$ to $\mathrm{Rx_j}$ will be:

$$y_{i,j}(t) = S_i(t) * \alpha_{ij}^2 h_{0,ij}(t) = \alpha_{ij}^2 \sum_{k=-\infty}^{\infty} b_k \Gamma_{i,j}(t - kT_b) \tag{6.13}$$

with $\Gamma_{i,j}(t) = P_i(t) * h_{0,ij}(t)$. The signals transmitted from all the transmitters are captured at the *j*th receiver each with its channel impulse response i.e. at the *j*th receiver, the optical signal received will be $y_j(t) = \sum_{i=1}^{M} y_{i,j}(t)$.

Now, the receiver output is given by $U = N + \xi$, in which N is a poisson distributed Random variable (RV) with mean $m^{(b_0)}$that includes dark current and background radiation for $b_0 \in \{1,0\}$, and ξ is a zero mean Gaussian distributed RV with variance σ^2. The GA probability of error is then [202]:

$$P_e = Q\left(\frac{m^{(1)} - m^{(0)}}{\sqrt{m^{(1)} + \sigma^2} + \sqrt{m^{(0)} + \sigma^2}}\right) \tag{6.14}$$

where $Q(x) = \left(1/\sqrt{2\pi}\right) \int_x^{\infty} \exp(-y^2/2)\, dy$ is the Gaussian Q-function.

The system BER established using the SPA can be expressed as [202]:

$$P_e = \frac{1}{2}[q_+(\beta) + q_-(\beta)] \tag{6.15}$$

where $q_+(\beta)$ and $q_-(\beta)$ are the error probabilities when binary "0" and "1" are sent respectively, namely that the photoelectron count at the output of the receiver, z, fulfils:

$$q_+(\beta) = Pr(z > \beta|\text{zero}) \approx \frac{\exp[\phi_0(s_0)]}{\sqrt{2\pi\phi_0''(s_0)}} \tag{6.16a}$$

$$q_-(\beta) = Pr(z \leq \beta|\text{one}) \approx \frac{\exp[\phi_1(s_1)]}{\sqrt{2\pi\phi_1''(s_1)}} \tag{6.16b}$$

$$\phi_{b_\text{i}}(s) = \ln\left[\psi_{z(b_\text{i})}(s)\right] - s\beta - \ln|s| \tag{6.16c}$$

where $b_\text{i} = 0{,}1$ and $\psi_{z(b_\text{i})}(s)$ is the moment generating function (MGF) of the receiver output when binary value b_i is sent. Moreover, s_0 is the positive, real root of $\phi_0'(s)$ and s_1 is the negative, real root of $\phi_1'(s)$. The receiver optimum threshold β is chosen so that it reduces the probability of error (i.e. $P_{be}/d\beta = 0$).

The next sub sections present the required expressions for both the GA and SPA for the different link configurations when EGC is used.

6.4.1 SISO UOWC Link

From the previous section, the received SISO photodetected signal can be expressed as:

$$r_{SISO}^{b_0} = y_{SISO}^{(b_0)} + v_{th} \tag{6.17}$$

Here, $y_{SISO}^{(b_0)}$ is a Poisson distributed RV with mean $m^{(b_0)}$, conditioned on α and $\{b_k\}_{k=-L}^{0}$, that is given by [161]:

$$m^{(b_0)} = \frac{\eta\alpha^2}{hf}\left\{\sum_{k=-L}^{0} b_k \Gamma_k^{\mathrm{Int}}\right\} + (\gamma_b + \gamma_d)T_b \tag{6.18a}$$

$$\Gamma_k^{\mathrm{Int}} = \int_0^{T_b} \Gamma(t - kT_b)dt \tag{6.18b}$$

where η, f, h, and L are the quantum efficiency, Planck's constant, carrier frequency of the optical source and channel memory, respectively. The mean count rates of the Poisson distributed dark current noise and background radiation are γ_d and γ_b, respectively.

The other noise contribution, v_{th} is a zero mean Gaussian distributed RV corresponding to the integrated thermal noise with variance σ_{th}^2, given by:

$$\sigma_{th}^2 = \frac{2k_b T_b T_r}{R_L\, q^2} \tag{6.19}$$

where $k_b, T_r, R_{L,} q$ are Boltzmann's constant, receiver equivalent temperature, load resistance and the electronic charge respectively.

The receiver output MGF conditioned on α is given below [83]:

$$\psi_{z\ \ {}^{(b_0)}_{SISO}|\alpha}(s) = M_{\mathrm{T}}(s) M_{\mathrm{SISO}}(s) M_{\mathrm{SISO-ISI}}(s) \tag{6.20a}$$

$$M_{\mathrm{SISO}}(s) = \exp\left(\left[\gamma_{SISO}^{(bd)} + \alpha^2 b_0 \gamma^{(0)}\right] E(s)\right) \tag{6.20b}$$

$$M_{\mathrm{T}}(s) = \exp\left(\frac{s^2\sigma_{th}^2}{2}\right) \tag{6.20c}$$

$$M_{\mathrm{SISO-ISI}}(s) = \prod_{k=-L}^{-1}\left[\frac{1 + \exp\{\alpha^2\gamma^{(k)}E(s)\}}{2}\right] \tag{6.20d}$$

where $E(s) = e^s - 1$, $\gamma_{SISO}^{(bd)} = (\gamma_b + \gamma_d)T_b$ and $\gamma^{(k)} = \frac{\eta}{hf}\int_{-kT_b}^{-(k-1)T_b} \Gamma(t)dt$.

In physical terms, $\gamma^{(k\neq 0)}$ indicates the effect of ISI and $\gamma^{(k=0)}$ illustrates the desired signal contribution (i.e. $\gamma^{(k=0)} = \gamma^{(s)}$). This MGF can be utilized in the SPA equation (16c) or to find the appropriate variance for the GA, both conditioned on α. Thus, the final BER can be obtained into the conditional BER $P_{e|\alpha}$and by averaging over the fading coefficient α.

$$P_e = E_\alpha\left[P_{e|\alpha}\right] = \int P_{e|\alpha}\, f_\alpha(\alpha)d\alpha \tag{6.21}$$

6.4.2 MIMO UOWC Link

Each of the N receiving apertures receives the sum of all transmitted signals, which then are photodetected and experience noise. Hence, at the jth receiver, the photo-detected signal can be expressed as:

$$r_j^{b_0} = y_j^{b_0} + v_{th,j} \tag{6.22}$$

In this case, $y^{(b_0)}$ is a Poisson distributed RV with mean $m_j{}^{(b_0)}$, conditioned on $\{\alpha\}_{i=1}^{M}$ and $\{b_k\}_{k=-L_{ij}}^{0}$, thus [83]:

$$m_j{}^{(b_0)} = \frac{\eta}{hf}\sum_{i=1}^{M}\left\{\sum_{k=-Lij}^{0}\alpha_{ij}^2 b_k \Gamma_{i,j}^{\mathrm{Int}}\right\} + \left(\gamma_{b_j} + \gamma_{dj}\right)T_b \tag{6.23a}$$

$$\Gamma_{i,j}^{\mathrm{Int}} = \int_0^{T_b}\Gamma_{i,j}(t - kT_b)dt \tag{6.23b}$$

The mean count rates of the Poisson distributed dark current noise and background radiation at the jth Rx are γ_{d_j} and γ_{b_j}, respectively; L_{ij} is the channel memory between TX_i and RX_j.

Once again, the other noise contribution, $v_{th,j}$ is a zero mean Gaussian distributed RV with variance $\sigma_{th,j}^2 = \sigma_{th}^2$, which is equivalent to the combined thermal noise of the jth Rx.

The MIMO output MGF is then, conditioned on the fading coefficient vector $\vec{\alpha}$, [83]:

$$\psi_{r(b_0),MIMO|\vec{\alpha}}(s) = M_{\mathrm{T}}\left(\sqrt{N}s\right) M_{\mathrm{MIMO}}(s) \prod_{j=1}^{N} M_{\mathrm{MIMO-ISI}}(s) \tag{6.24a}$$

$$M_{\mathrm{MIMO}}(s) = \exp\left(\left[\gamma_{MIMO}^{(bd)} + X_{\mathrm{MIMO}}\right] E(s)\right) \tag{6.24b}$$

$$X_{\mathrm{MIMO}} = \sum_{j=1}^{N} \sum_{i=1}^{M} b_0 A_{ij}^{(0)} \tag{6.24c}$$

$$M_{\mathrm{MIMO-ISI}}(s) = \prod_{k=-L_{\max}}^{-1} \frac{1}{2}\left[1 + \prod_{i=1}^{M} \exp\left(A_{ij}^{(k)} E(s)\right)\right] \tag{6.24d}$$

$$A_{ij}^{(k)} = \alpha_{ij}^2 \gamma_{i,j}^{(k)} \tag{6.24e}$$

where $\gamma_{i,j}^{(k)} = \frac{\eta}{hf} \int_{-kT_b}^{(-k+1)T_b} \Gamma_{i,j}(t)dt$, $\gamma_{MIMO}^{(bd)} = (\gamma_b + N\gamma_d)T_b$ and $L_{\max} = \max\{L_{11}, L_{12}, \ldots . L_{MN}\}$.

For the SIMO and MISO schemes, the output MGFs can be easily found by substituting $M = 1$ and $N = 1$ respectively in (6.24a-e). In a similar way to SISO, the conditional BER results from inserting (6.24a-e) into (6.16a-c) and the final BER from averaging over fading coefficients $\vec{\alpha}$ similarly to (6.21).

For the GA conditioned on $\vec{\alpha}$ and b_k, the zero mean Gaussian RV has variance $N\sigma_{th}^2$ while the Poisson RV has mean and variance $m^{(b_0)}$ given by [161]:

$$m_{MIMO}^{b_0} = \gamma_{MIMO}^{(bd)} + \sum_{j=1}^{N} \sum_{i=1}^{M} \left[\tau_{i,j}^{(b_0)} \alpha_{ij}^2\right] \tag{6.25}$$

where $\tau_{i,j}^{(b_0)} = b_0 \gamma_{i,j}^{(s)} + \sum_{k=-Lij}^{-1} b_k \gamma_{i,j}^{(k)}$ conditioned on $\{b_k\}_{k=-L_{ij}}^{0}$.

Then, the average BER of the system becomes:

$$P_e \approx Q\left(\frac{m_{MIMO}^{(1)} - m_{MIMO}^{(0)}}{\sqrt{m_{MIMO}^{(1)} + N\sigma_{th}^2} + \sqrt{m_{MIMO}^{(0)} + N\sigma_{th}^2}}\right) \tag{6.26}$$

6.5 *Upper BER Bound for ISI*

To deal totally comprehensively with ISI would require consideration of an infinite stream of previous bits that could influence the current bit. Since, the effects of ISI on the current bit are reduced as the previous bits become further in the past, a truncation of the number of bits is employed as captured here by L and $L_{\max}$ in (6.20d) and (6.24d) respectively.

In addition, methods based on the expectation on the values of previous bits may also be employed [210], which can utilize the GA [211]. Here, we use a particular bit sequence to produce an upper bound, which is known to be effective for UOWC [83]. When transmitting a zero, i.e. $\mathrm{b}_0 = 0$, we take $\mathrm{b}_{\mathrm{k}\neq 0} = 1$ and when transmitting a one, i.e. $\mathrm{b}_0 = 1$, we take $\mathrm{b}_{\mathrm{k}\neq 0} = 0$. These conditions ensure that for a zero, there is maximum chance that ISI will cause an excessive count that exceeds the decision threshold and for a one, there is no addition to the pulse size from ISI.

6.5.1 SISO-UOWC Link

Using similar procedures as the previous section (section 6.4) and assuming the above considered special order, the MGF of the Rx's output will be:

$$\psi_{r(b_0),SISO|\alpha}(s) = exp\left(\frac{\sigma_{th}^2}{2}s^2 + \left[\gamma_{SISO}^{(bd)} + b_0\alpha^2\gamma^{(s)} + \sum_{k=-L}^{-1} b_0^{'}\alpha^2\gamma^{(k)}\right]E(s)\right) \quad (6.27)$$

In which b_0' is the compliment of b_0 (i.e. when $b_0 = 1$, then $b_0^{'}$ =0 and vice versa).

6.5.2 MIMO UOWC Link

For the MIMO scheme and using EGC combining with the assumed special order for transmission, the MGF of the Rx output is [83];

$$\psi_{r(b_0),MIMO|\alpha}(s) = exp\left(\frac{N\sigma_{th}^2}{2}s^2 + \left[\gamma_{MIMO}^{(bd)} + \sum_{j=1}^{N}\sum_{i=1}^{M}\alpha_{ij}^2\left(b_0\gamma_{i,j}^{(s)} + b_0^{'}\sum_{k=-L_{ij}}^{-1}\gamma_{i,j}^{(k)}\right)\right]E(s)\right) \quad (6.28)$$

The MGFs for SIMO and MISO can be extracted by substituting $M = 1$ and $N = 1$ in (6.28) respectively.

6.6 Results and Discussion

This section presents the numerical results for the BER of various NLOS UOWC system scenarios. A log-normal distribution has been considered for the fading statistics with the same log-amplitude variance for all of the links, the transmitters employ equal power of P/M and the receivers have equal aperture areas of A/N, where A is the SISO aperture area. The turbulence free fading impulse response was simulated via MC simulation in coastal water with the parameters shown in Table 6.1 since this was the most likely environment for NLOS applications. Table 6.1 also shows the key noise parameters that affect the received signal. Background radiation had a negligible effect in the system given the significant attenuation of sunlight at likely orating depths. Based on further values in [133] and [50], the noise characteristics were $\gamma_b \approx 1.8094 \times 10^8 \mathrm{s}^{-1}$, $\gamma_d \approx 76.625 \times 10^8 \mathrm{s}^{-1}$, and $\sigma_{th}^2/T_b = 3.12 \times 10^{15} \mathrm{s}^{-1}$.

Table 6.1: Channel parameters from [133] [50] [30]

Parameter	Symbol	Value
Coastal water absorption coefficient	a	$0.179\ \mathrm{m}^{-1}$
Coastal water scattering coefficient	b	$0.219\ \mathrm{m}^{-1}$
Coastal water attenuation coefficient	c	$0.398\ \mathrm{m}^{-1}$
Receiver half angle FOV	θ_{FOV}	40^0
Aperture diameter	D_0	20 cm
Source wavelength	λ	532 nm
Refractive index of coastal water	n	1.331
Transmitter beam divergence	θ_{div}	0.02^0
Rx photon weight threshold	w_{th}	10^{-6}
Sample time		0.01 s
Optical filter bandwidth	$\Delta\lambda$	10 nm
Optical filter transmissivity	T_F	0.8
Quantum efficiency	η	0.8
Load resistance	R_{L}	$100\ \Omega$
Dark Current	I_{dc}	1.226 nA
Equivalent temperature	T_{e}	290K
Channel memory	$L_{\max}$	3

The proposed scheme was simulated in MATLAB using Lambertian LED sources located at (y, z) coordinates $(\pm 2.5\ \mathrm{m}, \pm 2.5\ \mathrm{m})$, taking x as the propagation direction. At first OOK and CPM were compared (using $l = 4$) in a 2x2 MIMO 1 Gbps NLOS configuration by simulation through 20 m of coastal water using $\sigma_X = 0.4$ to compare the performance of both modulation schemes. As can be seen from the results in Fig. 6.3, CPM was superior to OOK, at a BER of 10^{-4} CPM offered an advantage in excess of 7 dB over OOK that rises to some 10 dB at 10^{-5}. Thus, CPM was taken as the modulation scheme for the rest of what follows.

Next, the results obtained were compared using the GA and SPA, to ascertain which should be employed. This investigation is to make sure that the GA gives accurate results. Fig. 6.4 shows the results for a range of configurations using the same parameters as in Fig. 6.3 with the photon counting approach rather than simulation. It can be observed that the results from the GA and SPA are in excellent agreement, meaning that the former can be employed here without the need for the extra computation entailed in the latter. Hence, the GA was employed to obtain the remaining results that follow.

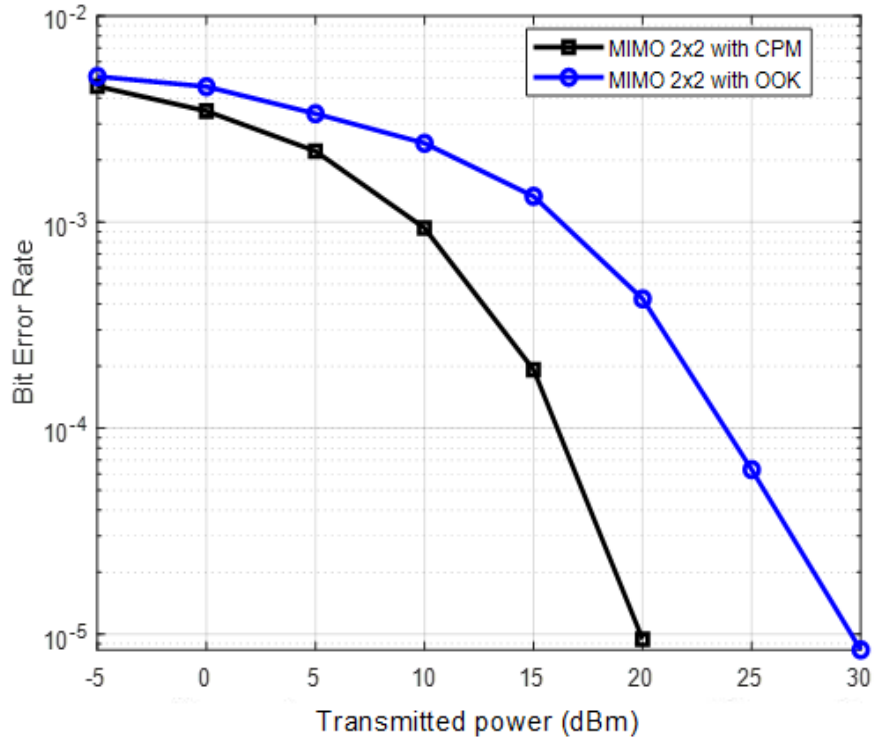

Fig. 6.3: Comparison of BER for OOK and CPM

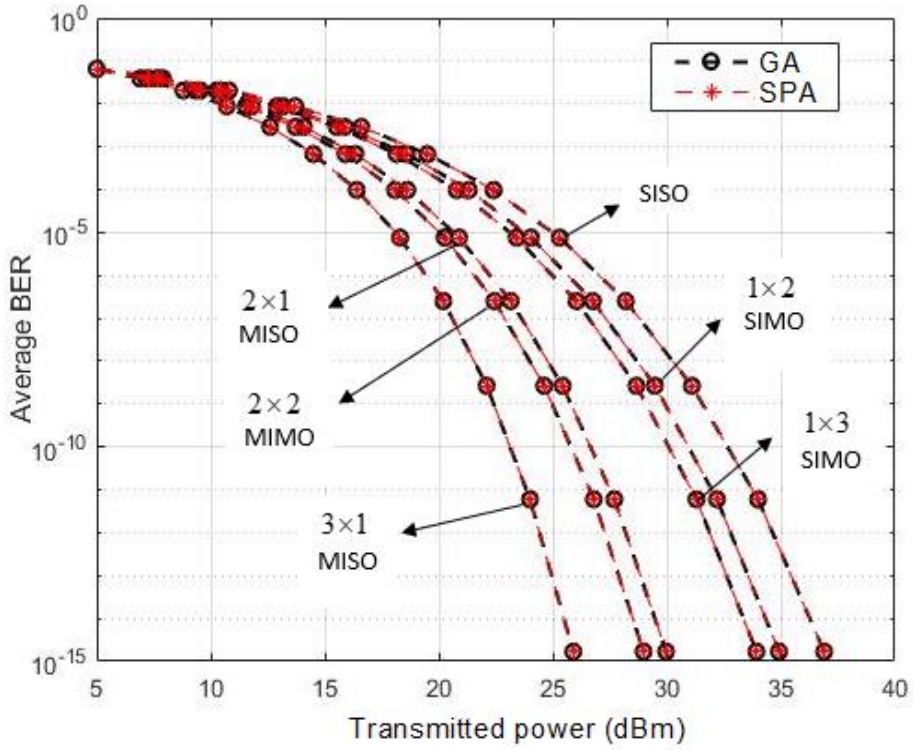

Fig. 6.4: Comparison of GA and SPA

Fig. 6.5 shows the results of employing the GA to evaluate the upper bound and exact BER of the system with various configurations (2×2 MIMO, $1 \times$

2 SIMO, and 1×3 SIMO) at a 1 Gbps transmission rate in 20 m of coastal water. Two regimes were considered, namely the moderately strong turbulent channel with $\sigma_X = 0.4$ used previously and a weakly turbulent channel having $\sigma_X = 0.1$. There is an excellent match between the exact and upper bound BER curves, which are tight in all configurations. In the $\sigma_X = 0.4$ regime, the 1×3 SIMO configuration gives better performance than 1×2 SIMO at high SNRs, where fading has a more degrading effect than ISI and absorption. This is understandable because each Rx in 1×3 SIMO has reduced aperture area but higher dark current and thermal noise than 1×2 SIMO. In the weaker regime of $\sigma_X = 0.1$, fading has a negligible effect on the system BER and absorption; scattering including noise has the more dominant effect. Hence, for low SNRs 1×2 SIMO provides better performance than 1×3 SIMO. Realistically, since the underwater channel suffers notably from turbulence, 1×3 SIMO offers greater fading mitigation as well as compensating for the effects of excess noise and smaller receiver apertures area since it benefits from one more independent link than 1×2 SIMO. Nevertheless, 2×2 MIMO has the same receiver aperture area as 1×2 SIMO but gives better performance in all regimes as it benefits from independent links. It is clear that Tx diversity yields better results than Rx diversity because of the effects of aperture size and noise power.

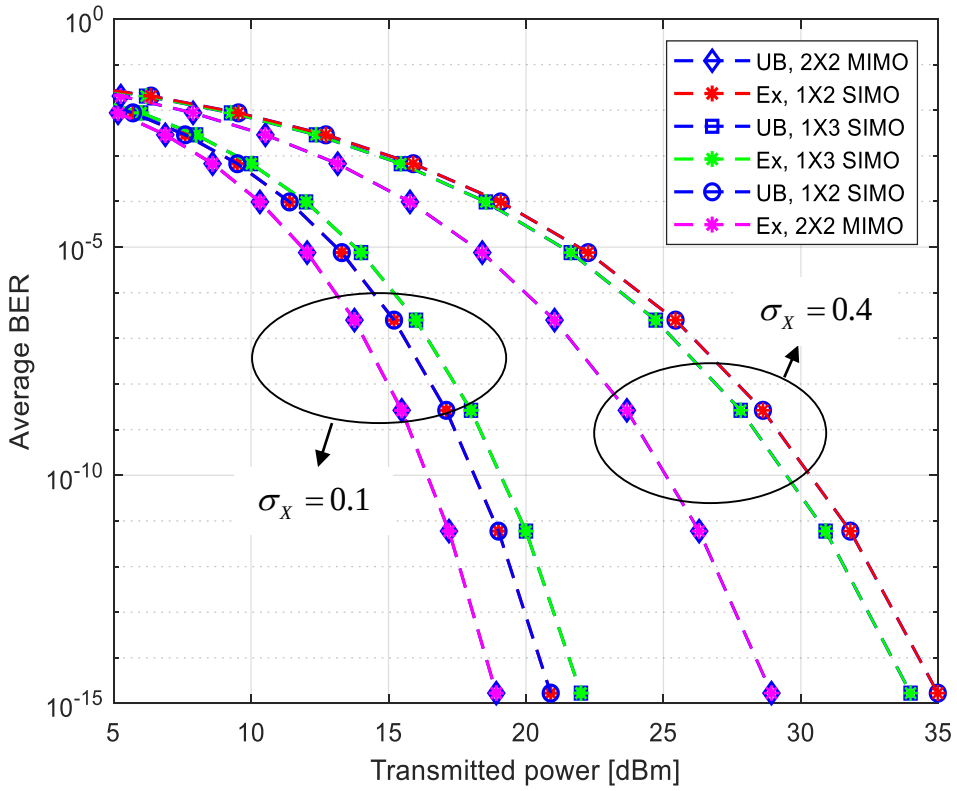

Fig. 6.5: Exact (Ex) and Upper bound (UB) BER at 1 Gbps in a 20 m coastal water link for various configurations

Fig. 6.6 investigates the effect of ISI on the performance of the system for various configurations. The figure depicts the upper bound BER results with $\sigma_X = 0.4$ in coastal water for different configurations (SISO, 2×1 MISO, 1×2 SIMO, 3×1MISO, 1×3 SIMO and 2×2 MIMO) using a typical NLOS data rate of 0.3 Gbps and a significantly higher data rate of 30 Gbps. At the lower data rate, significant improvements in system

At the lower data rate, 10^{-9} sensitivity improvements over SISO are seen for all diversity configurations. These range from 2.7 dB for 1×2 SIMO to 9.3 dB using 3×1 MISO. Thus, transmitter diversity is superior to receiver diversity; in the MISO structure all the transmitters are pointed at one receiver which means that the photons received by this single receiver experience less scattering. However, in the SIMO configuration, the transmitter source points more towards one of the detectors and then photons that experience relatively high scattering are captured by the other receivers through indirect paths causing ISI. The use of MIMO does produce

a further (albeit reduced) benefit, for example 2×1 MISO offers an improvement of 6.8 dB and 2×2 MIMO 7.7 dB. It is also apparent that increasing the data rate significantly impacts the system performance of some configurations via ISI. All the receiver diversity schemes (1×2 SIMO, 1×3 SIMO and 2×2 MIMO) exhibit error floors at 30 Gbps. Transmitter diversity fares much better, with 2×1MISO and 3×1 MISO delivering 10^{-9} sensitivity improvements of 8.4 dB and 11.6 dB, respectively.

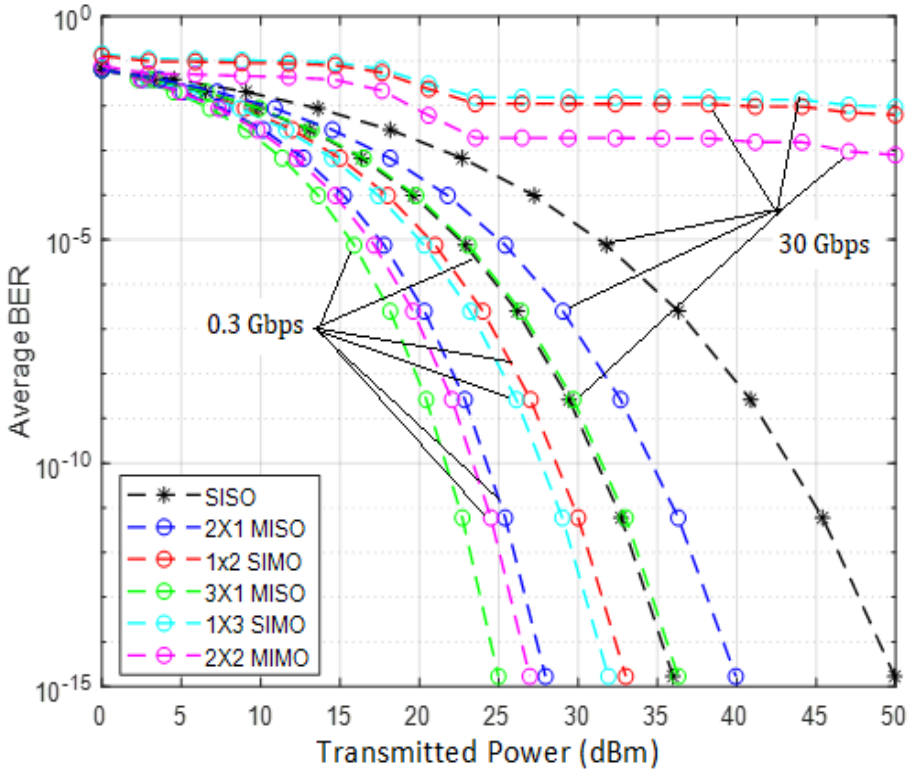

Fig.6.6: Effect of ISI on 20 m coastal water link for various configurations at 0.3 Gbps and 30 Gbps.

6.7 Conclusions

In this chapter, the performance of MIMO NLOS UOWC employing EGC at the receiver side has been studied. The effects of absorption, scattering and turbulence were all taken into account. The NLOS channel impulse response in the absence of fading was obtained using MC numerical simulations and turbulence effect was included as a multiplicative fading coefficient. CPM modulation was shown to give better BER results than OOK because of its

higher spectral efficiency. The system BER performance was evaluated using a photon counting approach with spatial diversity. Further investigation using the GA and SPA to produce the final results was done and both gave very similar results for the BER. Thus, the GA was adopted for later calculations since it was computationally simpler and so faster, which was of great benefit once the configurations increased in complexity. Coastal waters are the most likely environment for NLOS systems, given the preponderance of clutter close to land. The BER for these waters was thus determined, where 10^{-9} sensitivity gains of up to 8 dB was seen using MISO using a 1 Gbps data rate over a 20 m link with 0.16 log-amplitude variance; with SIMO was less beneficial and there was a small gain over MISO by using MIMO. An established tight upper bound was adopted for determining the impact of ISI. In the same water conditions, using a high bit rate of 30 Gbps showed the effects of ISI. Whilst MISO still delivered benefits of up to 11.6 dB, SIMO and MIMO developed error floors, preventing low BER values. Thus, multiple transmitter schemes are highly recommended in NLOS coastal transmission to improve the achievable bit rates. The numerical results have shown that spatial diversity can compensate the ISI effects by mitigating the fading effects and possibly extend communication ranges.

CHAPTER 7

Conclusions and Future work

7.1 Conclusions

Underwater optical wireless communications present a unique opportunity for low latency and high data rates communications in the Ocean world. Previously, the underwater communications were limited to very low data rate acoustic technology or to tethered applications using underwater cables. While for many years, this has served as a reasonable solution, applications requiring large data rates such as real-time video and real-time control of underwater vehicles such as ROVs and AUVs have been unachievable. Many attainable applications using the benefits of UOWC as discussed in chapter one could be explored. Over the years there has been significant work to establish a universal analytical model to estimate the overall performance of UOWC links. However, this is not an easy task to complete due to the high variability of the properties of light under the water and the resulting complexity. Thus, in this thesis, a more flexible method utilizing MC simulation as well as some analytical modelling was used to characterize the underwater channel and estimate its performance particularly with respect to NLOS links.

The objectives of the research highlighted in section 1.3 of chapter have been achieved.

Chapter two gave overview of the state of the art which started with the history of wireless communications under the water. This was followed by an introduction to the various technologies used in underwater communications, highlighting their respective advantages and disadvantages. Until substantial work was completed on extending the communication range of the UOWC, it has often been seen as a complementary technology to the incumbent acoustic technology, rather than a complete alternative as it supports high bandwidths but only over moderate distances. The UOWC link configurations and the system

components were discussed in the subsequent section, concluding with a review of the prototypes and experimental work in UOWC.

In chapter three, the underwater optical channel was considered which started with a brief introduction of light and energy, then the background theory on the properties of light under the water was discussed with particular emphasis on absorption and scattering processes which are the main inherent optical properties of the water. The subsequent section presented the challenges of the channel and the channel modelling schemes was discussed together with introduction to the main equation used to describe the light underwater, the RTE, highlighting the complexity of the equation indicating the need to use an MC numerical approach to solve it.

The MC simulation method in modelling the light beam in the underwater environment was presented in chapter four. The theory, details of the simulation including mathematical algorithms and equations were discussed. Then the performance of NLOS UOWC was studied. The effect of losses due to absorption, scattering and attenuation were incorporated using MC simulation method based on the RTE. Initially, the CIR of clear ocean, coastal and turbid water was characterized. Then the impact of FOV for different modulation schemes (QPSK, 8-PSK, 16-QAM and 64-QAM) in coastal water was considered since coastal water is the most likely application environment for NLOS UOWC links. The results in this chapter showed that 64-QAM modulation gives the better performance due to higher spectral efficiency and less susceptibility to noise. The effect of the receiver lens diameter based on the simulation was also shown and it was found that a receiver with a large aperture diameter increased the channel impulse response performance. The BER and throughput performance of the system were also presented.

Building on the NLOS simulation of chapter four, the temporal dispersion of the links as a result of multiple scattering in turbid water environments (coastal and harbor) were investigated in chapter five utilizing different scattering phase function models discussed in chapter three. The impulse response was then modelled using DGF and WDGF and both were shown to

produce a very good fit with the MC impulse response with the WDGF giving a little better numerical performance than the DGF in terms of modelling the NLOS UOWC channel, reaching 0.99 at best.

Finally, in chapter six, the NLOS design of the previous chapters was extended to multiple input multiple output employing EGC at the receiver side and the performance of the system was investigated. In this chapter, the effects of absorption, scattering as well as turbulence which are the major degrading effects of the channel were all taken into account. Spatial diversity was shown to provide significant performance enhancement of the NLOS UOWC system especially for weak oceanic turbulence. The BER performance of the system was evaluated using photon counting approach with spatial diversity technique for the Exact and Upper bound case. Excellent tightness between the Exact and Upper bound BER for various configurations was also observed. This chapter also showed that spatial diversity can compensate the ISI effects by mitigating the fading effects and possibly extend the communication range.

7.2 Future Research

It is clear that there is substantial scope for further work in the field of UOWC. There are several future works that can be done as extensions to the work documented in this research.

- ❖ Improvement of the efficiency of MC simulation.

The long simulation time of MC technique due to tracking of millions of photons propagating through the channel is its main disadvantage. Therefore, to boost the performance of the MC technique, a method to improve the simulation time is needed. Various approaches that have been used in accelerating MC simulation time in biomedical applications [212] can be interesting methods to be applied in UOWC.

- Modulation and Coding schemes

Several modulation schemes (such as OOK, QPSK, 8-PSK, 16-QAM, 64-QAM, CPM) have been used throughout the thesis which offer performance improvement. This opens up for further research direction in UOWC to design adaptive modulation techniques and coding schemes taking into consideration the characteristics of the underwater environment in the spirit of [105]. The routine inclusion of error correction coding can also enhance system reliability since error correction coding has been shown to be beneficial in FSO.

- MIMO Improvement

Chapter 6 of this thesis investigates the performance of MIMO NLOS UOWC which has shown to offer performance improvement compared to SISO configuration. Therefore, since the coverage area of UOWC for many real-time applications, for example, monitoring an undersea pipeline, is required to be large. The application of MIMO technology to improve transmission scheme and system performance needs to be further extensively investigated and studied. Only a limited amount of work has considered MIMO in UOWC.

- Higher layers network architecture

This research only focuses on the physical layer which is natural for an emerging medium. However, when designing a practical UOWC link, the higher layers of the network architecture need to be investigated (Medium Access, Data Link Control, Transport, and Application layers).

- Experimental work and Internet of underwater things

This thesis is based on computational models and hence experimental verification is needed in order to design practical UOWC systems for full scale implementation of UWSNs. There has also been an interest in the development of Internet of Underwater Things (IoUT) for various underwater applications [213]. Most recently, there has been discussion of self-powering [214] but in recent years there has been work to develop IoUT techniques such as routing, scheduling and data analytics [215] but this research is in its infancy and needs to be explored.

References

[1] K. Arun and C. Jennifer, Free-Space Laser Communications : Principles and Advances, Springer Science and Business Media, 2010.

[2] NOAA, “How much water is in the ocean?,” [Online]. Available: https://oceanservice.noaa.gov/facts/oceanwater.html, online. [Accessed 10 May 2020].

[3] M.Stojanovic, “Underwater Wireless Communications: Current Achievements and Research Challenges,” *IEEE Oceanic Engineering Society Newsletter,* no. 41, pp. 2-7, 2006.

[4] K. Hemani and G. Kaddoum, “Underwater Optical Wireless Communications,” *IEEE Access,* vol. 4, pp. 1518-1547, 2016.

[5] Q. Seibert, “Light in the Sea,” *Journal of the Optical Society of America,* vol. 53, no. 2, pp. 214-233, 1963.

[6] G. D. Gilbert, T. R. Stoner and J. L. Jernigan, “Underwater Experiments On The Polarization, Coherence, And Scattering Properties Of A Pulsed Blue-Green Laser,” in *Underwater Photo-Optical Instrumentation Applications*, Santa Barbara, United States, 1966.

[7] M. Callaham, “Submarine communications,” *IEEE Communications Magazine,* vol. 19, no. 6, 1981.

[8] J. Puschell, R. Giannaris and L. Stotts, “The Autonomous Data Optical Relay Experiment: first two way laser communication between an aircraft and submarine,” in *NTC-92: National Telesystems Conference*, Washington, DC, USA, 1992.

[9] T. F. Wiener and S. Karp, “The Role of Blue/Green Laser Systems in Strategic Submarine Communications,” *IEEE TRANSACTIONS ON COMMUNICATIONS,* vol. 28, no. 9, pp. 1602-1607, 1980.

[10] C. Wang, H.-Y. Yu and Y.-J. Zhu, “A Long Distance Underwater Visible Light Communication System With Single Photon Avalanche Diode,” *IEEE Photonics Journal,* vol. 8, no. 5, 2016.

[11] “BLUECOMM 100 – WIRELESS UNDERWATER OPTICAL COMMUNICATION,” Sonardyne, 2019. [Online]. Available:

https://www.sonardyne.com/product/bluecomm-underwater-optical-communication-system/. [Accessed 16 March 2020].

[12] N.Tollinsky, “Penguin unveils optical technology,” SUDBURY Mining Solutions, [Online]. Available: http://www.sudburyminingsolutions.com/penguin-unveils-optical-technology. [Accessed 20 March 2020].

[13] I. Vasilescu, K. Kotay, D. Rus and M. Dunbabin, “Data collection, storage, and retrieval with an underwater sensor network,” in *3rd international conference on Embedded networked sensor systems*, San Diego, USA, 2005.

[14] Z. Zeng, S. Fu, H. Zhang, Y. Dong and J. Cheng, “A Survey of Underwater Optical Wireless Communications,” *IEEE Communications Surveys & Tutorials,* vol. 19, no. 1, pp. 204-238, 2017.

[15] ERI, “Bermuda bio-optics project,” [Online]. Available: http://www.oceancolor.ucsb.edu/. [Accessed 2 February 2021].

[16] W. P. Bissett *et al.,* “Coastal ocean optics and dynamics,” *Oceanography,* vol. 17, no. 2, pp. 5-48, 2004.

[17] AOSN, “Autonomous ocean sampling network (AOSN),” [Online]. Available: https://www3.mbari.org/aosn/. [Accessed 2 February 2021].

[18] S. Srinivas, P. Ranjitha, R. Ramya and G. K. Narendra, “Investigation of oceanic environment using large-scale UWSN and UANETs,” in *8th International Conference on Wireless Commununication Network and Mobile Comp*, 2012.

[19] M. Waldmeyer, H. P. Tan and W. K. G. Seah, “Multi-stage AUV-aided localization for underwater wireless sensor networks,” in *IEEE Workshops of Int. Conf. on Adv. Infor. Netw. and Applications*, 2011.

[20] F. Akhoundi, A. Minoofar and J. A. Salehi, “Underwater positioning system based on cellular underwater wireless optical cdma networks,” in *Wireless and Opt. Commun. Conf., (WOCC),*, 2017.

[21] E. Cayirci, H. Tezcan, Y. Dogan and V. Coskun, “Wireless sensor networks for underwater survelliance systems,” *Ad Hoc Network,* vol. 4, no. 4, pp. 431-446, 2006.

[22] K. Munasinghe, M. Aseeri, S. Almorqi, M. F. Hossain, M. B. Wali and A. Jamalipour, “EM-based high speed wireless sensor networks for underwater surveillance and target tracking,” *Jornal of Sensors,* vol. 20, no. 17, p. 6731204, 2016.

[23] D. P. Williams, “On optimal AUV track-spacing for underwater mine detection,” in *IEEE Int. Conference on Robotics and Automation*, 2010.

[24] J. Keller, “Wide-area maritime surveillance with intelligent floats is goal of DARPA ocean of things project,” [Online]. Available: http://www.militaryaerospace.com/articles/2017/12/surveillance-ocean-floats.html. [Accessed 4 February 2021].

[25] K. Casey, A. Lim and G. Dozier, “A sensor network architecture for tsunami detection and response,” *International Journal of Distributed Sensor Network,* vol. 4, no. 1, pp. 28-43, 2008.

[26] OceanOne, “Robotic diver recovers treasures,” [Online]. Available: http: // news. stanford. edu/ 2016/ 04/27/ robotic diver-recovers-treasures/. [Accessed 25 April 2020].

[27] C. Gabriel, M. A. Khalighi, S. Bourennane, P. Leon and V. Rigaud, “Monte-Carlo-based channel characterization for underwater optical communication systems,” *IEEE/OSA Journal of Optical Communications and Networking,* vol. 5, no. 1, pp. 1-12, 2013.

[28] L. J. Johnson, F. Jasman, R. J. Green and M. S. Leeson, “Recent advances in underwater optical wireless communications,” *Underwater Technology,* vol. 32, no. 3, pp. 167-175, 2014.

[29] A. B. Umar and M. S. Leeson, “Advances in Underwater Optical Wireless Communications,” *International Journal of Photonics and Optical Technology,* vol. 7, no. 1, pp. 1-14, 2021.

[30] A. B. Umar and M. S. Leeson, “Performance of Non-Line-of-Sight Underwater Optical Wireless Communications,” in *2019 IEEE 2nd British and Irish Conference on Optics and Photonics (BICOP)*, London, UK, 2019.

[31] A. B. Umar and M. S. Leeson, “Performance of Non-line of Sight Underwater Optical Wireless Communication Links,” *International Journal of Photonics and Optical Technology,* vol. 6, no. 1, pp. 5-10, 2020.

[32] A. B. Umar, M. S. Leeson and I. Abdullahi, “Modelling Impulse Response for NLOS Underwater Optical Wireless Communications,” in *15th International Conference on Electronics, Computer and Computation (ICECCO)*, 2019.

[33] A. B. Umar and M. S. Leeson, “Performance of Non-line of sight Underwater optical wireless communication links with spatial diversity,” Accepted in *American Journal of Electrical and Computer Engineering, 2021.*

[34] NOAA, “How much water is in the ocean,” [Online]. Available: https://oceanservice.noaa.gov/facts/oceanwater.html. [Accessed 11 June 2020].

[35] S. J. Murray, “Report on the Scientific Results of the Voyage of H.M.S. Challenger During the Years 1873-76 Under the Command of Captain George S. Nares and the Late Captain Frank Tourle Thomson,” Nabu Press, Charleston, South Carolina, 2006.

[36] E. J. Prager and S. A. Earle, The Oceans, New york, US: McGraw-Hill, 2001.

[37] M. N. Hill, The Sea, Cambridge, US: Harvard University press, 2001.

[38] J. Hjort, J. S. Murray and J. J. Adolf, The Depths of the Oceans, New Hampshire, US: Wentworth Press, 2016.

[39] R. W. Fairbridge, The encyclopedia of oceanography, New York, US: Reinhold Pub, 1966.

[40] O. Kruemmel, Handbuch der Ozeanographie, Bremen, Germany: Europaischer Hochschulverlag Gmbh, 2014.

[41] A. F. Laloe, The Geography of the Ocean: Knowing the ocean as a space (Studies in Historical Geography), Howick Place, London: Routledge, 2016.

[42] L. Jane and G. Steven D, “A new narrative for the ocean,” *Science,* vol. 364, no. 6444, p. 911, 2019.

[43] A. G. Bell, “On the production and reproduction of sound by light,” *American Journal of Science,* vol. 3, pp. 305-324, 1880.

[44] H. Lichte, “On the influence of horizontal temperature layers in sea water on the range of underwater sound signals,” WHOI Unnumbered Reports, 1919.

[45] S. Q. Duntley, “Underwater lighting by submerged lasers and incandescent sources,” DTIC Tehnical report document, 1971.

[46] R. W. Preisendorfer, “Hydrologic optics volume 2. foundations. Technical report,” US Dept. of Commerce, National Oceanic and Atmospheric Administration, environmental Research Laboratories, Honolulu, US, 1976.

[47] N. G. Jerlov, “Marine Optics,” *Elsevier Oceanography Series,* vol. 14, pp. iii-vii, 1-231, 1976.

[48] B. Jensen, “Advances in luminescence instrument Systems,” *Radiation Measurements,* vol. 32, no. 5, pp. 523-528, 2000.

[49] J. Smart, “Underwater optical communications systems part 1: variability of water optical Parameters,” in *IEEE Military Communications Conference (MILCOM)*, 2005.

[50] J. W. Giles and I. N. Bankman, “Underwater optical communications systems. part 2: basic design Considerations,” in *IEEE Military Communications Conference (MILCOM)*, 2005.

[51] X. Che, I. Wells, G. Dickers, P. Kear and X. Gong, “Re-evaluation of RF electromagnetic communication in underwater sensor networks,” *IEEE Communication Magazine,* vol. 48, no. 12, pp. 143-151, 2010.

[52] D. Pompili and I. F. Akyildiz, “Overview of networking protocols for underwater wireless communications,” *IEEE Communication Magazine,* vol. 47, no. 1, pp. 97-102, 2009.

[53] C. A. Altgelt, “The world's largest 'radio' station. Technical report,” [Online]. Available: https://www.hep.wisc.edu/~Prepost/ELF.pdf. [Accessed 18 September 2019].

[54] P. M. C. P. C. d. Freitas, “Evaluation of Wi-Fi underwater networks in freshwater, Ph.D. dissertation,” Faculdade Engenharia Univ. Porto, Porto, Portugal, 2014.

[55] J. Lloret, S. Sendra, M. Ardid and J. J. Rodrigues, “J. Lloret, S. SendUnderwater wireless sensor communications in the 2.4 GHz ISM frequency band,” *Sensors,* vol. 12, no. 4, pp. 4237-4264, 2012.

[56] M. R. Frater, M. J. Ryan and R. M. Dunbar, “Electromagnetic communications within swarms of autonomous underwater vehicles,” in *ACM Underwater Network*, 2006.

[57] H. Kulhandjian, “Inside out: Underwater communications,” *J. Ocean Technol.,* vol. 9, no. 2, pp. 104-105, 2014.

[58] R. E. Race, J. C. Piskura and D. Sanford, “Towed Antenna System Allows Two-Way, Real-Time Communication with UUVs,” 11 May 2011. [Online]. Available: http://www.seatechnology.com/features/2011/0511/towed-antenna.php. [Accessed 9 April 2019].

[59] J. Shi, S. Zhang and C. J. Yang, “High frequency RF based non-contact underwater communication,” in *IEEE OCEANS*, Yeosu, South Korea, 2012.

[60] J. Partan, J. Kurose and B. N. Levine, “A survey of practical issues in underwater networks,” *ACM SIGMOBILE Mobile Comput. Commun. Rev.,* vol. 11, no. 4, pp. 23-33, 2007.

[61] W. W. Au, P. E. Nachtigall and J. L. Pawloski, “Acoustic effects of the ATOC signal (75 Hz, 195 dB) on dolphins and whales,” *The Journal of the Acoustic Society of America,* vol. 101, no. 5, pp. 2973-2977, 1997.

[62] M. Stojanovic, “Recent advances in high-speed underwater acoustic communications I, vol. 21, no. 2, pp. 125–136, Apr. 1996.,” *IEEE Journal of Oceanic Engineering,* vol. 21, no. 2, pp. 125-136, 1996.

[63] A. Zielinski, Y. H. Yoon and L. Wu, “Performance analysis of digital acoustic communication in a shallow water channel,” *IEEE Journal of Oceanic Engineering,* vol. 20, no. 4, pp. 293-299, 1995.

[64] H. Ochi, Y. Watanabe and T. Shimura, “Basic Study of Underwater Acoustic Communication Using 32-Quadrature Amplitude Modulation,” *Japanese Journal of Applied Physics,* vol. 44, no. 6S, p. 4689, 2005.

[65] H. C. Song and W. S. Hodgkiss, “Efficient use of bandwidth for underwater acoustic communication,” *The Journal of the Acoustic Society of America,* vol. 134, no. 2, pp. 905-908, 2013.

[66] F. Lu, S. Lee, J. Mounzer and C. Schurgers, “Low-cost medium-range optical underwater modem,” in *4th ACM International Workshop for Underwater Networks*, 2009.

[67] X. Yi, Z. Li and Z. Liu, “Underwater optical communication performance for laser beam propagation through weak oceanic turbulence,” *Applied Optics,* vol. 54, no. 6, pp. 1273-1278, 2015.

[68] B. Tu, L. Liu, Y. Liu, Y. Jin and J. Tang, “B. Tu, L. Liu, Y. Liu, Y. JiAcquisition probability analysis of ultra-wide FOV acquisition scheme in optical links under impact of atmospheric turbulence,” *Applied Optics,* vol. 52, no. 14, pp. 3147-3155, 2013.

[69] J. W. Bales and C. Chryssostomidis, “High-bandwidth, low-power, short-range optical communication underwater,” in *9th Int. Symp. Unmanned, Untethered Submersible Technol.,*, Durham , NH, USA, 1995.

[70] F. Hanson and S. Radic, “High bandwidth underwater optical communication,” *Applied Optics,* vol. 47, no. 2, pp. 277-283, 2008.

[71] N. Farr *et al.,* “Optical modem technology for sea floor observatories,” in *IEEE OCEANS*, Boston, MA, USA, 2006.

[72] S. Arnon, “Underwater optical wireless communication network,” *Journal of Optical Engineering,* vol. 49, no. 1, pp. 015001-1_015001-6, 2010.

[73] W. C. Cox, B. L. Hughes and J. F. Muth, “A polarization shift-keying system for underwater optical communications,” in *IEEE OCEANS*, Biloxi, MS, USA, 2009.

[74] B. Cochenour, L. Mullen, W. Rabinovich and R. Mahon, “Underwater optical communications with a modulating retro-reflector,” in *SPIE defense, Security and Sensing*, 2009.

[75] L. Mullen, B. Cochenour, W. Rabinovich, R. Mahon and J. Muth, “Backscatter suppression for underwater modulating retroreflector links using polarization discrimination,” *Applied Optics,* vol. 48, no. 2, pp. 328-337, 2009.

[76] S. Arnon and D. Kedar, “Non-line-of-sight underwater optical wireless communication network,” *Journal of Optical Society of America,* vol. 26, no. 3, pp. 530-539, 2009.

[77] G. Baiden, Y. Bissiri and A. Masoti, “Paving the way for a future underwater omni-directional wireless optical communication systems,” *Ocean Engineering,* vol. 36, no. 9, pp. 633-640, 2009.

[78] G. Giuliano, “Underwater optical communication systems. EngD Thesis,” University of Glasgow, Glasgow, UK, 2019.

[79] N. E. Farr, L. Freitag, j. Preisig, D. R. Yoerger, S. N. White and A. D. Chave, “Systems and methods for underwater optical communication”. US Patent 7953326 B2, 2006.

[80] M. Doniec *et al.,* “A lightweight device for high-rate long-range underwater point-to-point communication,” *OCEANS,* pp. 1-6, 2009.

[81] C. Creatore, M. A. Parker, S. Emmott and A. W. Chin, “Efficient biologically inspired photocell enhanced by delocalized quantum states,” *Phys. Rev. Lett. ,* vol. 111, no. 25, pp. 253601-1-253601-5, 2013.

[82] H. Oubei *et al.,* “4.8 Gbit/s 16-QAM-OFDM transmission based on compact 450-nm laser for underwater wireless optical communication,” *Optics Express,* vol. 23, no. 18, pp. 23302-23309, 2015.

[83] M. V. Jamali, J. A. Salehi and F. Akhoundi, “Performance studies of underwater wireless optical communication systems with spatial diversity: MIMO scheme,” *IEEE Transactions on Communications,* vol. 65, no. 3, pp. 1176-1192, 2017.

[84] F. Akhoundi, J. A. Salehi and A. Tashakori, “Cellular Underwater Wireless Optical CDMA Network: Performance Analysis and Implementation Concepts,” *IEEE Transactions on Communications,* vol. 63, no. 3, pp. 882-891, 2015.

[85] X. He and J. Yan, “Study on performance of M-ary PPM underwater optical communication Systems using vector radiative transfer theory,” in *International Symposium on Antennas, Propagation, and Electromagnetic Theory*, 2012.

[86] M. Chen, S. Zhou and T. Li, “The Implementation of PPM in Underwater Laser Communication System,” in *Int. Conf. on Comm., Circ. and Sys.*, 2006.

[87] M. A. Khalighi and M. Uysal, “Survey on Free Space Optical Communication: A Communication Theory Perspective,” *IEEE Communications Surveys Tutorials,* vol. 16, no. 4, pp. 2231-2258, 2014.

[88] M. Doniec and W. Rus, " BiDirectional optical communication with AquaOptical II.," in *IEEE International Conference on Communication Systems*, 2010.

[89] M. W. Doniec, C. Detweiler, I. Vasilescu and D. Rus, "Using optical communication for remote underwater robot operation," in *IEEE/RSJ Int. Conf. on Intelligent Robots and Sys.*, 2010.

[90] B. M. Cochenour, L. J. Mullen and A. E. Laux, "Phase coherent digital communications for wireless optical links in turbid underwater environments," *OCEANS,* pp. 1-5, 2007.

[91] Y. Dong, T. Zhang and X. Zhang, "Polarized pulse position modulation for wireless optical communications," in *47th Annual Conf. on Info. Sci. and Sys., (CISS)*, 2013.

[92] S. Meihong, Y. Xinsheng and Z. Fengli, "The evaluation of modulation techniques for underwater wireless optical communications," in *IEEE Int. Conf. Comm. Software Net.,*, 2009.

[93] X. Yu, W. Jin, M. Sui and L. Lan, "Evaluation of forward error correction scheme for underwater wireless optical communication," in *3rd Int. Conf. Comm. Mobile Computing*, 2011.

[94] Cox *et al.,* "An underwater optical communication system implementing Reed-Solomon channel coding," *OCEANS,* pp. 1-6, 2008.

[95] J. Everett, "Forward-error correction coding for underwater free-space optical communication. M.S. thesis, Dept. Elect. Eng.," North Carolina State University, Raleigh, NC, USA, 2009.

[96] Snow *et al.,* "Underwater propagation of high data rate laser communications pulses," in *SPIE*, 1992.

[97] Farr *et al.,* "Optical modem technology for seafloor observatories," *OCEANS,* pp. 1-6, 2005.

[98] Pontbriand *et al.,* "Diffuse high-bandwidth optical communications," *OCEANS,* pp. 1-4, 2008.

[99] K. Nakamura, I. Mizukoshi and M. Hanawa, "Optical wireless transmission of 405 nm, 1.45 Gbit/s optical IM/DD-OFDM signals through a 4.8 m underwater channel," *Optics Express,* vol. 23, no. 2, pp. 1558-1566, 2015.

[100] L. Sun, J. Wang, K. Yang, M. Xia and J. Han, “The Research of Optical Turbulence Model in Underwater Imaging System,” *Sensors and Transducers,* vol. 163, no. 1, pp. 107-112, 2014.

[101] D. Anguita, D. Brizzolara and G. Parodi, “Optical wireless communication for underwater Wireless Sensor Networks: Hardware modules and circuits design and implementation,” in *OCEANS*, Seattle, WA, 2010.

[102] M. Doniec, M. Angermann and D. Rus, “An end-to-end signal strength model for underwater optical communications,” *IEEE Journal of Oceanic Engineering,* vol. 38, no. 4, pp. 743-757, 2013.

[103] I. Vasilescu, P. Varshavskaya, K. Kota and D. Rus, “Vasilescu, I., Varshavskaya, P., Kotay, K, Rus, D.: Autonomous modular optical underwater robot (AMOUR) design, prototype and feasibility study,” in *IEEE Int. Conf. Robot. Autom. (ICRA)*, 2005.

[104] J. A. Simpson, B. Hughes and J. Muth, “A spatial diversity system to measure optical fading in an underwater communications channel. In: OCEANS2009, pp. 1–6 (2009).,” in *OCEANS*, 2009.

[105] J. A. Simpson, B. L. Hughes and J. F. Muth, “Smart transmitters and receivers for underwater free-space optical communication,” *IEEE Journal of Selected Areas in Communications,* vol. 30, no. 5, pp. 964-974, 2012.

[106] M. A. Chancey, “Short Range Underwater Optical Communication links,” North Carolina State University, NC, USA, 2005.

[107] W. C. Cox. Jr, “A 1 Mbps Underwater Communication System Using 405nm LAsr Diodes and Photomultiplier Tube, M.S. thesis, Dept. Elect. and Comp. Eng,” North Carolina State University, NC, USA, 2008.

[108] J. A. Simpson, “A 1 Mbps Underwater Communication System Using 405 nm LEDs and Photodiodes with Signal Processing Capability, M.S. thesis, Dept. Elect. and Comp Eng,” North Carolina State University, NC, USA, 2008.

[109] H. Brundage, “Designing a wireless underwater optical communication system. M.S. Thesis, Department of Mechanical Engineering,” Massachusetts Institute of Technology, Cambridge, US, 2010.

[110] P. Swathi and S. Prince, “Designing issues in design of underwater wireless optical communication system,” in *Int. Conf. Comm. Signal Process. (ICCSP)*, 2014.

[111] T. Szili, B. Matolcsy and G. Fekete, “Water pollution investigations by underwater visible light communications,” in *International Conference on Transparent Optical Networks*, 2015.

[112] Oubei *et al.,* “2.3 Gbit/s underwater wireless optical communications using directly modulated 520 nm laser diode,” *Optics Express,* vol. 23, no. 16, pp. 20743-20748, 2015.

[113] B. M. Cochenour, “Experimental measurements of temporal dispersion for underwater laser communications and imaging. Ph.D. Thesis, Department of Electrical Engineering,” North Carolina State University, NC, USA, 2013.

[114] I. Mizukoshi, N. Kazuhiko and M. Hanawa, “Underwater optical wireless transmission of 405nm, 968Mbit/s optical IM/DD-OFDM signals,” in *OptoElectron. Comm. Conf. Aust. Conf. Opt. Fibre Technol. (OECC/ACOFT)*, 2014.

[115] Y. Li, H. Yin, X. Ji and B. Wu, “Design and Implementation of Underwater Wireless Optical Communication System with High-Speed and Full-Duplex Using Blue/Green Light,” in *10th Int. Conf. on Comm. Software and Networks*, 2018.

[116] Y. B. Band, Light and matter: electromagnetism, optics, spectroscopy and lasers, volume 1, John Wiley & Sons, 2006.

[117] D. Halliday, R. Resnick and J. Walker, Fundamentals of physics extended, volume 1, John Wiley & Sons, 2010.

[118] V. I. Haltrin, “Absorption and scattering of light in natural waters,” *Light Scattering Reviews Springer,* pp. 445-486, 2006.

[119] A. Morel and H. Loisel, “Apparent optical properties of oceanic water: Dependence on the molecular scattering contribution,” *Applied Optics,* vol. 37, no. 21, pp. 4765-4776, 1998.

[120] R. E. Green and H. M. Sosik, “Analysis of apparent optical properties and ocean color models using measurements of seawater constituents in New

England continental shelf surface waters," *J. Geophys. Res. Oceans ,* vol. 10, no. 9, 2004.

[121] J. R. Apel, Principles of Ocean Physics. London, London: Academic Press , 1987.

[122] G. C. Mooradian and M. Geller, "Temporal and angular spreading of blue-green pulses in clouds," *Applied Optics,* vol. 21, no. 9, pp. 1572-1577, 1982.

[123] B. Cochenour, L. Mullen and A. Laux, "Spatial and temporal dispersion in high bandwidth underwater laser communication links," in *IEEE Military Communications Conference*, San Diego, 2008.

[124] B. Cochenour, L. Mullen and J. Muth, "Temporal response of the underwater optical channel for high-bandwidth wireless laser communications," *IEEE Journal of Oceanic Engineering,* vol. 38, no. 4, pp. 730-742, 2013.

[125] H. Zhang, l. Hui and Y. Dong, "Angle of Arrival Analysis for Underwater Wireless Optical Links," *IEEE Communications Letter,* vol. 19, no. 12, pp. 2162-2165, 2015.

[126] Vali *et al.,* "Experimental study of the turbulence effect on underwater optical wireless communications," *Applied Optics,* vol. 57, no. 28, pp. 8314-8319, 2018.

[127] O. Korotkova, N. Farwell and E. Shchepakina, "Light scintillation in oceanic turbulence," *Waves in Random and Complex Media,* vol. 22, no. 2, pp. 260-266, 2012.

[128] F. Yang, J. Cheng and T. A. Tsiftsis, "Free-space optical communication with nonzero boresight pointing errors," *IEEE Transactions on Communications,* vol. 62, no. 2, pp. 713-725, 2014.

[129] R. Sanchez and N. J. McCormick, "Analytic beam spread function for ocean optics applications," *Applied Optics,* vol. 41, no. 30, pp. 6276-6288, 2002.

[130] Gabriel *et al.,* "Misalignment considerations in point-to-point underwater wireless optical links," in *OCEANS*, 2013.

[131] Y. Dong, S. Tang and X. Zhang, “Effect of random sea surface on downlink underwater wireless optical communications,” *IEEE Communications Letter,* vol. 17, no. 11, pp. 2164-2167, 2013.

[132] Lu *et al.,* “An 8 m/9.6 Gbps Underwater Wireless Optical Communication System,” *IEEE Photonics Journal,* vol. 8, no. 5, 2016.

[133] S. Jaruwatanadilok, “Underwater wireless optical communication channel modeling and performance evaluation using vector radiative transfer theory,” *IEEE Journal of Selected Areas in Communications,* vol. 26, no. 9, pp. 1620-1627, 2008.

[134] Z. Ahmad and R. J. Green, “Link design for multi-hop underwater optical wireless sensor network,” in *International Conference on Systems and Networks Communications*, 2012.

[135] T. J. Petzold, “Volume scattering functions for selected ocean waters. Tech. Report 72-78,” Scripps Institution of Oceanography, San Diego, 1972.

[136] H. Tan, R. Doerffer, T. Oishi and A. Tanaka, “A new approach to measure the volume scattering function,” *Optics Express,* vol. 21, no. 16, pp. 18697-18711, 2013.

[137] H. V. Hulst, Light Scattering by Small Particles, New York: Dover, 1981.

[138] T. Binzoni, T. S. Leung, A. H. Gandjbakhche, D. Rüfenacht and D. T. Delpy, “The use of the Henyey-Greenstein phase function in Monte Carlo simulations in biomedical optics,” *Physics in medicine and biology,* vol. 51, p. L39–L41, 2006.

[139] S. A. Prahl, “Light transport in tissue,” University of Texas, Austin, USA, 1988.

[140] L. Wang and S. L. Jacques, “Monte Carlo modeling of light transport in multi-layered tissues in standard C,” The University of Texas, MD Anderson Cancer Center, Houston, 1992.

[141] J. Huang, Y. Zhang, D. Li and S. Ren, “Analyzation and Simulation of Underwater Laser Communication Based on Monte Carlo Mechanism,” in *7th International Conference on Intelligent Human-Machine Systems and Cybernetics*, 2015.

[142] V. I. Haltrin, “Two-term Henyey–Greenstein light scattering phase function for seawater,” in *International Geoscience and Remote Sensing Symposium (IGARSS)*, 1999.

[143] G. Fournier and F. Forand, “ Analytic phase function for ocean water,” in *SPIE Proceedings* , 1994.

[144] S. Arnon, J. Barry, G. Karagiannidis, R. Schober and R. Uysal, M. (eds.) Advanced Optical Wireless Communication Systems, Cambridge: Cambridge University Press, 2012.

[145] C. D. Mobley, E. Boss and C. Roesler, “Ocean Optics Book,” [Online]. Available: http://www.oceanopticsbook.info. [Accessed 19 March 2020].

[146] L. J. J. R. J. Green and M. S. Leeson, “A Survey of Channel Models for Underwater Optical Wireless Communication,” in *International Workshop on Optical Wireless Communications*, 2013.

[147] B. M. Cochenour, L. J. Mullen and A. E. Laux, “Characterization of the beam-spread function for underwater wireless optical communications links,” *IEEE Journal of Oceanic Engineering,* vol. 33, no. 4, pp. 513-521, 2008.

[148] Mobley *et al.,* “Comparison of numerical models for computing underwater light fields,” *Applied Optics,* vol. 32, no. 36, pp. 7484-7504, 1993.

[149] C. Li, K. H. Park and M. S. Alouini, “On the use of a direct radiative transfer equation solver for path loss calculation in underwater optical wireless channels,” *IEEE Wireless Communications Letter,* vol. 4, no. 5, pp. 561-564, 2015.

[150] R. A. Downes, C. O. Davis and C. D. Mobley, “Monte Carlo radiative transfer simulations for ocean optics: a practical guide,” Naval Research Lab. Tech. Report, Washington DC, 2004.

[151] Li *et al.,* “Monte Carlo study on pulse response of underwater optical channel,” *Optical Engineering,* vol. 51, no. 6, p. 066001, 2012.

[152] Gabriel *et al.,* “Channel modeling for underwater optical communication,” in *IEEE GLOBECOM Workshops*, 2011.

[153] J. Li, Y. Ma, Q. Zhou and B. Zhou, “Channel capacity study of underwater wireless optical communications links based on monte carlo simulation,” J. of Opt. 14(1), 1–7 (2012).,” *Journal of Optics,* vol. 14, no. 1, pp. 1-7, 2012.

[154] W. Cox and J. Muth, “Simulating channel losses in an underwater optical communication system,” *Journal of the Optical Society of America,* vol. 31, no. 5, pp. 920-934, 2014.

[155] W. Cox, “Photonator,” GitHub, 2012. [Online]. Available: https://github.com/gallamine/Photonator. [Accessed 30 March 2020].

[156] G. Zaccanti, P. Bruscaglioni and M. Dami, “Simple inexpensive method of measuring the temporal spreading of a light pulse propagating in a turbid medium,” *Applied Optics,* vol. 29, no. 27, pp. 3938-3944, 1990.

[157] S. Tang, Y. Dong and X. Zhang, “Impulse response modeling for underwater wireless optical communication links,” *IEEE Transactions on Communications,* vol. 62, no. 1, pp. 226-234, 2014.

[158] Y. Dong, H. Zhang and X. Zhang, “On impulse response modelling for underwater wireless optical MIMO links,” in *IEEE/CIC International Conference on Communications in China (ICCC)*, 2014.

[159] H. Zhang and Y. Dong, “ Impulse response modeling for general underwater wireless optical MIMO links,” *IEEE Communications Magazine,* vol. 54, no. 2, pp. 56-61, 2016.

[160] F. Hanson and M. Lasher, “Effects of underwater turbulence on laser beam propagation and coupling into single-mode optical fiber,” *Applied Optics,* vol. 49, no. 16, pp. 3224-3230, 2010.

[161] W. Liu, Z. Xu and L. Yang, “SIMO detection schemes for underwater optical wireless communication under turbulence,” *Photonics Research,* vol. 3, no. 3, pp. 48-53, 2015.

[162] W. W. Hou, “A simple underwater imaging model,” *Optics Letter,* vol. 34, no. 17, pp. 2688-2690, 2009.

[163] S. Woods, W. Hou, W. Goode, E. Jarosz and A. Weidemann, “Measurements of turbulence for quantifying the impact of turbulence on underwater imaging,” in *10th IEEE/OES Current, Waves and Turbulence Measurements (CWTM)*, 2011.

[164] M. Holohan and J. Dainty, “Low-order adaptive optics: a possible use in underwater imaging,” *Optics and Laser Technology,* vol. 29, no. 1, pp. 51-55, 1997.

[165] Y. Ata and Y. Baykal, “Field correlation of spherical wave in underwater turbulent medium,” *Applied Optics,* vol. 53, no. 33, pp. 7968-7971, 2014.

[166] S. Tang, X. Zhang and Y. Dong, “Temporal statistics of irradiance in moving turbulent ocean,” in *OCEANS2013*, 2013.

[167] Y. Ata and Y. Baykal, “Scintillations of optical plane and spherical waves in underwater turbulence,” *Journal of the Optical Society of America,* vol. 31, no. 7, pp. 1552-1556, 2014.

[168] S. Tang, Y. Dong and X. Zhang, “On link misalignment for underwater wireless optical communications,” *IEEE Communications Letter,* vol. 16, no. 10, pp. 1688-1690, 2012.

[169] R. Sanchez and N. J. McCormick, “Analytic beam spread function for ocean optics applications,” *Applied Optics,* vol. 41, no. 30, pp. 6276-6288, 2002.

[170] H. Zhang and Y. Dong, “Link misalignment for underwater wireless optical communications. In: Adv. Wireless Opt. Comm. (RTUWO), pp. 215–218 (2015).,” in *IEEE Advances in Wireless and Optical Communications (RTUWO)*, 2015.

[171] N. Metropolis and S. Ulam, “The Monte Carlo method,” *Journal of the American Statistical Association,* vol. 44, no. 247, pp. 335-341, 1949.

[172] Dimitrov *et al.,* “Path Loss Simulation of an Infrared Optical Wireless System for Aircrafts,” in *IEEE Global Telecommununication Conference* , 2009.

[173] M. Grabner and V. Kvicera, “Multiple scattering in rain and fog on freespace optical links,” *Journal of Lightwave Technology,* vol. 32, no. 3, pp. 513-520, 2014.

[174] H. Ding, G. Chen, Z. Xu and B. Sadler, “Channel modelling and performance of non-line-of sight ultraviolet scattering communications,” *IET Communications,* vol. 6, no. 5, pp. 514-524, 2012.

[175] Dalgleish *et al.,* "Physical layer simulator for undersea free-space laser communications," *Optical Engineering,* vol. 53, no. 5, pp. 051410-05, 2014.

[176] E. Alerstam, "Optical spectroscopy of turbid media: time-domain measurements and accelerated Monte Carlo modelling, Ph.D. thesis," Lund University, Sweden, 2011.

[177] M. Chowdhury, W. Zhang and M. Kavehrad, "Combined deterministic and modified monte carlo method for calculating impulse responses of indoor optical wireless channels," *Journal of Lightwave Technology ,* vol. 32, no. 18, pp. 3132-3148, 2014.

[178] H. Ding, "Modeling and characterization of ultraviolet scattering communication channels, Ph.D. thesis," University of California, Riverside, USA, 2011.

[179] W. C. Cox, "Simulation, Modeling, and Design of Underwater Optical Communication Systems, Ph.D. thesis," Department of Electrical and Computer Engineering, North Carolina State University, NC, USA, 2012.

[180] E. Ghargomi and I. S. Attia, "Modeling of a focused Gaussian beam into multi-layered tissue with Monte Carlo simulation, M.S. thesis," Department of Electrical and Computer Engineering, Concordia University, Canada, 2004.

[181] O. Ertl, "Numerical Methods for Topography Simulation, Ph.D. thesis," Institute for Microelectronics, Vienna University of Technology, Austria, 2010.

[182] S. Prahl, M. Keijzer, S. Jacque and A. Welch, "A Monte Carlo model of light propagation in tissue," *Dosimetry of laser radiation in medicine and biology,* vol. 5, pp. 102-111, 1989.

[183] F. Jasman, "Modelling and Characterisation of Short Range Underwater Optical Wireless Communication Channels, Ph.D. thesis," University of Warwick, Coventry, United Kingdom, 2016.

[184] A. Choudhary, V. K. Jagadeesh and P. Muthuchidambaranathan, "Pathloss analysis of NLOS underwater wireless optical communication channel," in *IEEE International Conference on Electronics and Communication System (ICECS)*, 2014.

[185] V. K. Jagadeesh, A. Choudhary, F. M. Bui and P. Muthuchidambaranathan, “Characterization of Channel Impulse Responses for NLOS Underwater Wireless Optical Communications,” in *International Conference on Advances in Computing and Communications (ICAC)*, 2014.

[186] C. D. Mobley, Light and Water: Radiative Transfer in Natural Waters, San Diego: Academic Press, 1994.

[187] S. K. Sahu and P. Shanmugam, “A theoretical study on the impact of particle scattering on the channel characteristics of underwater optical communication system,” *Optics Communications,* vol. 40, no. 8, pp. 3-14, 2018.

[188] L. C. Henyey and J. L. Greenstein, “Diffuse radiation in the galaxy,” *Astrophysical Journal,* vol. 93, pp. 70-83, 1941.

[189] Harmel *et al.,* “Laboratory experiments for inter-comparison of three volume scattering meters to measure angular scattering properties of hydrosols,” *Optics Express,* vol. 24, no. 2, 2016.

[190] A. P. Huang and L. W. Tao, “Monte carlo based channel characteristics for underwater optical wireless communications,” *IEICE Transactions on Commununications,* vol. 100, pp. 612-618, 2017.

[191] H. C. V. Hulst, Light Scattering by Small Particles, Dover Publications, 1981.

[192] V. A. Timofeyeva, “Relation between Light-Field Parameters and between Scattering Phase Function Characteristics of Turbid Media, Including Seawater,” *Izvestiya, Atmospheric and Oceanic Physics,* vol. 14, pp. 843-848, 1978.

[193] V. Haltrin, “One-parameter two-term Henyey–Greenstein phase function for light scattering in seawater,” *Applied Optics,* vol. 41, no. 6, pp. 1022-1028, 2002.

[194] Y. Li, M. S. Leeson and X. Li, “Impulse response modelling for underwater optical wireless channels,” *Applied Optics,* 2018.

[195] N. J. Nagelkerke, “A note on a general definition of the coefficient of determination,” *Biometrika,* vol. 78, no. 3, pp. 691-692, 1991.

[196] N. Farwell and O. Korotkova, “Intensity and coherence properties of light in oceanic turbulence,” *Optics Communications,* vol. 285, no. 6, pp. 872-875, 2012.

[197] Vali *et al.,* “Modeling turbulence in underwater wireless optical communications based on Monte Carlo simulation,” *Journal of the Optical Society of America,* vol. 34, no. 7, pp. 1187-1193, 2017.

[198] Jansen *et al.,* “Long-haul transmission of 16 × 52.5 Gb/s polarization-division-multiplexed OFDM enabled by MIMO processing,” *Journal of Optical Networking,* vol. 7, no. 2, pp. 173-182, 2008.

[199] A. H. Azhar, T. Tran and D. C. O’Brien, “A Gigabit/s Indoor Wireless Transmission Using MIMO-OFDM Visible-Light Communications,” *IEEE Photonics Technology Letters,* vol. 25, no. 2, pp. 171-174, 2013.

[200] Y. Hong, T. Wu and L. K. Chen, “On the performance of adaptive MIMO-OFDM indoor visible light communications,” *IEEE Photonics Technology Letters,* vol. 28, no. 8, pp. 907-910, 2016.

[201] M. V. Jamali and J. A. Salehi, “On the BER of multiple-input multiple-output underwater wireless optical communication systems,” in *Optical Wireless Communications (IWOW)*, Istanbul, Turkey, 2015.

[202] G. Einarsson, Principles of Lightwave communications, Wiley, 1996.

[203] S. McCammon and G. A. Hollinger, “Planning and executing optimal non-entangling paths for tethered underwater vehicles,” in *IEEE International Conference on Robotics and Automation (ICRA)*, Singapore, 2017.

[204] M. E. Lee and E. N. Korchemkina, Volume Scattering Function of Seawater, Kokhanovsky A. (Ed.): Light Scattering, Radiative Transfer and Remote Sensing, Springer, 2018.

[205] L. C. Andrews, R. L. Philips and C. Y. Hopen, Laser Beam Scintillation with Applications, SPIE, 2001.

[206] R. Bian, I. Tavakkolnia and H. Haas, “10.2 Gb/s Visible Light Communication with Off-the-Shelf LEDs,” in *European Conference on Optical Communication (ECOC)*, Rome, Italy, 2018.

[207] A. Barbieri, D. Fertonani and G. Colavolpe, “Spectrally-efficient continuous phase modulations,” *IEEE Transactions on Wireless Communications,* vol. 8, no. 3, pp. 1564-1572, 2009.

[208] Detwiler *et al.,* “Continuous phase modulation for fiber-optic links,” *Journal of Lightwave Technology,* vol. 29, no. 24, pp. 3659-3671, 2011.

[209] O. Weikert and U. Zölzer, “A wireless MIMO CPM system with blind signal separation for incoherent demodulation,” *Advances in Radio Science,* vol. 6, pp. 101-105, 2008.

[210] M. S. Leeson, “A Fast Approximation for Bit Error Rate Calculations in Optically Preamplified Receivers,” *Electronics Letters,* vol. 33, no. 15, pp. 1329-1330, 1997.

[211] El-Howayek *et al.,* “On the Use of Gaussian Approximation in Analyzing the Performance of Optical Receivers,” *IEEE Photonics Journal,* vol. 6, no. 1, pp. 1-8, 2014.

[212] C. Zhu and Q. Liu, “Review of Monte Carlo modeling of light transport in tissues,” *Journal of Biomedical Optics,* vol. 18, no. 5, p. 050902, 2013.

[213] C. Domingo, “An overview of the internet of underwater things,” *Journal of Network and Computer Applications,* vol. 35, no. 6, pp. 1879-1890, 2012.

[214] Filho *et al.,* “Toward Self-Powered Internet of Underwater Things Devices,” *IEEE Communications Magazine,* vol. 58, no. 1, pp. 68-73, 2020.

[215] N. Saeed, A. Celik, T. Y. Al-Naffouri and M. S. Alouini, “Underwater optical wireless communications, networking, and localization: A survey. Ad Hoc Networks, 94, 101935 (2019).,” *Ad Hoc Networks,* vol. 94, p. 101935, 2019.